University of Oslo
Department of Informatics

UWB Impulse Radio Coding Strategy

Thesis
Master of Science

Tan, Chao

August, 2007

Acknowledgements

Thanks to my supervisor Tor Sverre Lande and Dag T. Wisland, for their many inspirations, and patient guidance and encouragement.

Thanks to my parents, for their ceaseless love and support.

Thanks to my friends, for their company and support through all or part of the time of my study in Oslo

Last but the most important, thanks to my Lord for blessing me in so many ways, including this thesis work

Preface

This thesis is submitted for fulfilment of the degree study of Master of Science in Microelectronic Systems, under the Master program in Electronics and Computer Science in the University of Oslo. This thesis project started in August 2006 and concluded in August 2007.

This thesis presents a PHY layer design for low data rate, power efficient and low cost UWB-IR communication systems like Wireless Sensor Network. The coding strategy for modulation and channelization is the main focus, while many efforts are also put in the transmitter and receiver design. A PSM modulation and multi-access method is proposed. A novel biphasic toggling operation in the transmitter is present, which is simple and hardware friendly, but remarkably alleviates the spectral spikes in the PSM signal. A spatial RAKE receiver is present, which utilize the multi-path effect of the UWB channel. Theoretical analyses and simulations both show that the system performance meet the expectation well. Trade-offs of the system is discussed for different channel conditions and different capacity requirement.

Contents

1. Introduction

Ultra Wideband (UWB) technology is a new radio technology that transmits radio signal over an ultra wide bandwidth. This technology has many appealing properties that are interesting for various applications including ground-penetrating radar, through-wall imaging, vehicular and surveillance systems, and wireless communication systems. To coexist with other existing narrow band (NB) communication systems like Global Positioning Systems (GPS), Wireless Local Area Networks (WLAN) and cellular systems, the signal of UWB need to be at a very low power level so that it seems noise-like to the existing NB systems.

Bandwidth has been opened up for this new technology, and regulations to limit the transmitting power have been issued. The Federal Communications Commission (FCC) of the US has allocated huge bandwidth for the deployment of UWB devices and systems in 2002, and for wireless communication systems, the bandwidth of 3.1GHz to 10.6GHz is issued. In December 2006, the European Commission approved UWB technology to be deployed in Europe and it is announced that the regulation will come out very soon. Many other authorities and countries are also considering opening up bandwidth for this new technology.

UWB receives great interests from research bodies from the government, universities and industry all over the world. Some of the applications are really near to the daily life, like medical imaging and near-body networks, home automation and entertainment networks, Wireless Personal Area Networks (WPAN), wireless USB and PC-peripheral connections.

Standardization is still on the way but some products have already hit the market. In short, UWB is a technology that is going to change the world of telecommunication and change our lives soon.

1.1. UWB-definition and history

A UWB system is a transmission system with an instantaneous spectral bandwidth of more than 500MHz, or with an instantaneous fractional bandwidth of more than 20%~25%. The definition of fractional bandwidth is:

$$\textit{Fractional bandwidth} = \frac{B}{f_c} \qquad \text{Equation 1-1}$$

where *B* denotes the -10dB bandwidth, $B = f_H - f_L$, and f_c denotes the centre frequency, $f_c = (f_H - f_L)/2$, with f_H being the upper frequency of the -10dB band and f_L being the lower frequency of the -10dB band. According to the FCC 'First Report and Order' (R&O) [1], which issued permission of deployment of UWB devices in the US, to be a UWB system, a transmission system with $f_c > 2.5GHz$ needs to have a -10dB bandwidth of at least 500MHz, while a transmission system with $f_c < 2.5GHz$ needs to have fractional bandwidth of at least 0.2. Notice that for a system with bandwidth of 2.5GHz, a 20% fractional bandwidth is 500MHz. Under this definition, UWB systems with bandwidth larger than 2.5GHz are allowed to have fractional bandwidth less than 20%, and UWB systems with bandwidth smaller than 2.5GHz are allowed to have absolute bandwidth smaller than 500MHz.

The principle idea of UWB radio systems is to transmit information with ultra-short (nanosecond scale) radio pulse that is carrier-less and can operate at baseband. The idea of UWB has a history of more than a century. When first invented by Guglielmo Marconi, the radio communication system utilized the spark-gap transmitters to convey information. This method used enormous bandwidth and can be seen as a first example of UWB idea. In 1960s, when the techniques for generating and receiving sub-nanosecond (baseband) pulses, which were first invented for microwave network system impulse response observation and measurement, came into being, the short pulses were considered to be used in radar and communication systems. Ross's patent in 1973, '*Transmission and Reception System for Generating and Receiving Base-Band Pulse Duration Pulse Signals without Distortion for Short Base-Band Communication System*', built the foundation of UWB communications.

In 1989, the U.S. department of Defence (DoD) used the term 'ultra wideband' for radio devices occupying at least 1.5GHz, or a -20dB fractional bandwidth exceeding 25%. Before that, this technology was commonly referred as 'short pulse' or 'carrier-less'. In 1998, FCC started rule making of UWB, and in 2002, the First R&O was released. In December 2006, the European Commission approved UWB technology to be deployed in Europe. The regulations have not been released yet but it has been announced that they will not be very different from the FCC version, with similar power level but more restrictive frequency range.

On the other hand, the standardization of UWB is discussed in two IEEE bodies, especially, two task groups in IEEE 802.15 Wireless Personnel Area Network (WPAN). The Task Group 3a (TG3a) focuses on using UWB as a High Rate Alternative physical layer (PHY) of WPAN, aiming at provide data rate of 100Mbps or more. This task group has been withdrawn because the two main technology proposals: the UWB-OFDM proposal of the Multi-band OFDM Alliance (MBOA) and the UWB-Direct Sequence (DS) proposal of the UWB Forum could not come to a joint standard. The Task Group 4a (TG4a) focuses on using UWB as a Low Rate Alternative PHY of WPAN. TG4a aims at investigating a PHY with low data rate, multi-month or even multi-year battery life, and very low complexity. The UWB Impulse Radio (UWB-IR) proposal is approved in this task group.

There is another thing worth mentioning here. Different from the typical UWB idea of carrier-less ultra short pulse, which conveys information with base band impulse, there is another approach: multi-band UWB (UWB-MB). According to the FCC UWB definition, that a signal is UWB if its bandwidth exceeds 500MHz, the MB approach divides the overall 7.5 GHz bandwidth into smaller frequency band of at least 500MHz. The transmission of data occurs on these sub-bands. Different modulation and multi-access schemes can be applied to this approach. The UWB-OFDM proposal mentioned just now is an OFDM modulation Multi-Band UWB.

1.2. UWB-IR in low rate, power efficient and low cost systems

This thesis focuses on UWB communication systems. A communication system can be described by an Open Systems Interconnection Basic Reference Model (OSI model for short), which is an abstract and layered description of communications and computer network protocols. The OSI model defines 7 layers. The first layer is called physical layer (PHY); it defines the physical specifications of the communication devices, as well as the relationship between the device and the physical medium. The UWB is a technology that transmit information with ultra short pulse, or ultra wide bandwidth through the air, and therefore it is a mainly a PHY technology.

As a PHY realization for wireless communication systems, there are mainly two directions of development of UWB. One direction is high rate short range

systems, like systems transmitting large video files real-time in a range of 3m to 10m. This data rate can be 100Mbps or more. Home entertainment system is one of the typical applications.

The data rate and the communication range is a trade-off: the longer communication range a system demand, the lower data rate it can expect. This is because, the longer distance the UWB signal needs to travel, the more attenuation and fading and noise it will experience. Given the very noise-like power spectrum limit, the system can not conquer this by enhance the transmitting power. According to Shannon-Hartley Theorem, for an Additive White Gaussian Noise (AWGN) channel

$$C = B\log_2\left(1+\frac{S}{N}\right) \quad \text{Equation 1-2}$$

Where C is the channel capacity in bit per second (bps), B is the channel bandwidth in Hz, S is the total signal power, and N is the total noise power. Given a certain bandwidth B and a certain transmitting power, the received total signal power S decrease will lead to the decrease of C. On the other hand, apart from AWGN, the UWB signal also tends to experience more multi-path fading. To maintain the system performance at long range, the system has to lower down the data rate to give a larger margin to the link budget.

The other direction is low data rate, power efficient and high simplicity systems; the transmission range is longer compared to the first one. The typical application is wireless sensor networks. A wireless sensor network is a network of devices that are spatially distributed and that cooperatively monitor physical or environmental conditions. In such a network, the transmissions are not frequent and the data rate is low. A long battery life is desirable for such devices, the system need to be power efficient. The size of the devices needs to be small and the number of them can be large; therefore the system needs to have simple and low cost hardware implementation. Due to the very low transmission power, the UWB technology is power efficient by nature compared to other Radio technologies. Low data rate and simple hardware can make the power consumption even lower.

Ultra Wideband Impulse Radio (UWB-IR) is one of the two main approaches to realize UWB technology. As suggested by the name, UWB-IR transmits information with sequence of ultra short impulses. The duration of the pulses is less than one nanosecond and the bandwidth of the signal is ultra wide. The other approach of realization is UWB-MB-OFDM. This approach splits up the allocated

7.5GHz bandwidth into 500MHz sub-bands, and uses an OFDM modulation scheme. This is an idea that deviates from the origin idea of the UWB but still has strong potential, especially for the high data rate applications.

The focus of this thesis is on the low data rate, power efficient and low cost systems with UWB-IR realization. The high data rate short range systems and the UWB-MB-OFDM realization will not be discussed in this thesis.

1.3. Coding strategy

The focus of this thesis is on UWB coding strategy. The term coding has several meanings: in speech and image processing it means data compression, error correcting or data encryption, while in communication systems it means modifying the signal spectrum (spectrum-spreading and scrambling), digital modulation or channelization. It also refers as digital representation of an analogue signal in Analogue/Digital or Digital/Analogue conversion. In this thesis, coding means both modulation and channelization. We present a Pulse Sequence Modulation (PSM), which serves both as a modulation scheme and as a multiple-access scheme.

The idea of PSM is to transmit information symbols with pulse sequence coded by Pseudo-Noise (PN) codes. In a transmission channel with n symbols, n PN codes are allocated to represent each of them. For another transmission channel with m symbols, m PN codes are allocated to represent each of them. Say that we have a system with 10 channels, and each channel has two data symbols; then there are totally 20 symbols that might be transmitted in this system, and it needs 20 different PN codes to represent them. All these PN codes should be distinguishable from each other. This makes two symbols in one channel distinguishable, and at same time, makes symbols from different channels distinguishable too. In this way, the PSM serves both as a modulation scheme and as a multiple-access scheme.

The properties of the PSM codes directly affect the performance and the capacity of the system. First of all is the code distinguishability: the ability of the code to be distinguished from other codes. The distinguishability of the PSM codes determines the distinguishability of the information symbols of the system. The detection of a PN codes is by correlation: correlate the target bit sequence with the PN code we are looking for, and if a peak value that equals to the autocorrelation

peak of the PN code is found, then the PN code is found. Therefore, the correlation property of the codes is crucial to the system performance.

The correlation properties of the codes refers to the autocorrelation of one code and the cross correlation between each two codes. For successful detection, the PN codes need to have autocorrelation function with sharp peak and low side lobe, and low cross correlation function. If a set of codes have zero cross correlation function, they are orthogonal to each other. There are several different PN code families to choose from and they have different advantages and disadvantages. For example, the code family of Walsh-Hadamard codes is orthogonal code. They have zero cross correlations. However, their autocorrelations have no sharp peak. Another code family, Barker codes, has autocorrelations with sharp peak, and the side lobe has only tow value, 1 and 0. However, the number of available codes in this family is very limited. Another two code families, Linear Feedback Shift Register (LFSR) PN codes and chaos-based PN codes are discussed in this thesis. These two code families have low cross correlations, but not orthogonal; sharp autocorrelation peak, but side lobe not as low as that of the Barker codes. Both of these two code families have large number of available codes. The LFSR codes are easy to generate and manage on each communication node, while the chaos-based PN codes have flexibility in code density, which leads to easy control in the data rate of the channel and the system capacity. All these code families will be discussed in detail in chapter 5 Code Selection.

The nonzero cross correlation function of the PSM codes leads to interferences between data symbols, because the code detection is done correlating the received bit sequence with the PSM codes, and finding the autocorrelation peak. The bit sequence, if correctly detected on the bit level, is made up of PSM codes. A nonzero cross correlation is interference to the detecting of the autocorrelation peak. In this thesis, this interference is named as Inter-Symbol-Interference. If the interfering symbols are data symbols from other channel, this interference can also be seen as inter-channel interference, or multiple-access-interference (MAI). In this thesis we use the term MAI to describe this kind of interference. It is easy to understand that the more channel a system have, the more interference each transmission channel may experience. To ensure a certain level of channel performance, the number of channels will be limited by the interference level, and thus the property of the PN codes.

The length of the codes, along with other parameters like the chip duration, determines the data rate of the system. The number of ‘1’s in a binary PN codes, called code density, affects the inter-channel-interference. The code density also

affects the transmission power of the system. And these two parameters have their impact on the correlation properties of the code.

The generation of the PN codes needs attention too. With a simple generation algorithm like LFSR each communication nodes can generate the PSM codes by itself and can potentially make the channel allocation of the system dynamic. This gives flexibility to the Media Access Control (MAC) layer protocol of the system. A MAC layer is a sub layer in the OSI model which is right on top of the PHY layer. However, an algorithm which is complicated and consume large amount of hardware may not be suitable to be implemented on each node.

The main task of this thesis is to make suggestions on coding strategy by studying the generation and properties of different PN codes and their impacts on the performance and capacity of the UWB system.

1.4. System frame work

Generally speaking, the transmission through the PHY layer includes three parts,

1 signalling, and transmitting, which includes pulse generating and symbol modulation
2 propagation through the channel
3 receiving and detecting, which includes demodulation of the data symbol

Besides the coding strategy of the UWB system, these three parts of the PHY layer of the UWB system will also be discussed in different extent of details. One focus among these is the receiver scheme, which is a spatial full RAKE receiver. The communication environment of UWB systems, especially indoor UWB systems, is non line of sight (NLOS) and contains many fading effects, among which the multipath is one of the most significant effects. Multipath effect brings signal distortion and spread, and inter-chip-interference to the channel and therefore degradation of the channel performance. The propagation of UWB signal through communication channel is discussed in detail in chapter 3 Channel Model. Thanks to the ultra-short pulse duration of the UWB-IR system, the multipath effect in UWB channels can potentially be counteracted by exploiting the multipath diversity with a RAKE receiver. The full RAKE receiver is a realization of the ideal concept of all-RAKE (ARAKE), which has a finger for each multipath component and captures all the signal power. Since a signal propagating in a multipath environment in theory has infinite number of multipath component, the implementation of an ARAKE receiver is impossible [Iano 2004].

The spatial Full RAKE receiver implementation is relatively simple and the performance is reasonably good shown by simulation.

The PHY layer described in this thesis has following advantages.

1.4.1. Hardware perspective

From the hardware perspective, the scheme requires no synchronization and low capacity of Data Processing, which leads to hardware simplicity, low power consumption and low cost device.

No Synchronization
As will be discussed in the following chapters, other existing modulation schemes that used in UWB-IR, like Pulse Position Modulation (PPM) and Pulse Amplitude Modulation (PAM) and Binary Phase Shift Keying (BPSK) with coherent demodulation, will need synchronization to the pulse level. For PPM modulation, and Time Hoping (TH) multiple-access method, where timing presents the information, the synchronization requirement will be even higher. PSM method requires no synchronization at all; this will significantly simplify the receiver.

Simple Data Processing
Conventionally, receiver performs Sampling and Analogue/Digital Converting (ADC) to the received signal, and than use Digital Signal Processing (DSP) circuit to perform the computation of detection and demodulation. According to the Nyquist-Shannon sampling theorem, to sampling a baseband signal without losing information, the sampling rate f_s and the bandwidth of the signal B should have such relation:

$$f_s > 2B \qquad \text{Equation 1-3}$$

For UWB signal with bandwidth of 7.5GHz, the baseband sampling and processing frequency will be to 15GHz. Assuming a 6bit digital representation of each sampling in the ADC, the receiver needs to process a data stream of 90Gps, which demands large memory and fast data processing. This speed is a very high demand on the hardware.

In the statistic full RAKE receiver, we convert the analogue received signal to continuous time antipodal signal, so functionally this is a 1bit continuous time ADC. The clock frequency in this receiver is the chip frequency. Say that we have chip duration of 30ns, the clock frequency is 33MHz and the data processing requirement is 33Mbps.

In short, the PSM modulation and multiple-access method, and statistic full RAKE receiver, will make the hardware implementation simple, power efficient and low cost.

1.4.2. Protocol perspective

From the perspective of protocol, the PHY scheme we present has 5 adjustable parameters.

- the pulse shape
- data rate
- number of active channel that transmit at the same time
- number of available channel for the whole system

Different transmitting pulse shape can potentially accommodate different regulations in different region of the world by fitting different transmission mask. The flexibility in system data rate and number of channels will accommodate different channel conditions, different system requirement on data rate and system scales. These parameters can potentially be adjusted by changing the settings of the same hardware.

This means the same device can be used in different region of the world, in different communication environment and for systems with different capacity and scale. This also means that, depending on the design of MAC layer protocol, these parameters can potentially be adjust on the fly, when the system is in use and accommodate the change of environment. Such flexible PHY layer is desirable for ad hoc networks which are suitable for wireless sensor network.

1.5. Outline of this thesis

In chapter 2 we discuss the signalling of the PHY, which includes pulse and spectrum shaping, PSM modulation and multiple-access. In chapter 3 we discuss the UWB channel models. In chapter 4 we discuss the statistic Full RAKE receiver. In chapter 6 we present simulation results and discuss the system parameters in detail.

2. Signalling and transmitter

In this chapter, we discuss the signalling of the physical layer (PHY), which includes pulse shape, signal spectrum, PSM modulation and multiple-access. As stated in chapter 1, the Power Spectral Density (PSD) of the transmitted signal needs to be under the FCC emission mask. As discussed in [Bene 2004] and many other literates, the transmission pulse shape, the modulation method and the multi-access method are the mains factors that shape the signal PSD. In [Bene 2004], it is proved that for both TH-UWB and DS-UWB, which are currently the two main multiple-access schemes for UWB-IR, the spectrum of the transmission pulse gives the signal spectrum the general shape, while the modulation method and the multiple-access method brings spectral lines or spikes to the general shape.

The spectral spikes are not desirable because it means that the transmitted energy concentrate on discrete spectral lines and thus the spectrum will be higher than the case in which the energy distributed smoothly over the spectrum. Having those spikes, to make the whole signal spectrum under the FCC emission mask, the transmission power must be tuned down.

According to the Fourier Transform theory, the spectral spikes come from the periodicity in the transmitted signal. Therefore, the more random the signal is, the less spikes the spectrum will have.

2.1. Pulse shape and spectrum

UWB-IR uses very short pulses to transmit information. The choice of transmission pulse shape is important because it will affect the PSD of the transmitted signal. There are different pulse shape proposals. So called good pulse spectrum means the pulse spectrum fit FCC emission mask well, so that more energy can be transmitted under the FCC emission mask and so that a better pulse

detection performance can potentially be achieved. The pulse spectrum also needs to have zero DC component. There are many proposals on UWB pulse waveform. Some of them provides very flat spectrum within the FCC open bandwidth, others even provide deep spectrum notch to avoid interference with narrow band systems. The design of pulse shape generator is out of the scope of this thesis. Here we choose the widely used Gaussian function and its derivatives as our pulse waveform, because these waveforms have spectra that can fit the FCC emission mask well and are easy to generate.

A Gaussian function $g(t)$ is defined as follow

$$g(t) = \frac{\sqrt{2}}{\alpha} \exp(-2\pi \frac{t^2}{\alpha^2}) \qquad \text{Equation 2-1}$$

where α is known as the shaping factor. The Gaussian derivatives, $g_k(t)$ are derived as follow, k denotes the order of derivative,

$$g_k(t) = \frac{d^k}{d^k t} g(t) \qquad \text{Equation 2-2}$$

The odd order Gaussian derivatives have zero DC value while the even order derivatives have non-zero DC value. Therefore only the odd order derivatives are suitable for radio transmission. It also can be seen that, the larger α is, the wider these functions will be, and the narrower the spectrum will be.

Some literatures state that the antenna in the transmitter and receiver has an effect of time-derivative. Considering this, at the transmitter side, if an even order, $2n^{th}$ Gaussian pulse is generated, an odd order $(2n+1)^{th}$ pulse will be sent in the air; at the receiver side, the signal output by the receiver antenna will be an even order $(2n+2)^{th}$ pulse. On the other side, given the ultra wide bandwidth of the UWB signal, and the fact that it is very difficult for the transmitting and receiving antenna to have a flat spectrum response over so wide a bandwidth and in all direction (omni direction), the antenna will bring distortion to the UWB pulses, both in time domain and in spectrum. In this thesis we will not discuss the design and property of the UWB antenna. For simplicity we assume that the antenna brings no time-derivative or distortion to the pulses. However, the principle of choosing waveform and considerations on pulse detection will not lose their generality.

Two key factors of the spectrum of Gaussian derivative, the peak frequency and the width of the spectrum, are decided by the shaping factor α and the order of derivative [Bene 2004]. The peak frequency and the shaping factor α has a relation as follow

$$f_{peak,k} = \sqrt{k}\frac{1}{\alpha\sqrt{\pi}} \quad \text{, Equation 2-3}$$

This equation shows that the higher order derivative has higher peak frequency.

In Figure 2-1 we plot the spectrum of the Gaussian derivative pulses with order of 5, 7, 9 and 11. We keep the peak frequency of the Gaussian derivatives at the central frequency of the emission mask, which is 6.85GHz. According to Equation 3-2, the peak frequency of the Gaussian derivatives increases as the order goes up and decreases as the shaping factor increase. To keep the peak frequency the same, the shaping factor will change following this relation:

$$\alpha = \sqrt{k}\frac{1}{f_{peak,k}\sqrt{\pi}} \quad \text{Equation 2-4}$$

This means higher order pulse needs to have larger shaping factor α, which leads to narrower spectrum. In Figure 2-1 we can see that the spectrum of the 11^{th} pulse is the narrowest and the spectrum of the 5^{th} pulse is the widest. It is easy to understand that he transmitted pulse energy is the area of the pulse spectrum. Therefore, the 5^{th} order pulse shape can transmit the largest energy in these four.

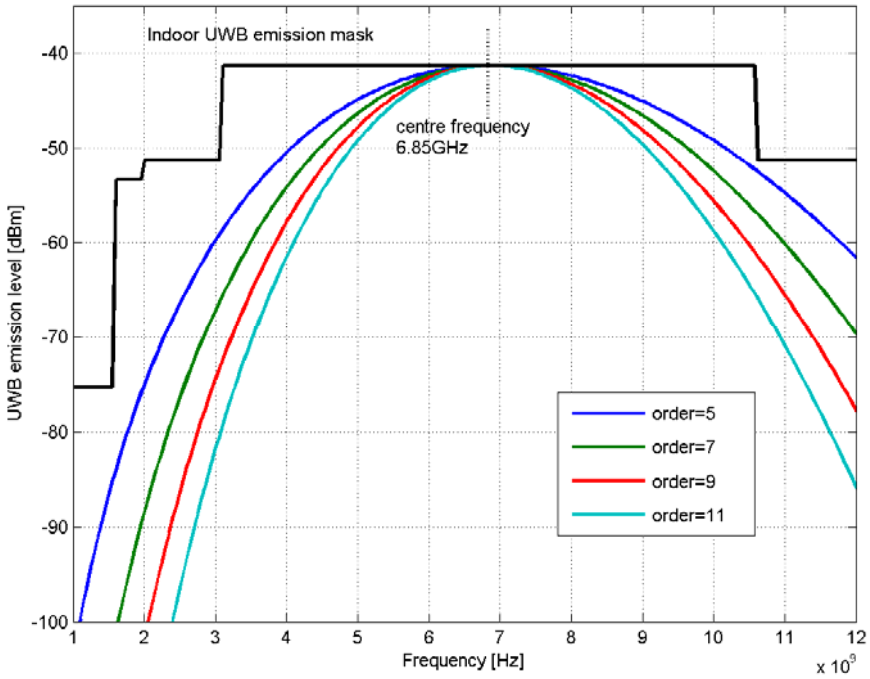

Figure 2-1 spectra of Gaussian derivatives

In Figure 2-2 we show the time domain waveform of the four pulses, the shaping factor α is also noted. All these Gaussian derivatives have some slopes in their waveform. Higher order derivatives tend to have more slopes. These pulse slopes are very important in our statistic pulse detection scheme, as will be discussed in chapter 5. More significant pulse slopes can potentially improve the performance of the statistic pulse detection.

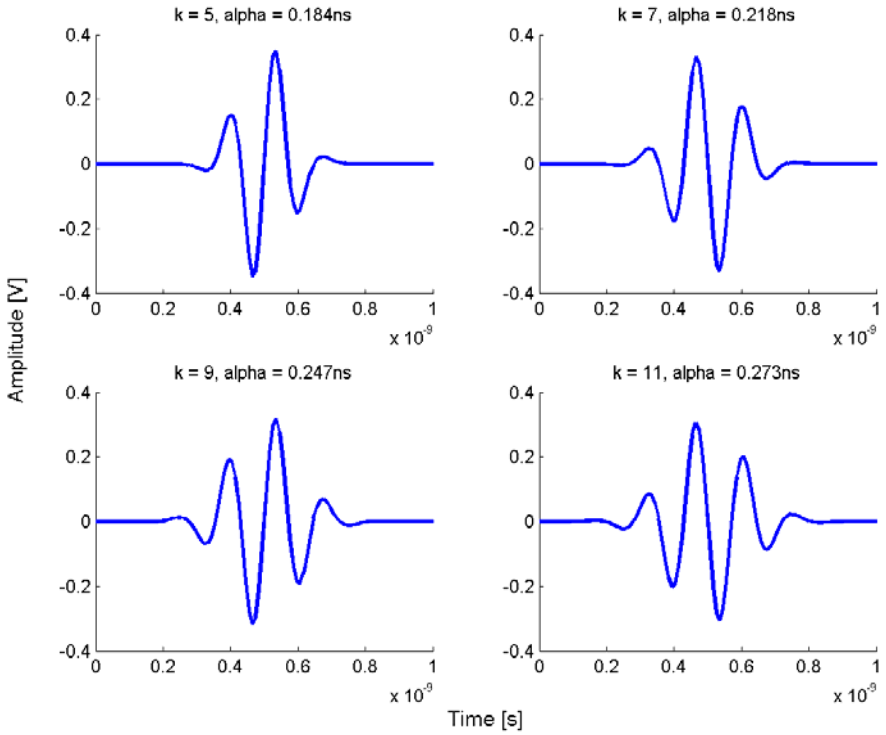

Figure 2-2 Time domain pulse shape of Gaussian derivatives

In the analysis and simulation of this thesis, we choose the 5th order Gaussian pulse as our transmission pulse because its spectrum fit the emission mask well and its four pulse slopes are convenient for our statistic pulse detection scheme.

2.2. Modulation and Multiple-Access in UWB systems

In a UWB-IR system, the transmitted signal is a sequence of radio pulses modulated by the information data. In narrow band systems, the signal may carry the information in the amplitude, phase or combination of these two. In UWB-IR, pulses can carry the information with amplitude, phase, and the position within a chip. In general, the more symbols a modulation scheme has, the more information one symbol of this scheme can convey. For each modulation scheme with M symbols, the information one symbol conveys is $I = \log_2 M$. Given certain symbol rate, higher transmitted data rate can be achieved with larger M. However, to achieve a certain symbol detection performance, larger M demands higher PSD, and more complex transceiver circuitry. In our system we choose to have modulation scheme with M=2.

In this section we discuss two modulation methods, Pulse Amplitude Modulation (PAM) and Pulse Position Method, and two multiple-access methods, Time Hoping (TH) and Direct Sequence (DS), to compare with the PSM method, which will be discussed in section 2.3. These are the major solutions for in current UWB-IR systems.

2.2.1. Modulation method: PPM, PAM

We name the wave form of a single pulse as $p(t)$. A time interval T_c which may contain a pulse is called a chip, and T_c is the chip duration. N_s denotes the number of pulses used to transmit one data symbol; the group of pulses that represent one data symbol is called one frame. The time duration of one frame is $T_s = N_s \cdot T_c$. $s(t)$ denotes the transmitted signal. The data sequence to be transmitted is denoted as **s** = (…, s_0, s_1, … s_k, s_{k+1}, …), $s_k = \{'0', \quad '1', \quad \ldots, \quad 'M-1'\}$ is a data symbol. These expressions will be used all through this thesis.

2PPM

The PPM method modulates the information by shift the pulse position within a chip by ε, $\varepsilon < T_c$. In Pulse Position Modulation, each symbol of the data sequence is repeated N_s time. This is called pulse repetition. The purpose of pulse repetition is to improve the symbol detection performance and to accommodate the multiple-access method. Data sequence after repetition is called bit sequence and denoted as **b** = (…, b_0, b_1, …, b_k, b_{k+1}, …). The bit sequence takes binary levels $b_k = \{0,1\}$

The PPM modulation can be expressed as follow,

$$s(t) = \sum_{j=-\infty}^{\infty} p(t - jT_c - b_j\varepsilon) \qquad \text{Equation 2-5}$$

2PAM

The PAM method also needs repetition. The process is the same as describe in the last paragraph. What is different is the signal level of bit sequence of 2PAM is antipodal, $b_k = \{+1, -1\}$.

$$s(t) = \sum_{j=-\infty}^{\infty} b_j \, p(t - jT_c) \qquad \text{Equation 2-6}$$

2.2.2. Multiple-Access method: TH, DS

Currently there are two main multiple-access methods, Time Hopping and Direct Sequence. Both of these two involve Pseudo Noise (PN) codes to perform channelization. Usually, the length of the channelization PN codes is equal to the pulse repetition number N_s, so that one frame can accommodate one complete channelization PN code.

TH

We denote $c_{TH} = (c_0, c_1, \ldots, c_k, c_{k+1}, \ldots, c_{L-1})$ as the TH code with code length L. The TH code is an integer-valued code. Apply the TH code to one data frame and this brings a time shift element $c_k T_{th}$ to each pulse. For all c_k, k=0, 1, …, L-1, we have $c_k T_{th} + T_{pulse} < T_c$, where T_{th} denotes the length of a pulse.

The UWB-TH-PPM signal, UWB signal with PPM modulation and TH multiple-access, can be expressed as follow:

$$s(t) = \sum_{j=-\infty}^{\infty} p\left(t - jT_c - c_j T_{th} - b_j \varepsilon\right) \qquad \text{Equation 2-7}$$

The UWB-TH-PAM signal, UWB signal with PAM modulation and TH multiple-access, can be expressed as follow:

$$s(t) = \sum_{j=-\infty}^{\infty} b_j \, p\left(t - jT_c - c_j T_{th}\right) \qquad \text{Equation 2-8}$$

DS

We denote $c_{DS} = (c_0, c_1, \ldots, c_k, c_{k+1}, \ldots, c_{L-1})$ as the DS code. DS codes are antipodal codes with $c_k = \{1, -1\}$. Apply the DS code to one data frame. The UWB-DS-PAM signal can be expressed as follow:

$$s(t) = \sum_{j=-\infty}^{\infty} c_j b_j p(t - jT_c) \qquad \text{Equation 2-9}$$

2.3. Pulse Sequence Modulation

As explained in Chapter 1, the PSM method is both modulation method and multiple-access method. We use $c_1 = (c_{1,0}, c_{1,1}, \ldots, c_{1,k}, \ldots, c_{1,L-1})$ and $c_0 = (c_{0,0}, c_{0,1}, \ldots, c_{0,k}, \ldots, c_{0,L-1})$ to denote the two PN codes to represent the data symbol '1', and '0'. Code c_1 and c_0 are binary PN codes, $c_{1,k}, c_{0,k} = \{1, 0\}$. In the PSM method, If we have a data sequence of $s = (\ldots, s_j, s_{j+1}, \ldots)$, after modulation, we get the bit sequence $b = (\ldots, c_{s_j,0}, \ldots, c_{s_j,L-1}, c_{s_{j+1},0}, \ldots, c_{s_{j+1}.L-1}, \ldots) = (\ldots, b_j, b_{j+1}, \ldots)$. The UWB-PSM signal can be expressed as follow:

$$s(t) = \sum_{j=-\infty}^{\infty} b_j p(t - jT_c) \qquad \text{Equation 2-10}$$

An example of PSM modulation is shown as follow. Say we now have a data sequence of 3 symbols: $s = ('1','0','1')$ and we have the following two PSM codes: $c_1 = (1,0,0,1,1,1,0)$ and $c_0 = (0,1,0,1,1,1,0)$. After PSM modulation, we get the bit sequence *b*:

$$b = (\underbrace{1\,0\,0\,1\,1\,1\,0}_{\text{Symbol '1'}}\ \underbrace{0\,1\,0\,1\,1\,1\,0}_{\text{Symbol '0'}}\ \underbrace{1\,0\,0\,1\,1\,1\,0}_{\text{Symbol '1'}})$$

Example 2-1 PSM modulation

An example of transmitted pulse sequence is shown in Figure 2-3. The bit sequence here is {1 1 0 1 0}. There is one pulse at the beginning in a chip of bit '1', but no pulse in a chip of bit '0'. We can see the 180 degree phase shift in the second pulse and this is because of the biphasic toggling, which will be discussed in subsection 2.3.2.

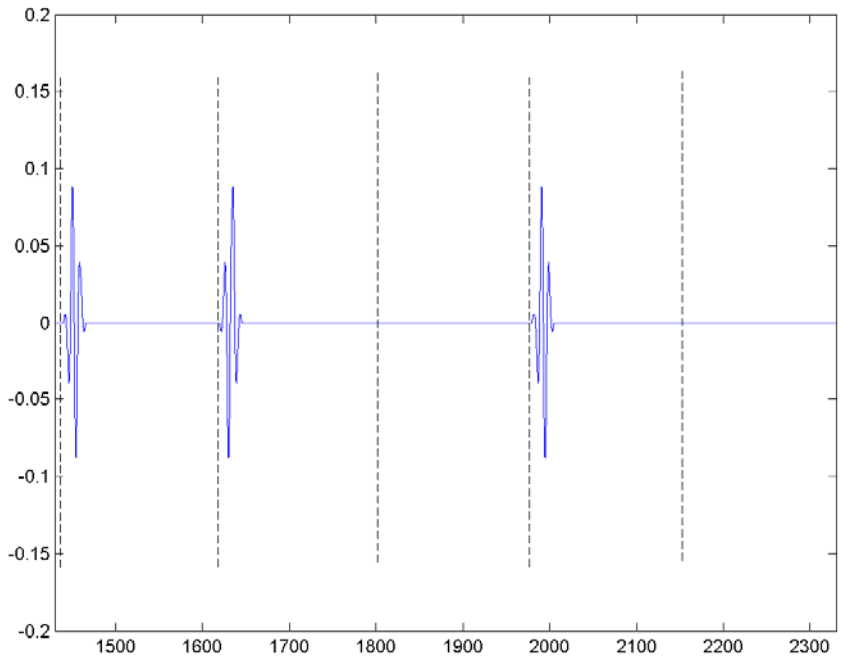

Figure 2-3 one piece of transmitted pulse sequence of PSM modulation

2.3.1. Comparison

The UWB-PSM signalling is different from all the other signalling in this way: for all the other signalling, there is one pulse in every chip, but in UWB-PSM signalling, it depends on the transmitted bit. If we have a PSM modulated bit sequence containing 20% of bit '1' we will transmit only one fifth of energy compared to the other signalling schemes. Therefore the PSM signalling can be more power-efficient than other signalling schemes by controlling the number of '1', which is called the density of '1'. The density of '1' in a bit sequence can be controlled by controlling the density of '1' in the PSM codes. We will discuss how this control can be achieved in chapter 5 code selection

In this subsection, we compare several UWB signalling schemes in respect to the fitting of the FCC emission mask. Figure 2-4, Figure 2-5, Figure 2-6 and Figure 2-7 show the power spectrum of different signalling methods. 5^{th} order Gaussian derivative is used as transmission pulse. In all these four cases, the energy per

pulse is the same. The chip duration T_c is the same. The frame length, i.e. the length of the TH code and length of the DS code and the length of the PSM codes, are the same. The emission mask shown in these four figures is the FCC indoor emission mask. The same PN code is used as TH code and DS code in these four case, and this code is one of the two pulse sequence code used in the PSM signalling. Given this conditions, the data rate of these four schemes is the same. We can now compare the spectrum of these different signalling schemes, with the same channel capacity and to see how the modulation and multiple-access affect the signal spectrum and how well they can comply with the power emission limit.

Figure 2-4 shows the power spectrum of UWB-PSM signalling. The energy per pulse is tuned to make sure that the PSD of UWB-PSM is just under the emission mask. And the same energy per pulse is used for the other figures. We can see that the spectra of the 2PPM-TH scheme and the 2PAM-TH scheme exceed the emission mask. This means, to comply with the FCC emission mask, with the same capacity, these two schemes have to lower done their transmitting power, and transmit less energy per pulse. Less energy per pulse tends to degrade the performance of detection.

Figure 2-6 shows that, the spectrum of the 2PAM-DS signalling has less significant spikes compared to the spectrum of the PSM signalling in Figure 2-4. With the same transmitting power, this makes the spectrum of the 2PAM-DS scheme has an around 7 dB margin under the emission mask. This means with 2PAM-DS signalling, the system can transmit pulse with energy 7dB higher. This margin can be used to improve the system performance by transmitting more energy per pulse, or to improve the system capacity by increasing the data rate or by employing higher order modulation scheme.

The reason why the 2PAM-DS scheme has this advantage over the PSM scheme is that, this signalling use the antipodal signal level, as oppose to the binary signal level in the PSM scheme. The antipodal signal level brings addition randomization to the signal, and the randomization of signal alleviates the problem of spectrum spikes.

To compensate the inadequate of randomization in the PSM signalling, we introduce biphasic toggling, which is discussed in subsection 2.3.2.

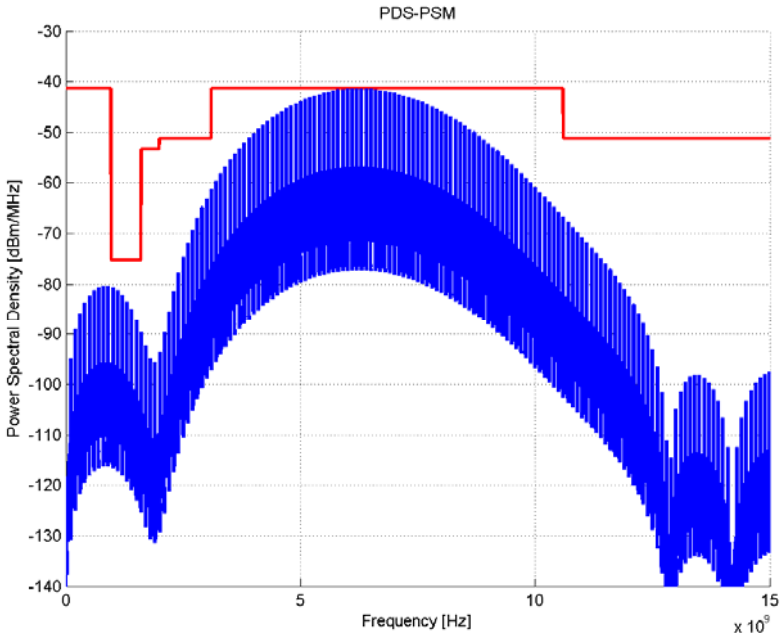

Figure 2-4 Power spectrum of PSM signalling

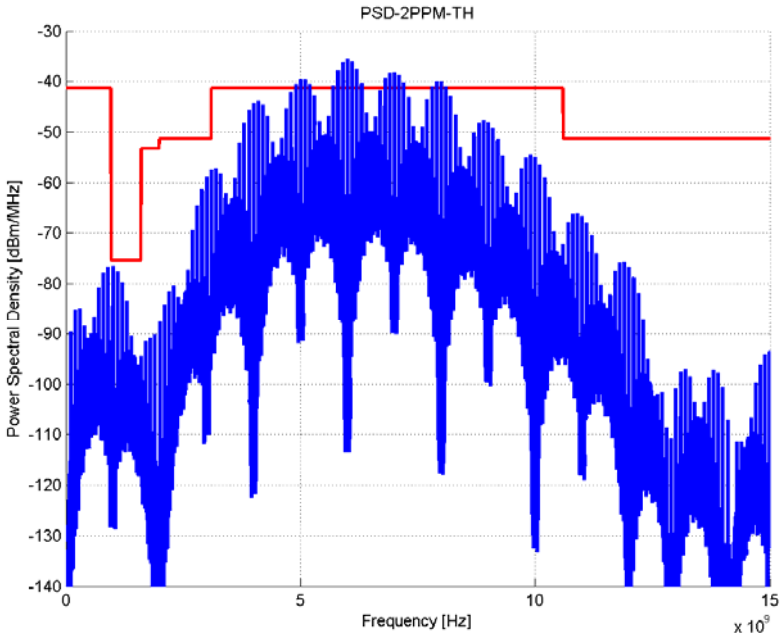

Figure 2-5 Power spectrum of 2PPM-TH signalling

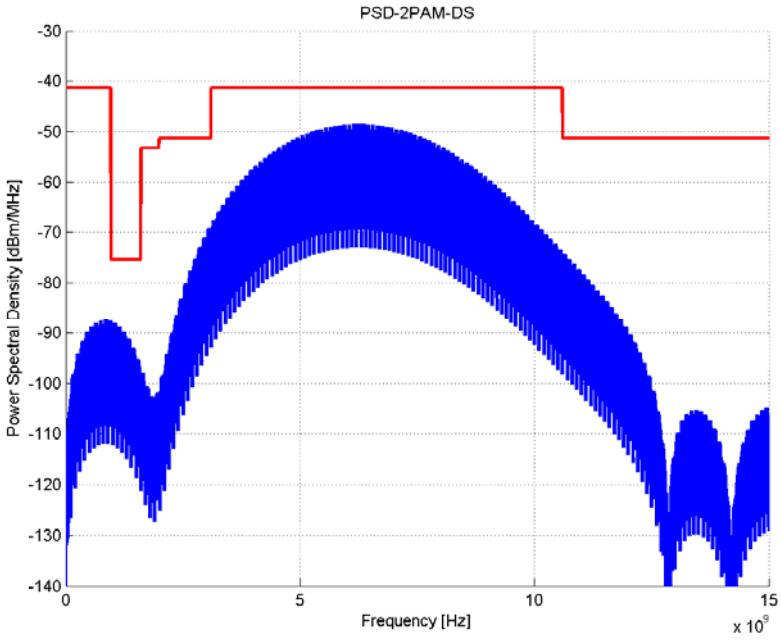

Figure 2-6 Power spectrum of 2PAM-DS signalling

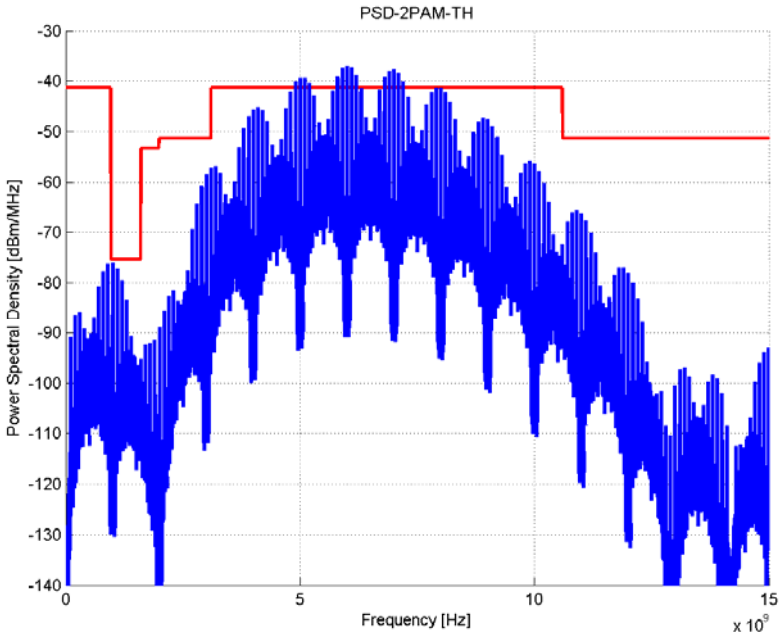

Figure 2-7 Power spectrum of 2PAM-TH signalling

2.3.2. Biphasic toggling

In this subsection we introduce a scrambling method that further randomizes our signal to smooth the signal spectrum. Scrambling process is often used in CDMA communication systems, to spread the narrow band signal over a wider bandwidth, or to provide multiple-user access. For example, in the 3th generation mobile communication system UMTS, which is a WCDMA system, the Hadamard codes are used in uplink channels as scrambling codes. In this system, the scrambling codes do not spread the signal spectrum because it does not further increase the chip rate, but provides multiple-user access to the channel.

Hadamard code is a PN code family who has the property to be orthogonal. Its orthogonal property makes ideal for the purpose of multiple-user access since it provide zero MAI. This code family will be discussed as a candidate for PSM modulation codes in chapter 5 Code selection.

Different from the mobile communication systems, the purpose of scrambling in our PHY is to randomize the signal to alleviate the spectrum spikes. Another way to understand randomization is to destroy the periodicity in the signal. In the light of comparison between the PSM signalling and the 2PAM-DS signalling, in the later extra randomization is achieve by antipodal signal level, we scramble the data by toggling every other '1' bit in the bit sequence to an opposite phase, which we called biphasic toggling.

The conventional way of data scrambling is to multiply a scrambling code with the bit sequence, as the data scrambling in UMTS system. To bring in antipodal signal level, we multiply the binary bit sequence with an antipodal scrambling code. We can use Hadamard codes as scrambling code here to because they are PN codes and have inherent randomization. We show and example of scrambling with an 8bit long Hadamard code as scrambling code. We use the same bit sequences as in Example 2-1 and the scrambling codes is:
$sc = (+1,-1,-1,+1,-1,+1,+1,-1)$. By multiplying the scrambling code to the bit sequence *b* be get *b'*. And much less periodicity can be seen in the sequence *b'* than in *b*.

b = (1 0 0 1 1 1 0 0 1 0 1 1 1 0 1 0 0 1 1 1 0)

.* sc = (+ - - + - + + - | + - - + - + + - | + - - + -)

b' = (1 0 0 1 -1 1 0 0 | 1 0 -1 1 -1 0 1 0 | 0 -1 -1 1 0)

Example 2-2 Data scrambling with Hadamard code

With simulation we found that using the Hadamard sequence as scrambling code improve the PSM spectrum by alleviate the spectrum spikes and brings in PSD margin under the emission mask. And the longer scrambling code is used, the larger PSD margin can be achieved. An 8bit long code can bring a margin of 4dB; a 16bit long code can bring a margin of 5.5dB; a 32bit long code can bring a margin of 6.5 dB and a 64bit long code can bring a margin of 7.5 dB, which is comparable with the 2PAM-DS scheme. This scrambling approach requires an additional code generation to the PHY layer, and additional code management to the MAC layer.

We introduce the approach of biphasic toggling. This approach use no scrambling code, but just toggle every other ‘1’ chip to ‘-1’. Simulation shows that this switching scrambling approach brings at least 9 dB improvement to the PSM spectrum. The idea is shown in Example 2-3:

b = (1 0 0 1 1 1 0 0 1 0 1 1 1 0 1 0 0 1 1 1 0)

b' = (1 0 0 -1 1 -1 0 0 1 0 -1 1 -1 0 1 0 0 -1 1-1 0)

Example 2-3 Data scrambling by shifting

Figure 2-8 shows the PSD of the PSM scheme with the biphasic toggling. We can see that the spectrum spikes are alleviated and about 9dB margin is achieved under the emission mask. The biphasic toggling method needs no additional code generation, and no additional management in MAC layer. The hardware implement is rather simple. Only a two-bit register and a inverter after the PSM modulator are needed. Therefore we employ the biphasic toggling approach in our PHY.

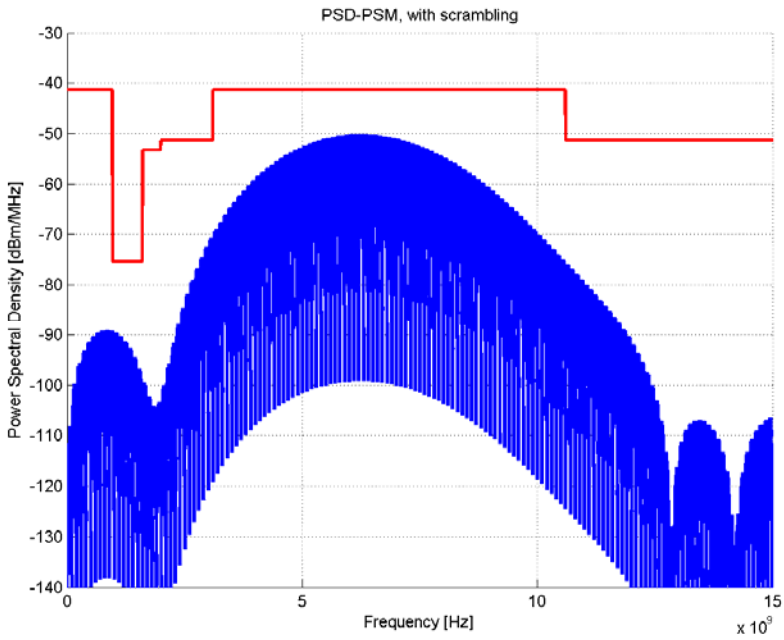

Figure 2-8 Power spectrum of PSM signalling with biphasic toggling

2.3.3. Analysis of the improvement

In this subsection we discuss why the biphasic toggling can achieve such improvement in the PSD of PSM signal. We start by model the transmitted signal as follow, where $\{a_n\}$ is the bit sequence, $p(t)$ is the pulse waveform, T_c is the chip duration and $\{\varepsilon_n\}$ is the time offset of each pulse.

$$s(t) = \sum_{n=-\infty}^{\infty} a_n p(t - nT_c - \varepsilon_n) \quad \text{Equation 2-11}$$

Equation 2-11 can be used to model all the four modulation and multiple access schemes discussed in this section: PSM, 2PPM-TH, 2PAM-TH and 2PAM-DS. To analysis the PSD of $s(t)$ we need to make some assumptions on the bit sequence $\{a_n\}$ and the time jitter $\{\varepsilon_n\}$. We model $\{a_n\}$ as a wide sense stationary (WSS) digital sequence and $\{\varepsilon_n\}$ as a sequence of independent identically

distributed (i.i.d) uniform random variables, which is independent of $\{a_n\}$, with probability density function (PDF)

$$f_{\varepsilon_n}(x)=\begin{cases}\dfrac{1}{\Delta} & \Delta_1 < x < \Delta_2 \\ 0 & otherwise...\end{cases} \qquad \text{Equation 2-12}$$

According to [Moez 1997], with these assumptions, the PSD of the signal $s(t)$, $S(f)$ consists of the continuous component $S^c(f)$ and the discrete component $S^d(f)$.

$$S^c(f)=\frac{1}{T_c}|W(f)|^2\left[R_a(0)-|\overline{a}|^2\left[\frac{\sin(\pi f\Delta)}{\pi f\Delta}\right]^2\right] + \frac{1}{T_c}|W(f)|^2\left\{\sum_{l\neq 0}\left[R_a(l)-|\overline{a}|^2\right]e^{-2\pi jlT_c}\right\}\cdot\left[\frac{\sin(\pi f\Delta)}{\pi f\Delta}\right]^2 \qquad \text{Equation 2-13}$$

$$S^d(f)=\frac{1}{T_c{}^2}\sum_{l=-\infty}^{\infty}\left|W\left(\frac{1}{T_c}\right)\right|^2|\overline{a}|^2\left[\frac{\sin(\pi f\Delta)}{\pi f\Delta}\right]^2\delta\left(f-\frac{l}{T_c}\right) \qquad \text{Equation 2-14}$$

In Equation 2-13 and Equation 2-14, $W(f)$ is the Fourier transform of the pulse waveform $p(t)$, $R_a(l)$ and $\overline{a}$ is the correlation function and mean of the bit sequence $\{a_n\}$. We can see that the continuous component and the discrete component of the PSD are shaped by the PSD of the pulse waveform, the statistic properties of the bit sequence, and a *sinc* function which is from the uniform distributed time jitter. In the discrete component we can see that the distance between spectrum lines is the chip frequency $1/T_c$.

In Figure 2-4 ~ Figure 2-7 we can see that, the PSD of the four schemes contain both continuous component and discrete component. In the 2PPM-TH scheme and the 2PAM-TH scheme, there is time offset in each chip. If we model the time offset in these two schemes as uniform distributed time jitter, we can see that the *sinc* function $\left[\dfrac{\sin(\pi f\Delta)}{\pi f\Delta}\right]^2$ shaped both the continuous component and the

discrete component of the PSDs, from the waves in the envelope of spectrum lines and the continuous PSD component.

In 2PAM-DS and PSM schemes there is no time offset in chips. In this model we can let $\Delta_1 \to \Delta_2$ so that $\Delta \to 0$. In this case the *sinc* function will be reduced to 1. And here we make another assumption on the sequence $\{a_n\}$: we assume that the bit sequence $\{a_n\}$ is uncorrelated. Then the correlation function will be

$$R_a(l) = \begin{cases} E\left(a_n a_n^*\right) & l = 0 \\ |\overline{a}|^2 & l \neq 0 \end{cases} \quad \text{Equation 2-15}$$

The Equation 2-13 and Equation 2-14 can be reduced to the following form.

$$S^c(f) = \frac{1}{T_c}|W(f)|^2 \left[R_a(0) - |\overline{a}|^2 \right] \quad \text{Equation 2-16}$$

$$S^d(f) = \frac{1}{T_c^2} \sum_{l=-\infty}^{\infty} \left| W\left(\frac{1}{T_c}\right) \right|^2 |\overline{a}|^2 \delta\left(f - \frac{l}{T_c}\right) \quad \text{Equation 2-17}$$

Now we qualitatively discuss with the same single pulse energy, why the 2PAM-DS scheme has a 7dB lower PSD than the PAM scheme, and why the biphasic toggling PAM can achieve a 9dB improvement compared to the un-toggled PAM.

2PAM-DS

We model the bit sequence $\{a_n\}$ as i.i.d digital sequence with PDF

$$P_r(a_n) = \begin{cases} p & a = 1 \\ 1-p & a = -1 \end{cases} \quad \text{Equation 2-18}$$

The correlation function will be as follow.

$$R_a(l) = \begin{cases} 1 & l = 0 \\ (2p-1)^2 & l \neq 0 \end{cases} \quad \text{Equation 2-19}$$

The continuous component and discrete component of the PSD will be

$$S^c(f)=\frac{1}{T_c}|W(f)|^2\left[1-(2p-1)^2\right] \quad \text{Equation 2-20}$$

$$S^d(f)=\frac{1}{T_c^2}\sum_{l=-\infty}^{\infty}|W(f)|^2(2p-1)^2\delta\left(f-\frac{l}{T_c}\right) \quad \text{Equation 2-21}$$

Both of these two parts are shaped by the PSD of the single pulse; the distribution of a_n affects the amplitude of them.

In the simulation in Figure 2-6, the number of 1s and 0s in the bit sequence is almost equal, which means in this model $p=0.5$. When $p=0.5$ we have

$$S^c(f)=\frac{1}{T_c}|W(f)|^2 \quad \text{Equation 2-22}$$

$$S^d(f)=0 \quad \text{Equation 2-23}$$

The discrete component of the PSD is vanished and the continuous component is equal to the PSD of a single pulse. In Figure 2-6 the PSD of the 2PAM-DS signal has very low discrete component and the shape of the PSD is the same with the PSD of single pulse. The simulation result confirms with the analysis result except that the simulation result still contains discrete component; this is because the bit sequence in the simulation is sequence of DS codes and is not exactly i.i.d distributed.

PSM

In the PSM scheme, the bit sequence $\{a_n\}$ is modelled as i.i.d digital sequence with PDF

$$P_r(a_n)=\begin{cases} p & a=1 \\ (1-p) & a=0 \end{cases} \quad \text{Equation 2-24}$$

The correlation function will be

$$R_a(l)=\begin{cases} p & l=0 \\ p^2 & l\neq 0 \end{cases} \quad \text{Equation 2-25}$$

The continuous component and discrete component of the PSD will be

$$S^c(f) = \frac{1}{T_c}\left|W(f)\right|^2 p(1-p) \qquad \text{Equation 2-26}$$

$$S^d(f) = \frac{1}{T_c^2}\sum_{l=-\infty}^{\infty}\left|W(f)\right|^2 p^2\delta\left(f - \frac{l}{T_c}\right) \qquad \text{Equation 2-27}$$

When $p = 0.5$

$$S^c(f) = \frac{1}{T_c}\left|W(f)\right|^2 \cdot \frac{1}{4} \qquad \text{Equation 2-28}$$

$$S^d(f) = \frac{1}{T_c^2}\sum_{l=-\infty}^{\infty}\left|W(f)\right|^2 \cdot \frac{1}{4}\cdot\delta\left(f - \frac{l}{T_c}\right) \qquad \text{Equation 2-29}$$

In Figure 2-4 we can see that the PSD of the PSM signal contains both continuous and discrete component; the discrete components, i.e. the spectral lines are very high. This confirms with the analysis results of Equation 2-28 and Equation 2-29. The analyses until here explain why with the same transmitted power per pulse, the 2PAM-DS contains much lower spectral lines than the PSM scheme does and thus has a lower PSD.

Biphasic toggled PSM

In the biphasic toggled PSM scheme, the bit sequence $\{a_n\}$ is modelled as i.i.d digital sequence with PDF

$$P_r(a_n) = \begin{cases} p_1 & a = 1 \\ p_2 & a = -1 \\ 1-(p_1+p_2) & a = 0 \end{cases} \qquad \text{Equation 2-30}$$

The correlation function will be

$$R_a(l) = \begin{cases} p_1 + p_2 & l = 0 \\ (p_1 - p_2)^2 & l \neq 0 \end{cases} \qquad \text{Equation 2-31}$$

The continuous component and discrete component of the PSD will be

$$S^c(f) = \frac{1}{T_c}|W(f)|^2\left[(p_1+p_2)-(p_1-p_2)^2\right] \qquad \text{Equation 2-32}$$

$$S^d(f) = \frac{1}{T_c^2}\sum_{l=-\infty}^{\infty}|W(f)|^2(p_1-p_2)^2\,\delta\left(f-\frac{l}{T_c}\right) \qquad \text{Equation 2-33}$$

In the simulation in subsection 2.3.2 Figure 2-8, the bit sequence is toggled in the way that every other '1' bit is toggled to '-1'. Therefore in this simulation we have $p_1 + p_2 = p$ (p is the same as in the previous analyses) and $p_1 = p_2 = \frac{1}{4}$. In this case,

$$S^c(f) = \frac{1}{T_c}|W(f)|^2\ p = \frac{1}{T_c}|W(f)|^2 \cdot \frac{1}{2} \qquad \text{Equation 2-34}$$

$$S^d(f) = 0 \qquad \text{Equation 2-35}$$

By toggling the bit sequence, the discrete component of the PSD is vanished. Compare Equation 2-34 with Equation 2-22, and we can see that the continuous component of the biphasic toggled PSM is 3dB lower than scheme the continuous component of the 2PAM-DS scheme. Compare Figure 2-6 and Figure 2-8 we can see that, both these two figures contains very low discrete components, and the PSD in Figure 2-8 is about 2dB lower than the PSD in Figure 2-6. The analysis results qualitatively confirm with the analysis results. The difference between these two is because the bit sequences in the 2PAM-DS and the biphasic toggled PSM scheme are not exactly i.i.d distributed sequence.

Summary

In this subsection we analysis the PSD of different modulation and multiple access schemes by modelling the bit sequence as i.i.d distributed uncorrelated digital sequence and the time offset as uniform distributed time jitter. By comparing the analytic expressions are achieved and they explain why the 2PAM-DS scheme has a large PSD margin compared with the PSM scheme, and why the biphasic toggled PSM can achieve a even larger margin than the 2PAM-DS scheme. The analyses confirm with the simulation results.

2.4. Transmitter

In the light of previous discussed pulse shape, modulation, multiple-access, and toggling scheme, our transmitter structure is as shown in Figure 2-1Figure 2-9.

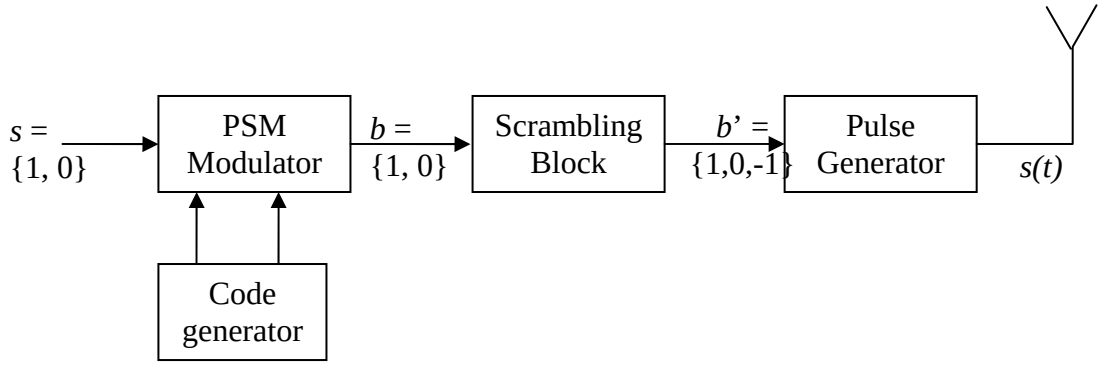

Figure 2-9 Transmitter block diagram

3. Channel Model

A channel model describes how a received signal will be different from the sent signal in a communication system. In a wireless communication system, a radio signal sent from the transmitter to the receiver may experience attenuation, reflection, diffraction, penetration and other effects that may change the signal both in time domain and in frequency domain. The channel is mainly catalogued into two, one is the Line of Sight (LOS) channel, which means the receiver can be seen from the transmitter directly and no object stand in the way, the other is the Non Line of Sight (NLOS) channel, which is just opposite, the receiver cannot be seen from the transmitter directly. The effects that the sent signal may experience in the channel are usually catalogued into two, large-scale effects and small-scale effects.

The specialities of UWB channel will bring new challenges and possibilities to the design of UWB PHY. In this chapter we will discuss the speciality of UWB channels, and introduce the IEEE channel model [IECM 2003]. The simulations in this thesis are done with this channel model.

3.1. Speciality of UWB channels and impacts on receiver design

What makes UWB channel model different from the conventional wireless communication channel model is its ultra wide bandwidth. According to [Jeff 2005], traditional channel models for path loss assume that diffraction coefficients, attenuation due to materials, and other propagation effects are constant over the band of interest. Additionally, narrowband models often incorporate antenna effects, such as the effective aperture, into the path loss, since the change in these antenna effects is negligible over the band. However, neither of these two assumptions is valid for UWB signals.

According to [Jeff 2005], there are also small-scale assumptions that may not hold for UWB systems. Narrowband and even wideband channel modes assume that the received signal is the sum of delayed, phase shifted and attenuated copies of the received signal. The interaction of these multiple signals results in fading and frequency distortion. However, it assumed that the individual copies are not distorted. For UWB signals, individual components of the received signal may be distorted, thus introducing pulse-level frequency distortion in addition to the distortion seen in the total received signal.

Channel model is important for the design of a communication system. It is important for design of the receiver structure, and also important for evaluating the performance of a design. The special properties of UWB channel decide that the UWB receiver will be different from the conventional counterparts. The multi-path effect of the UWB channel make RAKE receiver an attractive candidate for UWB system. But a RAKE receiver requires complicate synchronization and is not suitable for our requirement as simple and power effective receiver structure. In chapter 4 we introduce a spatial full RAKE receiver which requires no synchronization and has relatively simple hardware implementation.

3.2. The channel impulse response model

The most commonly used method for UWB channel model is to model the channel as a channel impulse response model, or Channel Impulse Response (CIR). In a CIR, each impulse represents one amplitude-scaled, time-delayed and phase-shifted multi-path component. The UWB channel is often modelled as time-variant because the transmitter or receiver or other objects surrounding may move during the transmission. The expression of a UWB CIR often looks like this: $h(t,\tau)$. The received signal can be expressed as follow:

$$r(t) = s(t) * h(t,\tau) + n(t), \quad \text{Equation 3-1}$$

Here, $s(t)$ represents the sent signal and $r(t)$ represents the received signal, $h(t,\tau)$ represents the time-varying CIR of the channel and $n(t)$ is AWGN.

$$h(t,\tau) = \sum_{k=0}^{N(t)-1} \beta_k(t) p_k(t) \delta(\tau - \tau_k(t)) \qquad \text{Equation 3-2}$$

Here, $\beta_k(t)$, $\tau_k(t)$ and $p_k(t)$ are the time-varying amplitude, delay and polarity of the k^{th} path respectively. The model here is a dynamic channel model, which means the CIR of the channel is changing from time to time. This is because in a realistic transmission channel, the distance between the transmitter and the receiver may change and the obstructive objects between them may move so that the multipath condition in this channel may change from time to time.

In this thesis, we use dynamic channel model but we assume that the channel is static during at least one data symbol. This means that we consider the channel will change from time to time but within the time duration of one data symbol, the channel condition will be the same. For chip duration of 30ns and a symbol length of 60, one data symbol will be 1.8us long and it is realistic to assume a static channel in such short time duration. The CIR in this case can be written as

$$h(t) = \sum_{k=0}^{N-1} \beta_k p_k \delta(t - \tau_k) \qquad \text{Equation 3-3}$$

And the received signal can be expressed as

$$r(t) = s(t) * h(t) + n(t) \qquad \text{Equation 3-4}$$

We can see from a simple calculation that the assumption of static channel model in one data burst is reasonable. Say we have a data burst of 100 Byte. We have our PSM codes of length 31, and we have chip duration of 30ns, then the length of this data burst is 0.744ms. It is acceptable to assume that the transmitter and receiver and other objects around them or in between them are static within this time.

The statistical channel models provide the statistics of the amplitude, phase and the arrival time-delay in a CIR and can be used to generate CIR in a simulation.

There are several channel models proposed that describe the large scale statistics of the UWB channels, like the $\Delta - K$ model and the Saleh-Valenzuela (S-V) Model. The IEEE channel model is a model based on a cluster approach and on S-V model. This model is used by the IEEE 802.15.3a group to estimate the performance of the proposed PHY design, so we also use this model in the simulation of our PHY. As we can understand, it will be difficult to model all the possible channel environments and characteristics, the IEEE model try to model the Root Mean Square (RMS) delay spread, the power delay profile and the

number of multi-path components of the UWB channel. They are large scale parameters.

As for small scale effects of the UWB model, we have not seen reports on the statistics of the pulse-level distortion, or any channel model that deal with the pulse-level distortion of the UWB channels when I started the work of this thesis. There is an algorithm named CLEAN that can extract the CIR from individual measurements. This algorithm is first introduced in 1974 and well-established in the radio astronomy and microwave communities, and now is often applied to UWB measurements [Jeff 2005]. Apart from extract the CIR to represent the large scale of the channel model, this algorithm can also extract CIR to simulate the pulse distortion. It generates multiple impulses, or taps as mentioned in other literature, to represent the distorted pulse. It behaves like an FIR filter to approximate the frequency distortion of the pulse [Jeff 2005]. With this algorithm, both the large scale and small scale effects of the UWB channel can be extracted and well modelled from measurements, in the form of CIR. In conclusion, pulse-level distortion modelling of the UWB channel needs to be exploited more and is out of the scope of this thesis.

In [AICT 2006], a statistical UWB channel model based on physical analysis is presented. This model is said to be more realistic than the IEEE UWB model because it models the reflection and diffraction mechanism of the channel and therefore models part of the pulse distortion.

3.3. IEEE Channel model

The IEEE channel model describes the statistics of the parameters in Equation 4-3. These are quite complicated descriptions with a lot of stochastic parameters and we have no need to list them here. Details can be found in [IECM 2003].One thing to mention is that, the IEEE channel suggest for type of channel conditions, with different parameter settings. The four type of channels respectively:

CM1: LOS channel, Transmitter-Receiver (TR) distance 0-4m.
CM2: NLOS channel, TR distance 0-4m.
CM3: NLOS channel, TR distance 4-10m.
CM4: Extreme NLOS multi-path channel.

These four types of channel conditions display different characteristics, for example, RMS delay spread, and different PHY layer parameters, for example the length of time interval between two pulses, can be set for them to avoid Inter-

Chip-Interference (ICI). This type of interference is often referred to as Inter-Symbol-Interference (ISI), in conventional systems and also some of the other literatures on UWB systems. However, in this thesis, the term 'symbol' is used to denote the information symbol to be conveyed by the PHY, so we avoid using it here. Instead, in this thesis we call the time interval to transmit a pulse a chip, and therefore we call the interference between multi-path components of two pulses ICI.

The RMS delay spread can be derived from the Equation 4-3

$$\tau_{RMS} = \sqrt{\frac{\sum_k \beta_k^2 \tau_k^2}{\sum_k \beta_k^2} - \tau_m^2} \qquad \text{Equation 3-5}$$

Here, τ_m is called excess delay.

$$\tau_m = \frac{\sum_k \beta_k^2 \tau_k}{\sum_k \beta_k^2} \qquad \text{Equation 3-6}$$

These two parameters describe how long time the multi-path components may spread over time after one pulse sent. This is important for making sure that the accountable multi-path components, less than10dB lower than the main path component, do not arrive after the first component of the next pulse arrives, in another word, to avoid inter chip interference.

The IEEE channel model gives the excess delay and RMS delay spread of the four channel models, listed in the following table.

	CM1	CM2	CM3	CM4
τ_m [ns]	5.05	10.38	14.18	
τ_{RMS} [ns]	5.28	8.03	14.28	25

Table 3-1 Mean excess delay and RMS delay spread of the four type channels in IEEE channel model

An example of CM3 type channel is shown in Figure 3-1. From this example we can see that, the RMS delay spread (RMS DS) does not means that no components will arrive after this time. It just means how the sent energy is spread over time. Therefore, to set the chip duration as the RMS DS of a channel cannot

make sure the avoidance of ICI. On the other hand, the measure of avoiding ICI in a transmission is not just literal, that no components arrive in the next chip, but also how severely this will affect the pulse detection. However, what we really care is not just the ICI, but the system performance. And the performance on the chip level shall be measured by the detection Chip Error Rate (CER). Therefore, we will discuss the relation between ICI and RMS DS of a channel in detail after we describe our receiver and our pulse detection method Statistic Pulse Detection (SPD).

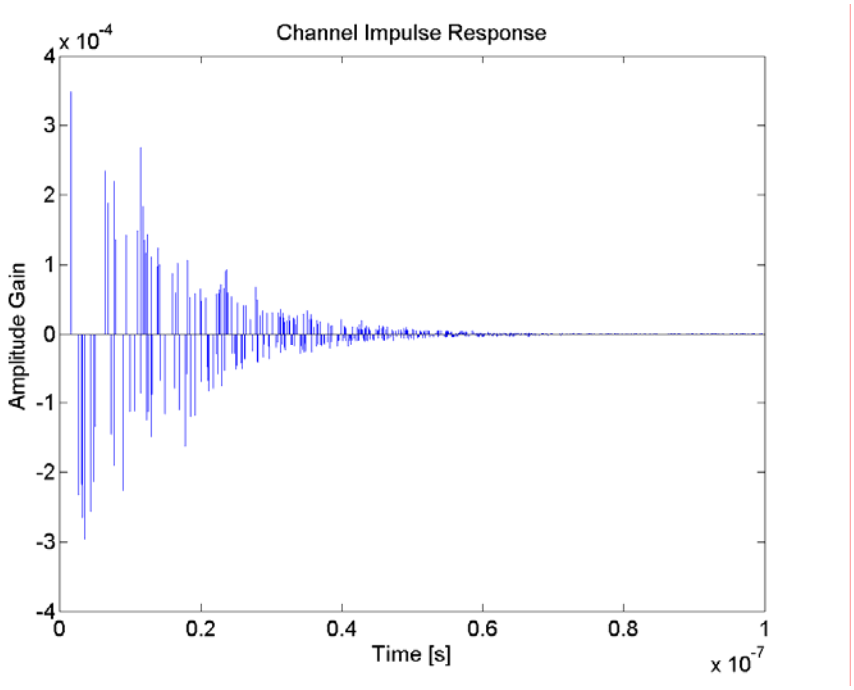

Figure 3-1 An example of CM3 type channel

4. Receiver

The structure of the spatial Full RAKE Receiver is as shown in Figure 4-1. It comprises of two parts: the statistic pulse detector, and the full RAKE symbol detector. Compared with others used in UWB system, this receiver has several appealing properties. First, it does not demand a high speed clock and a huge amount of signal processing as others do. Second, it needs no synchronization with the transmitter. Synchronization is a very significant issue for UWB receivers; given the ultra short UWB pulse on the level of nanosecond, the synchronization requires very high speed and very high accuracy of tracking the received pulse and adjusting the local clock. Third, it is a RAKE receiver and can take advantage of the unique high multipath resolution of the UWB signal and utilize time diversity to counteract the multipath fading. These advantages will be discussed in section 4.1

The function of the statistic pulse detector is to detect pulses, including multipath components, in the received signal *r(t)*. This detector is a hybrid circuit: its input *r(t)* is a pure analogue signal, but it processes and output continuous-time signals with digital value. The output signal *q(t)* is a continuous-time square wave signal with binary value, and each square wave represent one detected pulse. The statistic pulse detector will be discussed in section 4.2.

The full Rake symbol detector collects the energy of all the pulses detected by the statistic pulse detector, or in another word, it collects energy from all the detectable multipath components. Therefore it is call a full RAKE. This will be further discussed in section 4.3

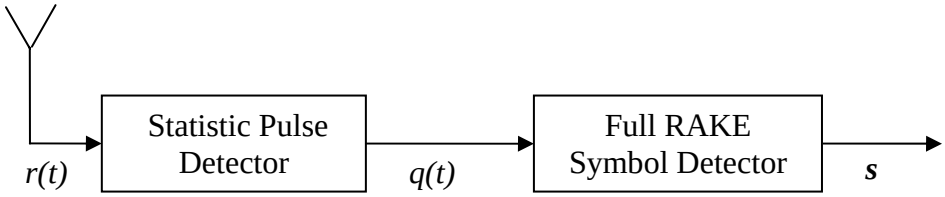

Figure 4-1 Spatial RAKE receiver

4.1. Advantages

The receiver shown above has the following advantages.

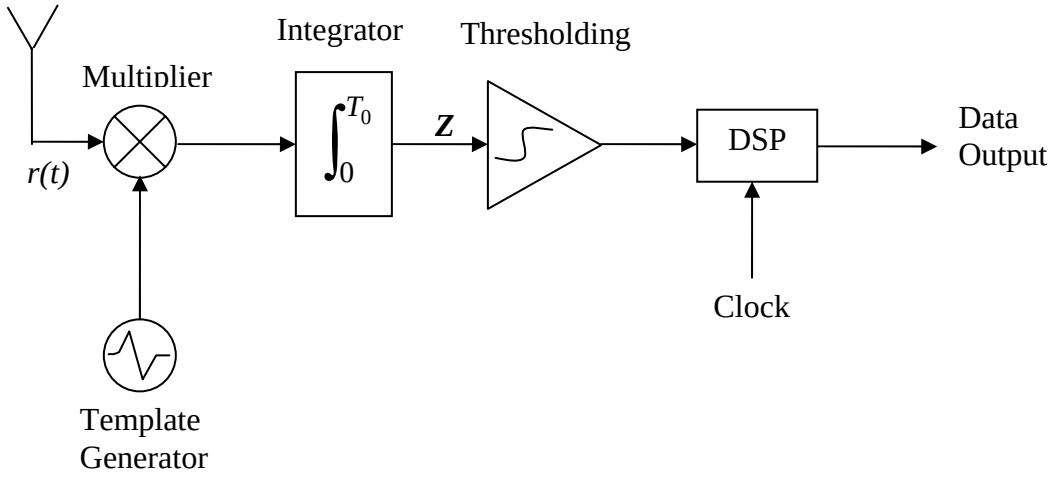

Figure 4-2 A basic correlation receiver

Signal processing issue
The most often used radio receiver is a DSP based correlation receiver; the concept is shown in Figure 4-2. It correlate the received signal *r(t)* with a template wave form *T(t)* and make a decision on the correlation result. The template waveform *T(t)* is decided by the modulation and demodulation scheme; usually it is a linear combination of the transmitted symbol. Figure 4-2 shows the algorithm

of this receiver, in real implementation the multiplying and integration operation, as well as the template generation are all in digital form and are performed by the DSP.

$$Z = \int r(t) * T(t)\, dt \qquad \text{Equation 4-1}$$

The design of correlating template and the method of arbitrating of the correlation receiver is not relevant and we will not discuss this further. Generally, this type of receiver requires high frequency clock and need to process a huge amount of data. According to the Nyquist-Shannom sampling theorem, the sampling rate f_s and the bandwidth of the signal should have such relation:

$$f_s > 2B \qquad \text{Equation 4-2}$$

For UWB signal with bandwidth of 7.5GHz, the base band sampling and processing frequency will be to 15GHz. Assuming a 6bit digital representation of each sampling in the ADC, the receiver needs to process a data stream of 90Gbps, which demands large memory and fast data processing. In ordinary RAKE receiver, the correlating operation also exists and the data processing is even more complex than the correlation receiver. This will be seen later in this section.

In the spatial RAKE receiver, the statistic pulse detector converts the analogue received signal to continuous time binary signal, so functionally it is a 1bit continuous time ADC. The clock frequency in this receiver is the chip frequency. Say that we have chip duration of 30ns, the clock frequency is 33MHz and the data processing requirement is 33Mbps. We also have correlation operation in this receiver, both in the Statistic pulse detector and the Full RAKE symbol detector, but our correlation operations are between binary or antipodal signals; these correlation operations are simple and can be implemented by ‘AND’ and ‘OR’ gates.

Synchronization issue

For both the basic correlation receiver and the ordinary RAKE receiver, timing and synchronization are extremely important. Timing offset will leads to mismatch between the received signal with the correlation template and dramatic drop in the Signal Noise Ratio (SNR). In addition to maintaining precise timing at the receiver, acquiring and synchronizing with the transmitted signal is extremely essential to UWB systems using timing information in modulation and multiple access purpose, namely PPM modulation and TH multiple access. The spatial

RAKE receiver needs no synchronization with the transmitted signal. This will be further discussed in section 4.3.

Immunity to near-far problem

In a wireless communication system with correlation receivers, a very common problem is the near-far problem. Consider such a scenario: two transmitters are transmitting simultaneously with the same transmitting power and a receiver is to receive signal from one of them. If the target transmitter stands further from the receiver than the interfering transmitter does, the signal arrived at the receiver from the interfering transmitter will be stronger than that of the target transmitter. This will bring high Signal Interference/Noise Ratio (SINR) and degradation of the detection performance. To some extent it will make the target signal impossible to be detected. This is called near-far problem.

In a cellular system like CDMA, the dynamic Automatic Power Control (APC) is implemented at the base station, to control the transmitting power dynamically so that when the signals of different users arrive at an end user receiver will be at the same power level. The APC involves complex algorithm, hardware and large communication overhead to the system; and this is why the APC is implemented only on the base station but never on an end user device.

The spatial full RAKE receiver is immune to near-far problem, no power control mechanism is needed in this system. This immunity comes from the statistic pulse detector. Different from the correlation receivers, the statistic pulse detector does not perform correlation operation directly on the received analogue signal. It first converts the received signal to a 3-valued {-1 0 1} continuous time digital signal, and then correlates. This threshold is set according to the noise level. It detects a pulse by detecting a pattern of positive/negative slope pattern, and this pattern is decided only by the time domain shape factor of the pulse but not by the amplitude of the pulse. In the scenario described in last paragraph, although a nearer interfering transmitter leads to interfering signal at the receiver with larger amplitude, the time domain pulse pattern will be the same no matter where the interfering transmitter stands; this will not brings higher interference to the system. In conclusion, with the statistic pulse detection, the system faces no near-far problem.

RAKE

The concept of RAKE receiver, as shown in figure 4-3, is to collect energy from the multiple signal replicas which propagate and arrive at the receiver by multiple signal paths. This is an approach to counteract multipath fading with temporal

diversity. In most of the conventional narrowband communication systems, the multipath components in the received signal are overlapping and cannot be distinguished from each other. A RAKE receiver cannot be used in such situation. For an indoor IR-UWB system, due to the ultra-short duration of the transmission pulse and the complex indoor propagating environment, there are rich distinguishable multipath components in the received signal. This has been discussed in Chapter 3.

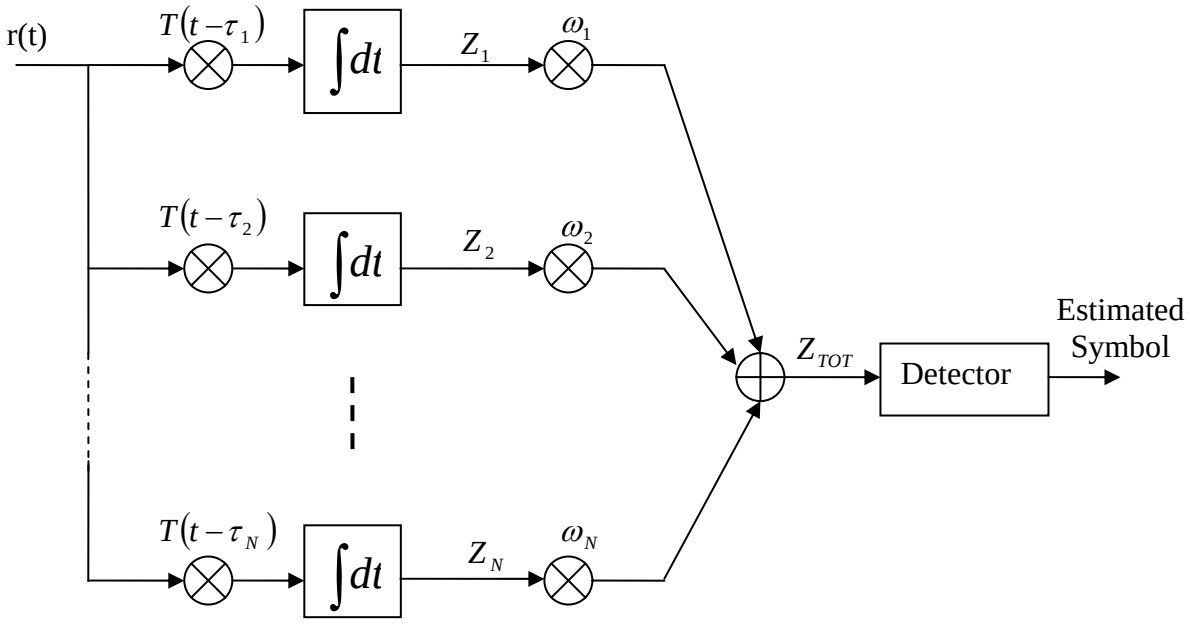

Figure 4-3 RAKE receiver

In a RAKE receiver, the received signal is correlated with time-shifted template waveform $T(t-\tau_j)$, j=1,2,…N, where N is the number of distinguishable and detectable multipath components and τ_j is the relevant arriving time difference of them. Each path is given a weight ω_j, j=1,2,…N. By setting different weight, different strategies for combining the multipath signals can be achieved. The N brunches of correlation is referred as ‘fingers’.

There are mainly three type of combination strategy. For in a Selection Diversity (SD) RAKE, the receiver tracks different signal paths, finding the strongest one,

and using this path for symbol estimation by setting the weight of this path as 1 but all the others as 0. For an Equal Gain Combining (EGC), all the detected paths are combined with all the weights are set the same. For a Maximal Ratio Combining (MRC), all the detected paths are taking account into the estimation, and the path weights are set proportional to signal strength of the paths. There is a partial RAKE, which stands in between of these two. Another way of cataloguing RAKE receiver is by how many multiple paths they combine. A Full Rake combines all the detectable signal paths and a partial RAKE takes only some of them.

Generally speaking, the main concerns of RAKE receiver are:

- Channel estimation. RAKE receiver needs to have knowledge of channel, specifically the number of multiple paths, the attenuation of the paths, and the arriving time. With this knowledge the receiver can set the time shift τ of the correlation template waveform for the fingers and the combination weights ω.
- Timing and synchronization: the reasons stated in previous section why timing and synchronization is important for basic correlation receiver are also applicable here. One thing worth mentioning here is each finger in the RAKE needs its own synchronization with the signal path it is tracking.
- Combining algorithm: combining algorithm refers to how the finger weights are set according to the result of channel estimation. Note that the UWB channels are time variant. This means The channel estimation needs to repeat from time to time and the weights of the fingers need to be adjusted dynamically (except for the EGC RAKE)

Up to now we can see that, the ordinary RAKE receivers impose very high requirement on hardware and are expensive to implement.

The Full RAKE symbol detector in the statistic RAKE receiver shares the same concept of collecting energy in multiple signal paths and exploring temporal diversity to counteract multipath fading. But the implementation is different. This RAKE structure is a full RAKE with EGC combination strategy: it combines all the detectable signal paths with the same weights. No channel estimation is needed since this receiver needs no synchronization. All the RAKE fingers in this receiver will share the same clock of the frequency equal to chip rate. The combining algorithm is an EGC algorithm.

4.2. Statistic Pulse Detection

The statistic pulse detector detects pulses in the received signal, no matter they are LOS received signal or multipath replicas. The received pulses are transformed into a binary square wave signal, and the width of the square wave is the same as the length of the pulse. The structure of the statistic pulse detector is shown in figure 4-4. It comprises of three parts: thresholding, statistic correlating and pulse stretching. This detector processing digital valued signal but is continuous time.

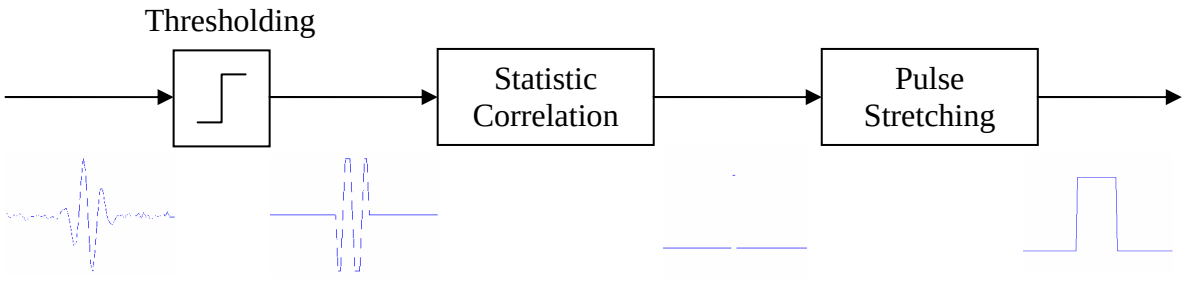

Figure 4-4 Statistic Pulse Detector

4.2.1. Function and implementation

Thresholding circuit
The threshold circuit converts the received signal *r(t)* to a digital-valued continuous signal *square(t)*, with the value of { 1, 0, -1}. This is done by compare the signal with a positive threshold and a negative threshold. The threshold circuit can be seen as a 2bit ADC.

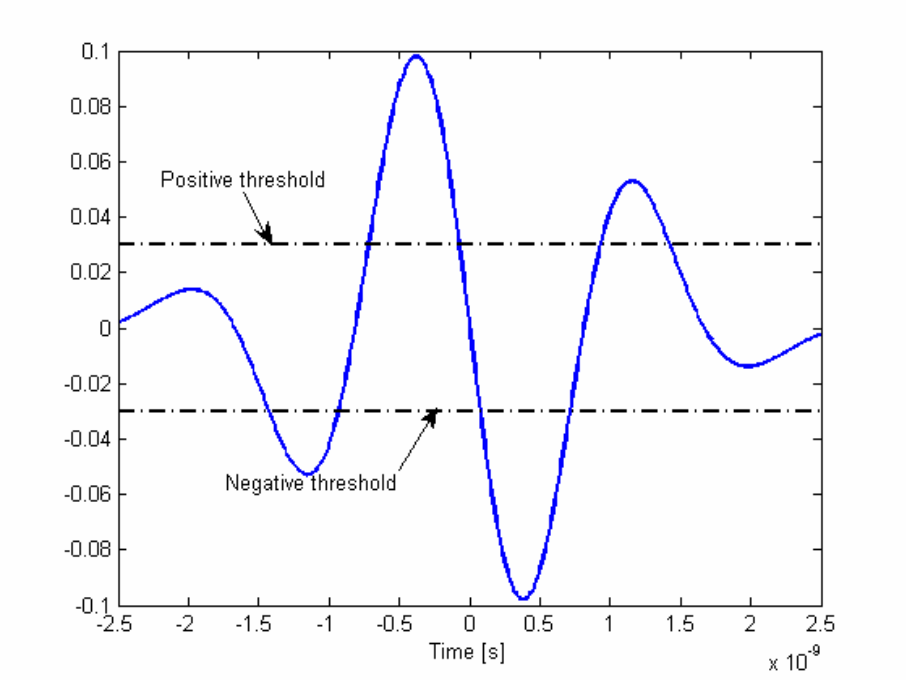

Figure 4-5 Pulse Thresholding

Statistic correlation

The statistic correlation circuit matches the square signal with a template, as shown in Figure 4-6. For a given pulse shape, the thresholded waveform shall be determined as shown in figure 4-4, the square wave form between the thresholding block and the statistic correlation block. In a conventional correlator, this wave form shall be used as the correlation template and be multiplied with the received signal and then integration.

However, in this block we let the signal propagate through several delay blocks, the amount of time delay of each block is the same as the width of the width of the slope in the transmitted pulse. The delay line here serves to convert a signal of certain time duration at one spatial point to a signal spread over several spatial points at one time. This is actually a time-space transformation. Here the delay line spread the time signal at four physical points, and actually functions as a sampling circuit of the square wave, but without a clock.

The four samples are multiplied with the template and than added together, and than go to the arbitrator. The Arbitrator is again thresholding the output of the adder Zi(t). When Zi(t) is larger than a arbitrating constant Zt. The output of the arbitrator spike(t) is a binary value continuous time signal. When a thresholded

pulse in the signal square(t) is propagating through the delay line, when and only when the four slopes stand in between delay blocks, the output of the adder Zi(t) will be at its biggest value and the spike(t) would be on its high level. This will not last longer than the time width of a slope so the spike(t) signal will look like spikes, as shown in figure 4-4.

Different pulse shape may use different length of delay line have different template to match. For the 7th Gaussian derivative pulse we are using, the template is a 4bit scalar [-1 +1 -1 +1]. For pulses of higher order, the template can be longer. The multiply-and-add function is actually a correlating function. But these operations are very easy to be implemented with combinational logic gates like inverter, AND, XOR and so on.

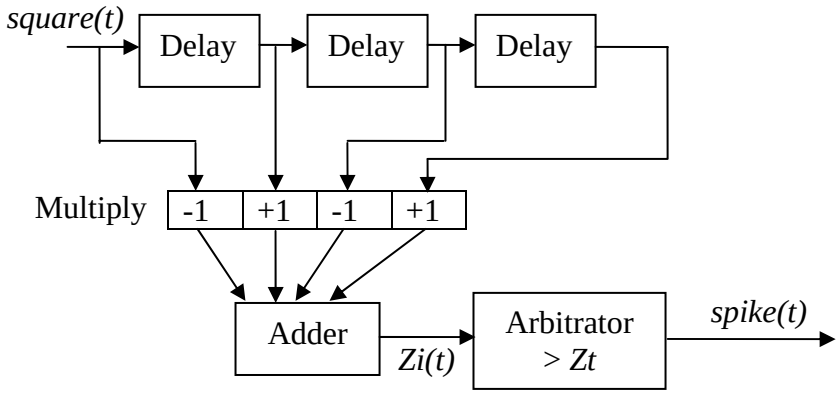

Figure 4-6 Statistic correlation circuit for pulse detection

Now we explain the statistic property of this detector. In chapter 4 we have described that the UWB channels are noisy and with multipath effect. Some received pulses can be quite weak, and when they are in a AWGN back ground of a certain level, it is quite possible that the pulses are distorted and the slopes are missing. When a pulse is detected, all the slopes are matched to the template and *Zi* will have a value of 4. But if one finger of the pulse is disappeared, *Zi* will be 3. The statistic correlator set the arbitrating constant Zt to be 3, so that even one slope of the pulse is missing, the pulse is still claimed. However, we should be aware that this can be a false alarm, which means, there is no pulse but the detector claimed a pulse. To think further on this direction, from figure 4-5 we can see that, the two slopes in the middle of the pulse wave form are stronger than the

other two. And statistically these two slopes are less possible missing. We can use this knowledge in the arbitrating: to claim a pulse when a middle slope is missing is more possible to be a false alarm than to claim a pulse when an outside slope is missing.

To give the pulse different weight, we can set our matching template as [-1 +2 -2 +1]. By doing this we give the two fingers in the middle double weight than the outside two. If we set $Zi = 5$, this means that the missing of one of the outside slope is acceptable but the missing of one of the middle slope is not.

Pulse stretcher
Stretch the spike signal to form a binary square wave, the width of the square wave is the same as the length of a pulse.

4.2.2. Pulse detection thresholding

In this subsection we discuss the setting of the pulse detection threshold. The purpose of the thresholding here is to detect the slopes of the pulse wave form we are looking for in the received signal. The received UWB signal experienced multi-path fading and AWGN. It contains multi-path components (each has its own time-delay, phase-shift (0 or180 degree) and amplitude attenuation), the background radio noise due to the indoor environment and the receiver thermal noise. The multi-path effect will be taken care of by the RAKE structure in the full RAKE symbol detector. Here we model the background radio noise due to the complicated indoor environment and the receiver thermal nose as AWGN.

A straightforward way is to set the threshold according to the height of the slopes we intend to detect, and the AWGN noise level. For example, assume that we know the expected slope has a peak value of a, and with a probability of 99.9%, the noise value falls into the range of $[-b, \infty]$. Then we can set our threshold at $t = a - b$. The probability that this slope can be detected is the same as that of the sum of the signal and noise falling into the range of $[t, \infty]$; this probability is also 99.9%.

One problem here is we do not know the level of the pulses we are expecting. It is difficult to assess the amplitude of the pulses that arrive at the receiver in the multi-path environment: the amplitude attenuation is unpredictable to the receiver unless it has a channel-estimating scheme. Channel-estimation is a scheme that

estimates the attenuation, time-delay and phase-shift effect of the channel. By providing this knowledge it helps the receiver to make better decision when detecting symbols from the received signal. However, channel-estimation bring large amount of signal processing requirement and costs a lot with respect to power consumption and hardware. In our power efficient, low cost system, we will not include this function.

Our solution is to set the threshold slightly higher than the noise level. We are aware that the received signal can be very weak and some of the pulses can be buried in the AWGN noise. Although we have no idea of how high the received slopes will be, we can make sure that they will be detected with a certain probability. We will explain this in the following discussion.

The AWGN is a zero-mean statistic variable with a PDF as follow:

$$P(noise = x) = W_N(x) = \frac{1}{\sigma\sqrt{2\pi}} \exp\left(-\frac{x^2}{2\sigma^2}\right) \qquad \text{Equation 4-3}$$

Where x is the noise voltage and σ is the standard derivation, or the average noise density. We can not predict the noise voltage at a certain time, but we predict the probability that the noise is higher than a certain level at a certain time.

$$P(x \geq b) = \int_{-\infty}^{b} W_N(x)dx = \int_{-\infty}^{0} W_N(x) + \int_{0}^{b} W_N(x) = \frac{1}{2}\left(1 + erf\left(\frac{b}{\sigma\sqrt{2}}\right)\right) \qquad \text{Equation 4-4}$$

Where $erf(x) = \frac{2}{\sqrt{\pi}} \int_0^x \exp(-t^2)dt$

Since signal value is a decide value and the noise value is an additive statistic value, the sum of the two should be a statistic value too, with the PDF function as follow.

$$P(signal + noise = x) = W_{S+N}(x) = \frac{1}{\sigma\sqrt{2\pi}} \exp\left(-\frac{(x-a)^2}{2\sigma^2}\right) \qquad \text{Equation 4-5}$$

The following figures show an example of the signal and noise level and their PDF function. We use a 5th Gaussian derivative pulse as an example. The discussion in this subsection also holds for other pulse. For the convenience of

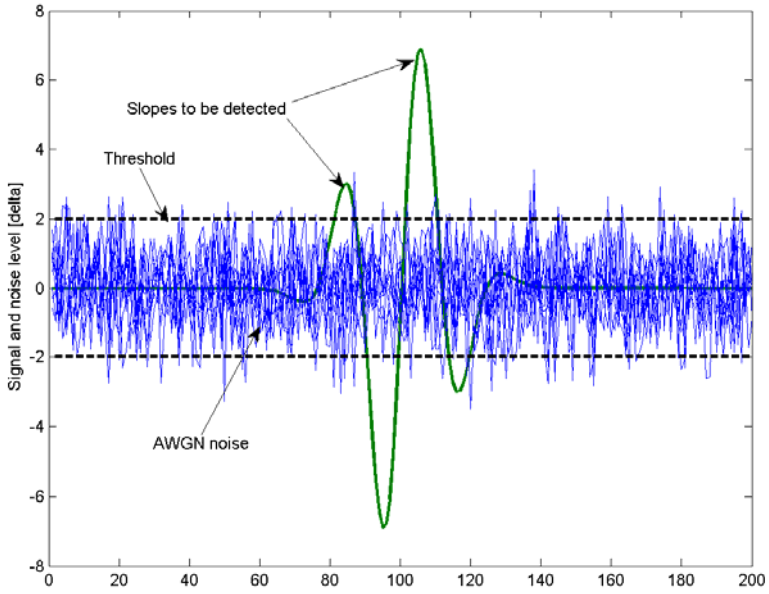

Figure 4-7 Signal and AWGN noise

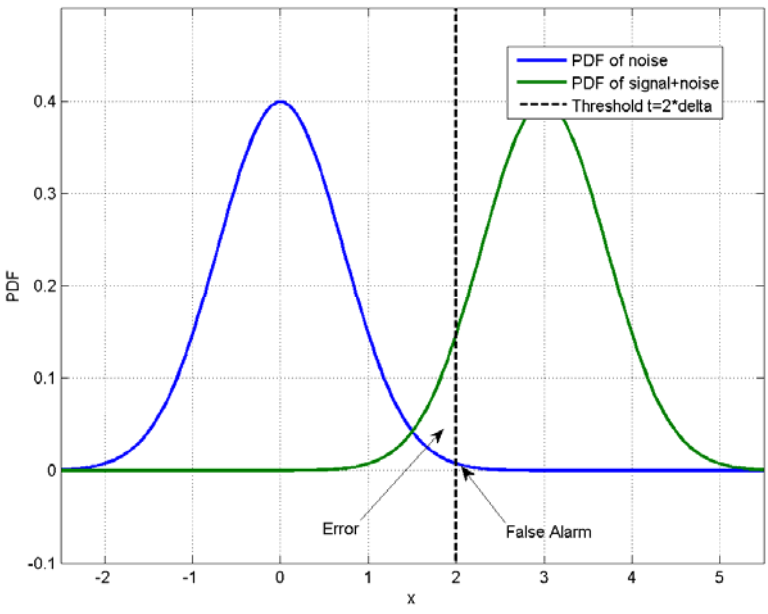

Figure 4-8 PDF functions of the signal and noise

discussion, we normalize the standard derivation of the AWGN noise $\sigma = 1$, and we consider the detection of the positive slopes only. The situation of detection of the negative slopes is the same. Assume that we have a weak pulse, with the height of the lower slope equal to 3σ. And we set our detection threshold $t = 2\sigma$. In Figure 4-7 can see that the lower slope is almost buried by the noise. The height of the higher slope here is 6.9σ.

Here we introduce several useful terms and their notations.

- P_D, detection probability, the probability that there is a slope and it is successfully detected,

  $$P_D = P(signal + noise \geq threshold) = \int_{-\infty}^{t} W_{S+N}(x)dx = \frac{1}{2}\left(1 + erf\left(\frac{a-t}{\sigma\sqrt{2}}\right)\right)$$

- P_e, error probability, the probability that there is a slope but it is not detected, $P_e = P(signal + noise < threshold)$, $P_D + P_e = 1$,
- P_{fa}, false alarm probability, the probability that there is no slope in the signal but one slope is claimed,

  $$P_{fa} = P(noise \geq threshold) = \int_{t}^{\infty} W_N(x)dx = 1 - \int_{-\infty}^{t} W_N(x)dx = 1 - \frac{1}{2}\left(1 + erf\left(\frac{t}{\sigma\sqrt{2}}\right)\right)$$

  $$= \frac{1}{2} erfc\left(\frac{t}{\sigma\sqrt{2}}\right)$$

Given the PDF of the noise and the signal+noise, we have the height of the lower slope $a = 3\sigma$, the height of the higher slope $a = 3\sigma$, and threshold $t = \sigma$.

Detection probability of the lower slope: $P_{D-lower} = \frac{1}{2}\left(1 + erf\left(\frac{2}{\sqrt{2}}\right)\right) = 0.9772$

Detection probability of the higher slope: $P_{D-higher} = \frac{1}{2}\left(1 + erf\left(\frac{5.9}{\sqrt{2}}\right)\right) \approx 1$

Error probability of the lower slope: $P_{e-lower} = 1 - P_{D-lower} = 0.0223$

Error probability of the higher slope: $P_{e-higher} = 1 - P_{D-jigher} \approx 0$

False alarm probability: $P_{fa-slope} = \frac{1}{2} erfc\left(\frac{1}{\sqrt{2}}\right) = 0.1587$

In the statistic pulse detection scheme, when we use a template [-1 1 -1 1] and an arbitrating constant Zt=4, we have

Detection probability of the pulse:
$P_{D-pulse} = P_{D-lower} * P_{D-higher} * P_{D-lower} * P_{D-higher} = 95.45\%$

False alarm probability: $P_{fa-pulse} = P_{fa-slope}^4 = 0.063\%$

When we use a template [-1 2 -2 1] and an arbitrating constant Zt=5, we have
$P_{D-pulse} = 1-(2P_{e-lower} + P_{e-lower}^2)/3 = 97\%$
$P_{fa-pulse} = P_{fa-slope}^3 = 0.4\%$

From these calculations we can see that, $P_{D-poulse}$ is decided by the signal level, the threshold, and the detection setting (template and Zt), while $P_{fa-pulse}$ is decided by the threshold and the detection setting. There is a trade-off between the pulse detection probability and the pulse false alarm probability. By setting a softer detection setting, a better detection probability is achieved, but we also have a higher probability of false-alarm.

These calculations are done for very weak pulses. It is easy to understand that, if we have stronger pulse, we can set a higher threshold and both $P_{D-pulse}$ and $P_{fa-pulse}$ will be more satisfactory.

4.2.3. De-toggling

Remember in chapter 2 Signalling and Transmitter, we have the signal scrambled by toggling every other '1' bit to '-1', and we get a bit sequence *b'* with three level: {1, 0, -1}. Thus in our transmitted signal $s(t)$, we have three types of chips, chips with a positive pulse, chips with no pulse, and chips with a negative pulse, which is just 180 degree phase shifted. A 180 degree phase shifted pulse can be detected with a 180 degree phase shifted matching template, this is no difficult.

A straightforward way of de-toggling is to detect positive and negative pulse; get a bit sequence of positive, negative and zero value; and then switch every other nonzero bit to '–bit'. However, there is a big problem in this approach: if one 1bit is miss-detected in the bit sequence, it will make the descrambling a chaos. Simulation result shows that the Chip Error Rate (CER) performance of this de-toggling approach is much higher than that when no scrambling is applied in the transmission. This means the scrambling brings big performance degradation.

Our approach of de-toggling is much simpler. We just ignore the 180 degree phase shift of any detected pulse and output a positive square wave. Simulation result shows that this approach brings no degradation to the pulse detection compared to transmission with on scrambling scheme.

4.3. Full RAKE Symbol Detection

The principle of the RAKE receiver is introduced in section 4.1. Here we discuss the function and implementation of the Full RAKE symbol detector. To make the discussion easier we quickly review the PSM modulation first.

PSM uses binary PN codes to represent symbols in the data sequence. In our system there are symbols: '1' and '0' in the data sequence, so we have two representing PN codes. After each data symbol is represented by the respective PN code we get a binary bit sequence. This bit sequence is then used to modulate the pulse sequence. The pulses are sent in chips of certain chip duration Tc. The positions of the pulses in the chips are the same, as oppose to the PPM modulation. Each chip represents one bit in the bit sequence; one pulse is sent in the chip for a 1bit and no pulse is sent in the chip for a 0bit

4.3.1. Full RAKE structure

The structure of the RAKE structure is shown in Figure 4-1. The square wave form shown above the delay blocks is the output from the statistic pulse detector. As discussed in section 4.2, each square wave stands for one detected pulse in the received signal. And the width of the square wave shall be equal to the pulse length. In this signal we see some of the squares are wider and this is because there are pulses overlapping with each other. This signal is a continuous time signal with binary digital value.

The output of the statistic pulse detector propagates through a line of time delay blocks. Each block provides a time delay of τ , and at the points before and after each block, the signal is sampled and sent to a RAKE finger, as illustrated in the figure. Again, the delay line serves to spread the time signal over a number of spatial points, and to convert the temporal diversity of the signal to a spatial diversity. The length of τ should be no longer than the width of a square pulse, and the total length of the delay line shall be equal to the chip duration Tc. This makes sure that the square pulse within one chip shall be captured by at least one RAKE finger.

People may think that there is such a situation: a signal path arrives just in between of two RAKE fingers and may be missed by both of them. It can be found out that this situation will not happen, because, each captured pulse is represented as a square wave of certain width, and this width is all ways longer than τ , the time interval between two RAKE fingers. The RAKE fingers read in at the edge of the clock so they behave as sampling the square(t) signal with time interval τ . Therefore, no matter when a pulse arrives at the receiver, as long as it is detected by the pulse detector, it will be captured by at least one RAKE finger.

We assume that the environment of the system will not change within the duration of one data session, and therefore the propagation channel will not change. We know that each received pulse comes from one signal path among many multiple paths and be transformed to a square wave. Although there are arriving time differences between different signal paths, but for pulses that propagate through one path, the time intervals between them are preserved. This means, if the pulses are sent out with chip duration Tc, when they arrive at the receiver through different signal path, they are still pulses with chip duration Tc, although there are time difference between different paths.

We set the clock of the RAKE the same as the chip rate. If one pulse is captured by a RAKE finger j at one clock edge, the next pulse coming through the same signal path will arrive after time of Tc; since the RAKE clock is the same as the chip rate, the next clock edge will also come after time of Tc and therefore the next pulse in this signal path will too be captured by the RAKE finger j. Actually all the pulse coming from one signal pulse will be captured by one and RAKE finger. It is explained that all the square pulse within one chip shall be captured. Therefore, these RAKE fingers together will capture all the detectable signal paths. This is why this structure is called a Full RAKE. Each RAKE finger outputs a bit sequence detected from one signal path.

No Synchronization

Now we explain why this receiver does not need to synchronize with its transmitter. In last paragraph we explained that pulses from a detectable signal path will always be captured by one RAKE finger at the clock edge, this is actually the same to say that, this RAKE finger is synchronized with this signal path. No matter what difference there will be between the transmitter clock and the receiver clock, a detectable signal path will always have a RAKE finger tracing it, i.e. a RAKE finger synchronized with it. We do not need to adjust the difference between the transmitter clock and the receiver clock, i.e. we need no synchronization between the transmitter and the receiver.

The delay line structure spread the duration of one chip over many spatial points; since the clock frequency is the same at the transmitter and at the receiver, all the possible phase difference between those two clocks are manipulated by one RAKE finger in a fine granularity (τ). Therefore the receiver needs not synchronize to set to its clock to a certain phase difference.

Requirement on the clock

Clock drift is the deviation of the clock speed. This is a very realistic problem in any hardware. In our system, in order to make sure one RAKE finger can keep track of one signal path within one symbol duration, we need to have the speed shift limited. To keep a RAKE finger track one signal path within one symbol duration, we need to have the accumulated time difference of the clock over one symbol duration less than the granularity of the RAKE fingers, i.e. the duration of a pulse. If the accumulated time difference is greater than the finger granularity (τ), then the pulse will be capture by the RAKE finger before or after.

$$\Delta t = N_s * \left(\frac{1}{f_{clk}} - \frac{1}{f_{clk} + \delta} \right) < T_m \qquad \text{Equation 4-6}$$

Here Δt is the accumulated time difference over one symbol duration, N_s is the length of the PSM code, i.e. the length of a symbol, f_{clk} is the clock frequency and δ is the clock drift. If we have pulse duration of 0.4ns, chip duration of 30ns, a PSM code length of 40, than we need to have the clock δ less than 11 KHz. Longer PSM codes will make this requirement stricter.

Another thing worth mentioning here is that, the pulses captured by these RAKE fingers in one clock may belong to two successive chips. As discussed in chapter 3, the chip duration should be longer than the channel delay spread and make sure

the inter chip interference be avoided. If this goal is achieved, we shall expect no pulse in one chip duration that is a replica of a pulse sent in the previous chip. However, since we are not synchronizing the receiver clock with the transmitter clock, with very high probability that the output bit sequences in some of the RAKE fingers are one bit earlier than those in the rest RAKE fingers. In the next section we will see that this will not bring any problem to our symbol detection.

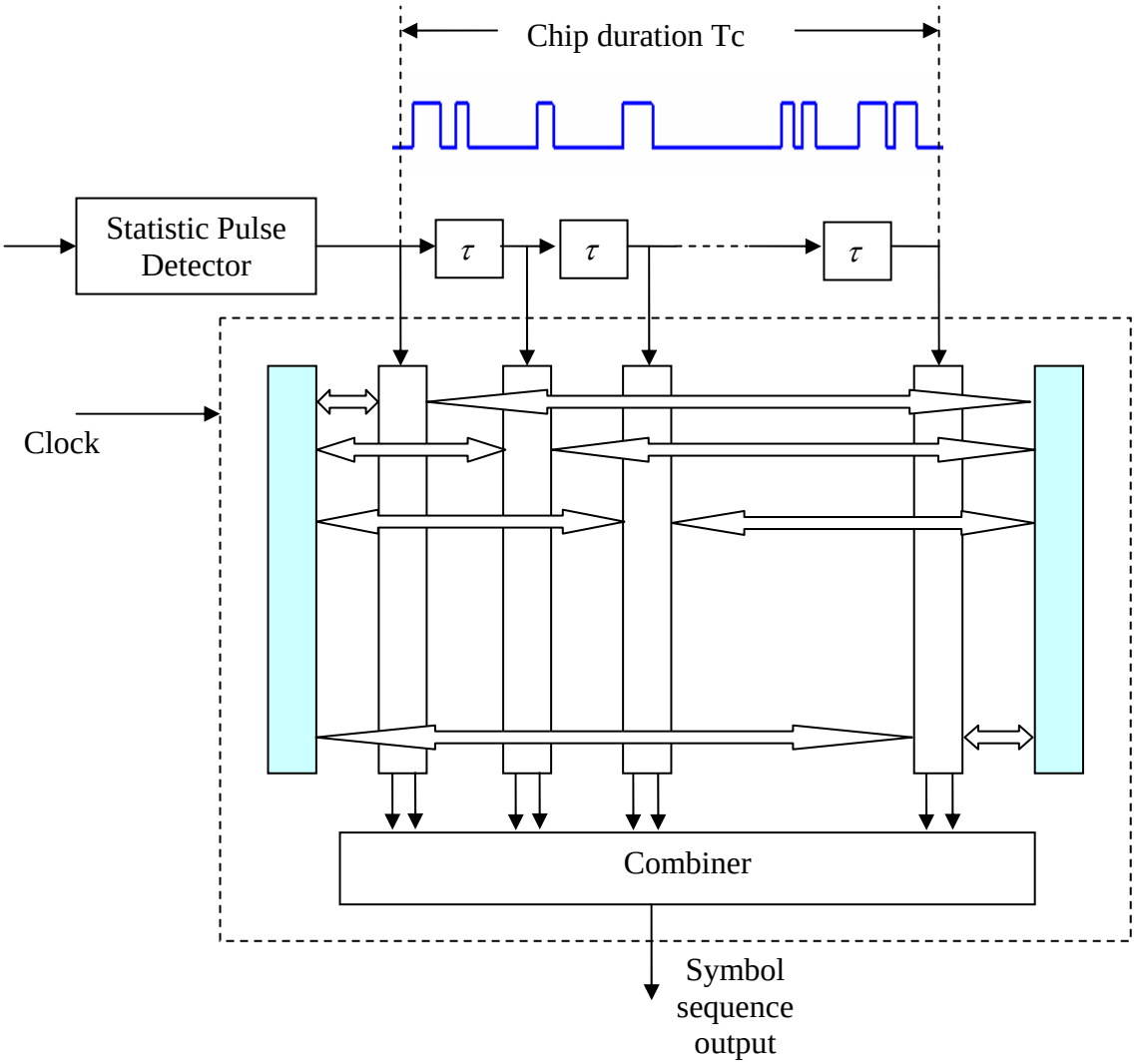

Figure 4-9 Full RAKE symbol detector

4.3.2. Demodulation/Symbol detection

The demodulation/symbol detection process detects the PSM PN codes in the received bit sequence: when a code representing symbol ‘1’ (denoted as code1) is detected, a symbol ‘1’ is claimed and when a code representing symbol ‘0’ (denoted as code0) is detected, a symbol ‘0’ is claimed. The detecting of the PN code is done by correlating the target PN codes, code1 and code0, with the received bit sequence and making decision on the correlation, {Z1} and {Z0}.

In this receiver, each bit sequence output from a RAKE finger is demodulated independently. The bit sequence is correlated with the two sequence template. The two correlation sequence {Z1} and {Z0} from each RAKE finger are sent to the Combiner.

$$\begin{cases} Z1_j = \sum_{i=1}^{N} code1(i) * b(j - N + i) \\ Z0_j = \sum_{i=1}^{N} code0(i) * b(j - N + i) \end{cases}$$

Equation 4-7

The correlation operation is multiplying and integration. For binary digital signal, this operation can be implemented with AND gates and Adder. When the binary signal level {1/0} is used, this operation can be seen as looking for a pattern of one, defined by correlation code, in the received bit sequence. This is because when a bit is ANDing with a ‘0’ in the correlation code, the result will always be ‘0’ and that means no matter this bit is 1 or 0, it will not affect the correlation output and thus will not affect the decision making of detection. Only the bits that are ANDing with the ‘1’s in the correlation code will affect the result.

As discussed in Chapter 3, the PN codes used in PSM modulation should have high and sharp autocorrelation and low cross correlation, so that they can be detected in the bit sequence and are distinguishable from each other. When the received bit sequence contains no error, it is made up of code1 and code0, therefore the correlation sequence {Z1} contains the autocorrelation of code1, the cross correlation of these two and something else, and the correlation sequence {Z0} contains the autocorrelation of code0, the cross correlation of these two and something else. When an autocorrelation peak is detected in the correlation sequence then a code is claimed. The autocorrelation peak is detected by thresholding the correlation sequence with a threshold Zt.

Threshold Zt

To detect the autocorrelation peak the threshold Zt should be set as a value between the peak value and the highest non peak value. The following figures show the correlation sequence in different circumstances. Say that we are detecting code1 from the bit sequence. When the bit sequence is made up of code1, {…code1 code1 ….}, then the correlation sequence will look exactly as shown in Figure 4-10, which is autocorrelation of code1. When the bit sequence is made up of code0, {…code0 code0…}, the correlation sequence will look like Figure 4-11, which is cross correlation of code1 and code0. In a more real world, the bit sequence is combined by code1 and code0 and the correlation sequence will look like shown in Figure 4-12 and 4-13. Figure 4-11 is correlation code0 with a bit sequence of {…code1 code0 code1…} and figure 5-11 is correlation code1 with a bit sequence of {…code0 code1 code0…}. These four figures cover all the situations one may meet in the correlation sequence. The autocorrelation peak is equal with the number of '1' in the binary code; by selecting proper codes, the cross correlation and the non peak value in the autocorrelation can be foreseen at most of the time. But care need to be taken for the situation described in Figure 4-11 and 4-12.

The correlation properties we expect from our PSM sequences are high autocorrelation peak and low autocorrelation side lobe and low cross correlation. We now define a measure to quantitatively evaluate how good the expectation is met. We call this peak distinguishablity (PD)

$$PD = \frac{AutocorrelationPeakValue - NonPeakValue}{AutocorrelationPeakValue} * 100\%$$

The threshold Zt needs to be higher than the PD value.

In these four figures, the two PN codes used are two 63bit long Gold codes, each containing 32 1bit. We can see the autocorrelation peak is 32 and the highest non peak value is 23. Here, PD = (32-23)/32=71.2%. The threshold Zt needs to be higher than this.

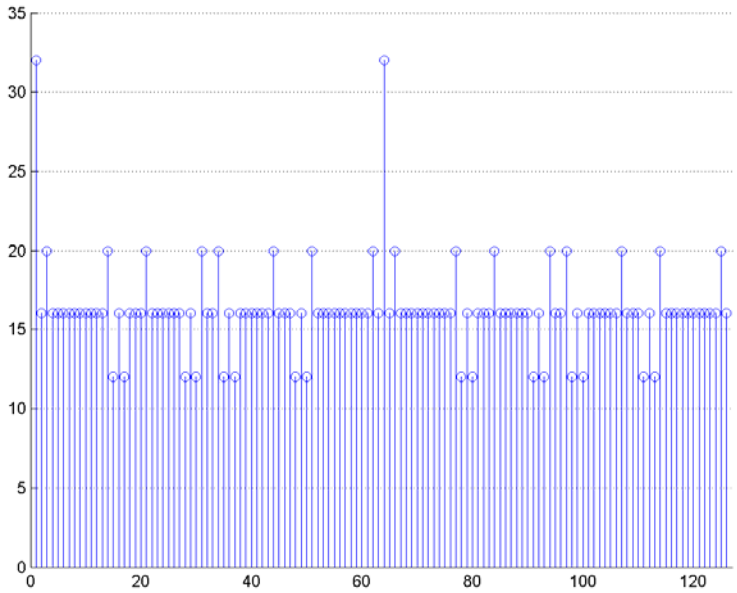

Figure 4-10 Autocorrelation of a binary version Gold code

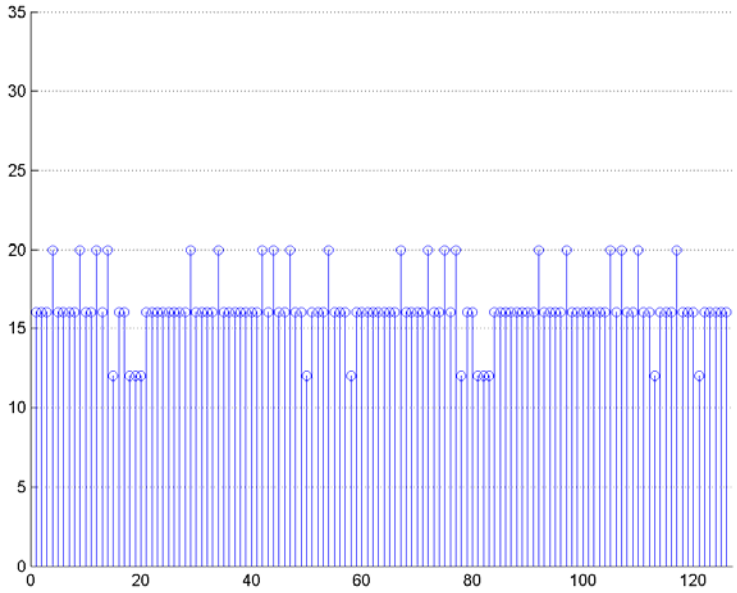

Figure 4-11 Cross correlation of a binary version Gold codes

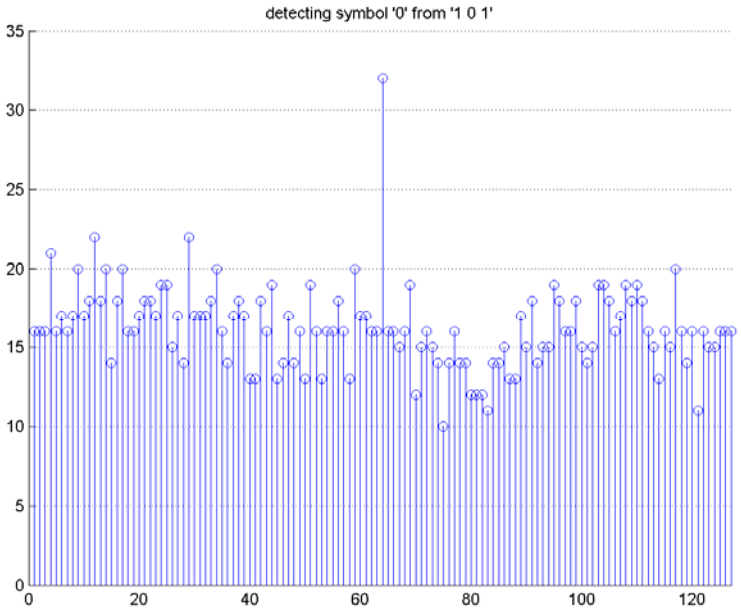

Figure 4-12 Correlation of detecting symbol ‘0’ from sequence ‘1 0 1’

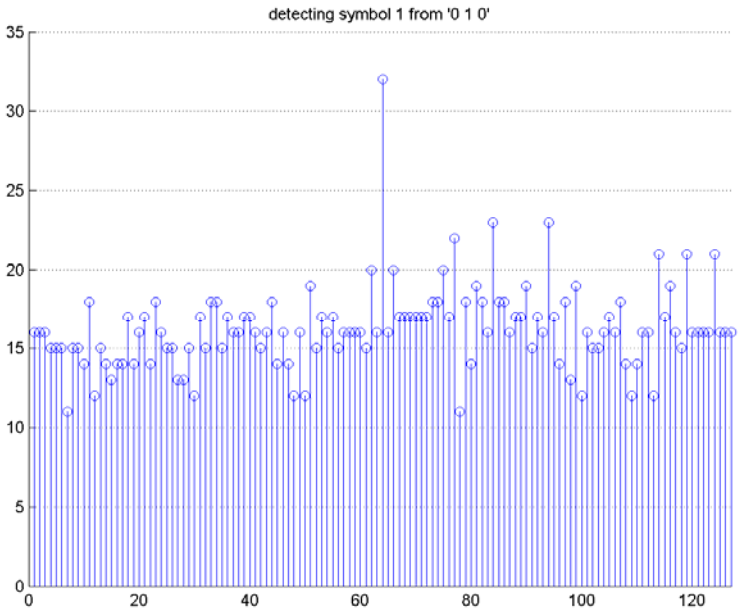

Figure 4-13 Correlation of detecting symbol ‘1’ from sequence ‘0 1 0’

4.3.3. Statistic symbol detection

As discussed previously, each RAKE finger output the bit sequence detected from the signal path it is tracking. These multiple paths can be very weak and some of the pulses might be missing, that means some of the '1bits' in the bit sequence might be missing. As mentioned in section 4.3.1, the correlation operation in this receive is looking for a pattern of '1's in the bit sequences, given the weak signal level a certain degree of missing '1' in the bit sequence can be accepted in the detection. The autocorrelation peak is equal to the number of '1' in the pattern. We can say that we accept it when we find a certain percentage of '1' of the pattern and claim a symbol detected. This is called statistic symbol detection.

When we set the threshold Zt less than 100%, this means we accept missing of '1' in the pattern we are looking for. But care need to be taken here because if the Zt is set too low, there might be false alarm, which means a symbol is claimed detected when there is no symbol at all.

4.3.4. Combiner

The combiner performs the following functions.

- As discussed previously in this chapter, with high probability, the bit sequences detected by some of the RAKE fingers are one bit ahead of the others. When correlating with the correlation template, the autocorrelation peak in some of the bit sequences will come one bit later than that in the others. The combiner algorithm needs to take care of it.

- Each RAKE finger outputs two correlation sequences {Z1} and {Z0}. The combiner thresholds these correlation sequences, detects autocorrelation peaks and make a decision on whether a symbol is detected and which symbol it is.

There might be three problematic situations:

1. No autocorrelation peak is detected in any of the correlation sequences from all the RAKE fingers
2. In some of the RAKE fingers, autocorrelation peak is detected in {Z1}; while in some of the other fingers, autocorrelation peak is detected in {Z0}.

3. In one RAKE finger, autocorrelation peak is detected in both sequence {Z1} and sequence {Z0}.

The reason that leads to situation 1 can be that the signal is too weak and too many pulses are missed in the pulse detection. There are not many things we can do in this case except increasing the transmission power to achieve a higher SNR in the pulse detection.

Situation 2 and situation 3 can happen when the receiver is under severe multiple access interference (MAI). There are too many pulses from many users so that in each RAKE fingers there are too many '1' bit detected. Imagine if a RAKE finger detected a bit sequence with all one, and given that our correlation operation is an operation looking for pattern of '1's, then whatever pattern of '1's it is looking for, it will find it. Nothing more can be done on the receiver side for these two cases. However, by selecting less dense PSM codes the MAI can be mitigated.

4.4. Performance of the receiver

Simulation is done to evaluate the performance of the Statistic Full Rake receiver. The single channel performance of the receiver is mainly limited by the channel condition and the SNR level. Another measure that is commonly used to evaluate the performance of a receiver against noise level is E_b / N_0 : the energy per bit per noise spectral density. This parameter is often considered as the normalized SNR and used to compare the bit error performance (BER) Our receiver does not output a general bit detection result: it detects all the pulses received and the full RAKE structure detects symbols from these pulses. Therefore, in this section we use E_b / N_0 vs Symbol Error Rake (SER) to measure the performance of our receiver.

In chapter 6 we will discuss the relation between modulation codes and the SER performance. Under the PSM modulation, different modulation codes use different number of bit to represent a symbol. To fairly compare the receiving performance of different modulation codes, we should use E_s / N_0: energy per symbol per noise spectral density. $E_s / N_0 = N_1 * (E_b / N_0)$, N_1 is the number of '1's in the modulation codes. For the time being, our purpose is to evaluate the receiving performance against the noise level and no comparison of modulation codes is involved. Therefore we use the parameter E_b / N_0.

Simulation results show that, by adjusting the threshold of the pulse detection and the threshold of the symbol detection, the receiver works well under different noise level. The results shown in Table 4-1 comply with the analysis in previous sections: higher threshold for higher SNR and lower thresholds for lower SNR.

E_b / N_0	Pulse detection threshold	Symbol detection threshold	SER
12dB	2.5σ	90%	<0.1%
3dB	σ	80%	0.58%

Table 4-1 Single channel performance, SER vs. Eb/No

5 Code Selection

In this section, we discuss the selection of PSM codes. As discussed in previous chapters, the properties of the PSM codes directly affect the performance and the capacity of the system. The correlation properties affect the detection performance of the PSM codes. The length of the codes decides the data rate of the system and the density of‘1’s of the codes affect the severity of MAI. Code generation and hardware implement issues also need attention. On one hand, the code generation may affect the MAC layer code management; on the other hand, simple generation circuits comply with our goal of power efficient and low cost device.

In section 5.1 we state the demand on the code selection. From section 5.1 to section 5.5 we study several candidate PN codes and make comparison between them. In section 5.6 a short summary of this chapter is made.

5.1 Demand on code selection

The following properties are desirable for PSM modulation and multiple-access method:

Sharp Autocorrelation and low cross correlation
This point has been stated in subsection 4.3.2, and a quantitative measure of how good the code correlation property is, Peak Distinguishability (PD), is introduced. This measure shall be used in the study in the candidate PSM codes. Under bad channel condition, higher PD value ensures better symbol detection performance.

Multiple choices on code length and code density
The PSM method use PN codes to present data symbols. The symbol rate of a channel R_s and the bit rate or chip rate after modulation R_b has such

relation: $R_s = R_b / N_s$, where N_s is the length of the PSM codes. In a UWB channel which is rich of multipath, the chip rate is limited by the delay spread of the channel. This point has been discussed in section 3.3. Under this condition, short PSM codes provide high symbol rate.

PSM code density has impact on MAI. The code density is defined as the number of '1' in a code divided by the code length. In last chapter it has been stated that the statistic symbol detector detect data symbols by looking for pattern of '1's in the bit sequence. The '0's in a PSM code are ignored in the detection. The code density has impact on MAI in this way. In a multiple user scenario, several transmitters are transmitting simultaneously. They are transmitting pulse sequences with a pulse population decided by the density of '1' of their PSM bit sequence. The more pulses are sent in one data symbol frame, the more possible that pulses from interfering transmitters may be detected by the RAKE fingers of the target receiver and this is the Multiple Access Interference. Lower code density brings lower MAI to the system.

On the other side, the codes length and code density usually has impact on the code correlation: longer code length and higher code density tend to have higher PD value than short ones. These trade-offs shall be further exploited in chapter 6.

Large number of codes
The larger number of available sequences we find, the more channels we can sustain at one time. This is one main limit on the capacity of the system.

5.2 Walsh-Hadamard codes.

Walsh-Hadamard sequence is also referred as Walsh sequence or OVSF (orthogonal variable spreading factor) codes. Walsh-Hadamard sequence has the advantage to be orthogonal, which means the cross correlation between sequences is zero. The orthogonality of Walsh-Hadamard codes is good for channelization, and is widely used in cellular systems for this purpose. Not only two sequences of the same length are orthogonal, two sequences of different length, if only the longer one is not generated directly or indirectly from the shorter one, are also orthogonal. This enables Walsh-Hadamard sequences of different lengths to be used in the same system. Different code length provides different data throughput, therefore this property of Walsh-Hadamard codes potentially provide flexible channel capacity management to the MAC layer.

If a set of Walsh-Hadamard sequences have the length of 2^n, the number of available sequences is 2^n.Walsh-Hadamard sequences are used in encryption and CDMA cellular communication systems.

Walsh sequence are defined as a set of N codes, W_j, j = 0, 1, …, N-1,

- W_j takes binary value of +1 and -1,
- The first digit of all the sequences is +1, $W_j(0) = 1$,
- W_j has exactly j zero crossing, for j = 0, 1, …, N-1,
- Orthogonality, $W_j W_k^T = \begin{cases} 0, j \neq k \\ N, j = k \end{cases}$

The algorithm for generating Walsh codes is (a', b') = (a +b, a -b). By using this algorithm recursively, Walsh codes with length of 2^n, where n is a nonnegative integer.

Hadamard sequences are generated based on Hadamard matrix, whose rows form a set of orthogonal codes. Hadamard matrix is generated by using the following algorithm recursively.

$$H_1 = [1] \qquad \text{Equation 5-1}$$

$$H_{2n} = \begin{bmatrix} H_n & H_n \\ H_n & -H_n \end{bmatrix} \qquad \text{Equation 5-2}$$

One major drawback of Walsh- Hadamard sequences is that they do not have sharp autocorrelation. This is not good for synchronization. The following figure gives an example of the autocorrelation function of a Walsh sequence, which contains no main peak.

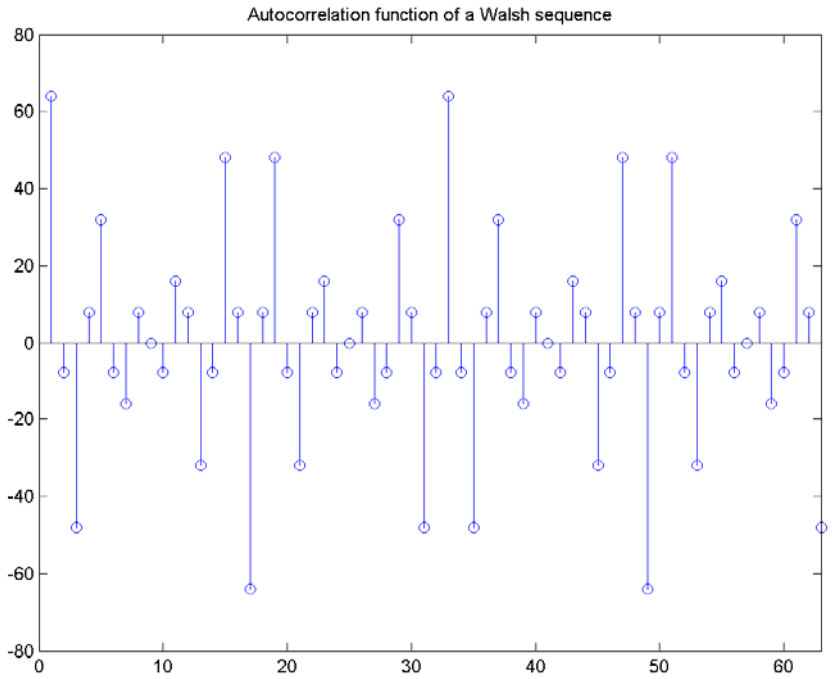

Figure 5-1 Autocorrelation of a Walsh sequence

5.3 Barker codes

The advantage of Barker codes is that they have sharp autocorrelation and low correlation side lobes.

A correlation side lobe is the correlation of a code word with a time-shifted version of itself. The correlation side lobe C_k, for a k-symbol shift of an N-bit code sequence, $\{X_j\}$, is given by

$$C_k = \sum_{j=1}^{N-k} X_j X_{j+k} \qquad \text{Equation 5-3}$$

where X_j is an individual code symbol taking values +1 or -1 for j=1, 2, 3, …, N. Correlation side lobe is different from the autocorrelation of a sequence. However, low correlation side lobes and a sharp autocorrelation are both important for sequence synchronization.

A barker code is a sequence of N values of +1 and -1, such that $|C_k| \leq 1$ for all$1 \leq k < N-1$. Barker codes are commonly used for frame synchronization in digital communication systems.

One drawback of Barker codes is that the, both the code length and the number of available codes are very limited. There are barker codes of lengths 2, 3, 4, 5, 7, 11 and 13, and it is conjectured that no longer Barker codes exist. A list of known Barker codes up to reversal of digits and negation is given below.

length	code
2	+ -, + +
3	+ + -
4	+ - + +, + - - -
5	+ + + - +
7	+ + + - - + -
11	+ + + - - - + - - + -
13	+ + + + + - - + + - + - +

5.4 Linear Feedback Shift Register Codes

5.4.1 Maximal Length Sequences

Maximal lengths sequences (MLS), also referred as n-sequence or m-sequence, are generated by Linear Feedback Shift Register (LFSR). The main advantage of MLS is that they have very sharp autocorrelation function. As its name suggests, they are the sequences of the maximal possible period (which is $N = 2^n - 1$) from an n-stage LFSR. A LFSR can be described by the Generator Polynomial parameters. For a binary polynomial in z, $g_r z^r + g_{r-1} z^{r-1} + g_{r-1} z^{r-1} + ... + g_0$, the coefficient g_k is 1 if there is a connection from the *k*th register, as labelled in the diagram below, to the adder. A necessary and sufficient condition for the sequence generated by a LFSR to be maximal length is that its corresponding polynomial be primitive. The leading term g_r and the constant term g_0 of the Generator Polynomial parameter must be 1 if the polynomial needs to be primitive.

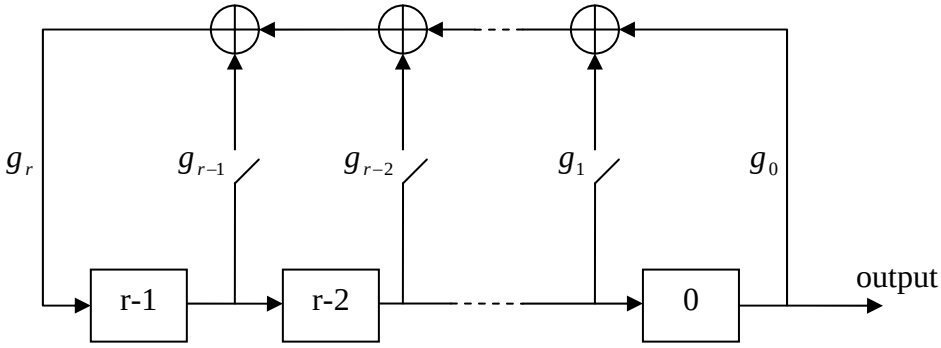

Figure 5-2 Linear feedback shift register

MLS have the following properties

- Balance property: the number of '1's in the sequence is one greater than the number of '-1's.
- Run property: of all the 'runs' in the sequence of each type(i.e. runs consisting of '1's and runs consisting of '-1'): one half of the runs are of length 1, one quarter of the runs are of length 2, one eighth of the runs are of length 3,…etc…. A 'run' is a subsequence of '1's or '-1's within the MLS concerned.
- The shift-and add property: $T^k u = T^i u \cdot T^j u$. Here T denotes the operator that shifts vectors cyclically to the left by one place. By combining two shifts of this sequence (relative shifts *i* and *j*) the same m-sequence is obtained, yet with another relative shift.
- The autocorrelation function is two-valued: $R_u(\tau) = \begin{cases} N & \tau = kN \\ -1 & \tau \neq kN \end{cases}$, where k is an integer value and τ is the relative shift as a multiple of a chip-duration. MLS has very sharp autocorrelation function. This property of MLS is commonly used in extraction of impulse responses of linear time invariant systems.
- Not orthogonal, but quite low cross correlation function.

The length of MLS can be quite long but the number of available sequence of a certain length is limited. The figures below show the autocorrelation function and cross-correlation function m-sequences of length $N = 63$. We see that the autocorrelation function takes on only two values: 63 and -1; the nonzero cross-

correlation function shows that m-sequences are not orthogonal, yet the cross-correlation is low compared to the autocorrelation peak.

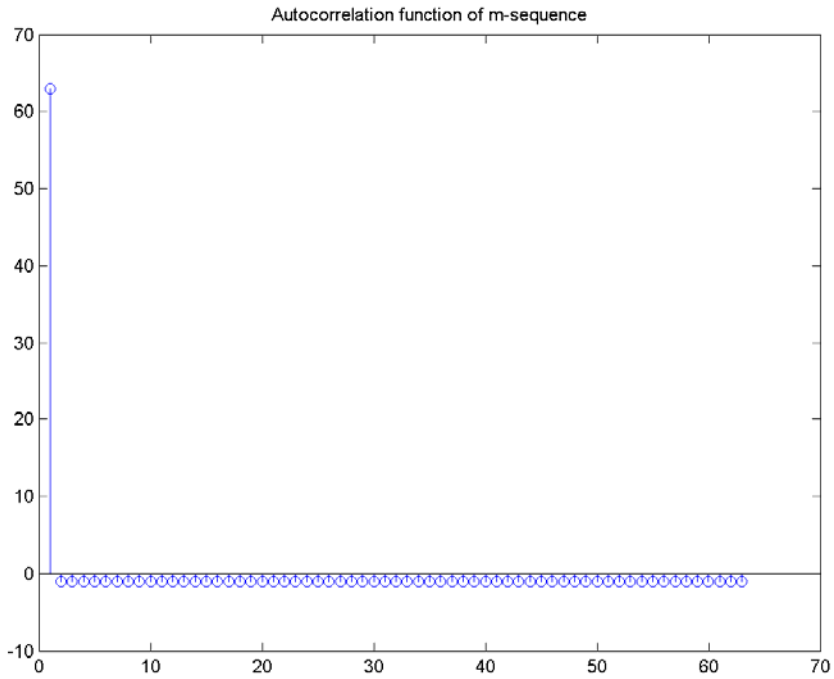

Figure 5-3 Autocorrelation of m-sequence

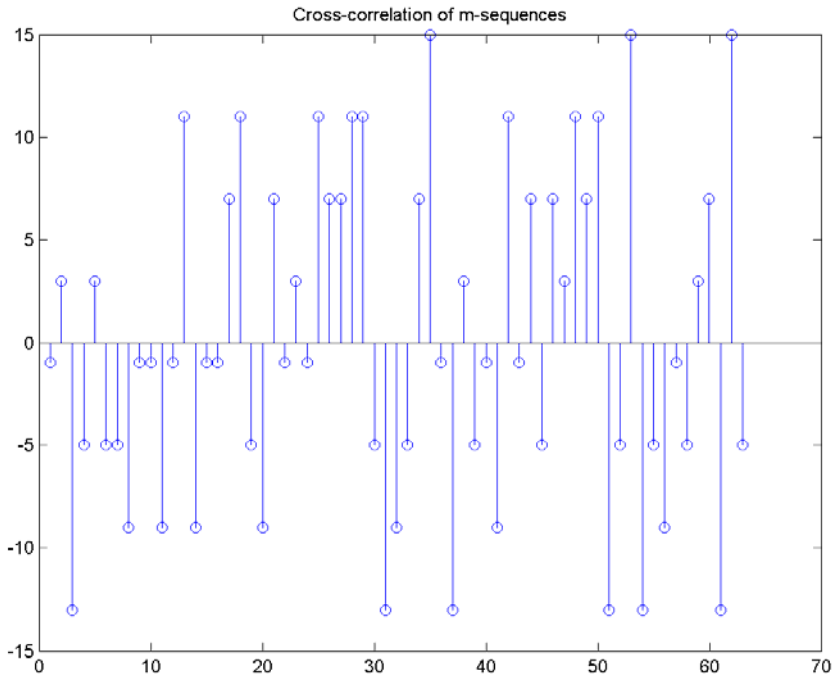

Figure 5-4 Cross correlation of m-sequence

5.4.2 Gold sequences

A 'preferred pair' of m-sequences added (XOR) together produce a so-called Gold sequence. Gold sequences have good cross correlation properties.
For a specified pair of sequences *u* and *v*, of period of $N = 2^n - 1$, the set *G(u, v)* of Gold sequence is defined by

$$G(u,v) = \{u, v, u \oplus v, u \oplus Tv, u \oplus T^2V, \ldots, u \oplus T^{N-1}v\} \qquad \text{Equation 5-4}$$

where *T* denotes the operator that shifts vectors cyclically to the left by one place, and $\oplus$ denotes addition modulo 2. $G(u,v)$ contains *N*+ 2 sequences of period *N*. Gold sequences have the property that the cross correlation between any two, or between shifted versions of them, takes on one of three values: $-t(n)$, -1 or $t(n)-2$, where

$$t(n) = \begin{cases} 1 + 2^{(n+1)/2} & n \quad odd \\ 1 + 2^{(n+2)/2} & n \quad even \end{cases}. \qquad \text{Equation 5-5}$$

A short list of preferred pairs is as below

n	N	Preferred Polynomial[1]	Preferred Polynomial[2]
5	31	[5 2 0]	[5 4 3 2 0]
6	63	[6 1 0]	[6 5 2 1 0]
7	127	[7 3 0]	[7 3 2 1 0]
9	511	[9 4 0]	[9 6 4 3 0]
10	1023	[10 3 0]	[10 8 3 2 0]
11	2047	[11 2 0]	[11 8 5 2 0]

Table 5-1

The autocorrelation function of Gold sequences is not as good as that of m-sequences but still has sharp peak and low side lobe.

The figures below show the autocorrelation function and the cross-correlation function of gold sequences. From the figures it can be seen that the autocorrelation function of Gold sequences is not two-valued, yet it has a sharp main peak. The cross-correlation function of Gold sequences takes on 3 values. For $n = 6, N = 63$, $t(n) = 17$. Therefore the cross-correlation function takes on values of -17, -1 and 15. The cross-correlation function is low compared to the main autocorrelation peak.

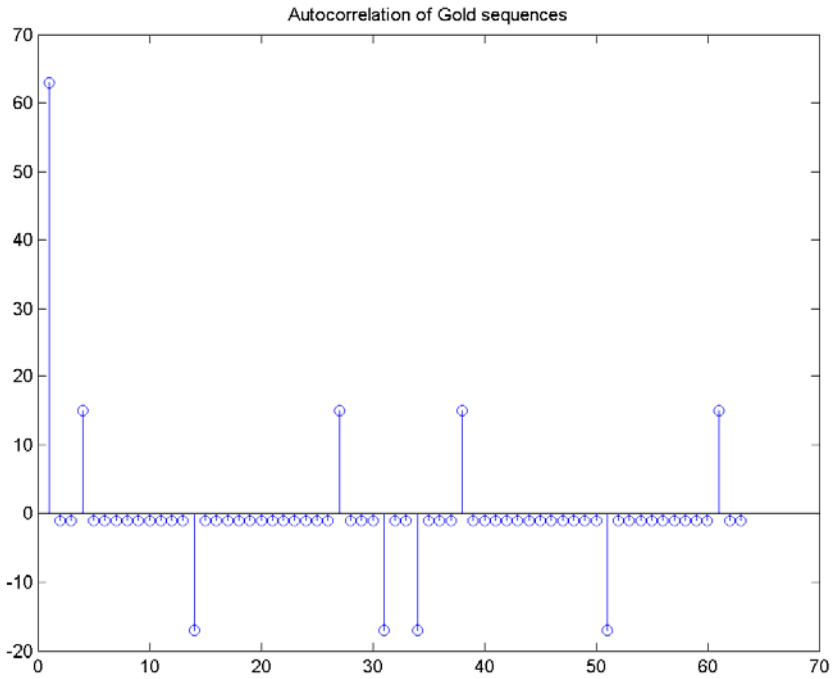

Figure 5-5 Autocorrelation of Gold sequence

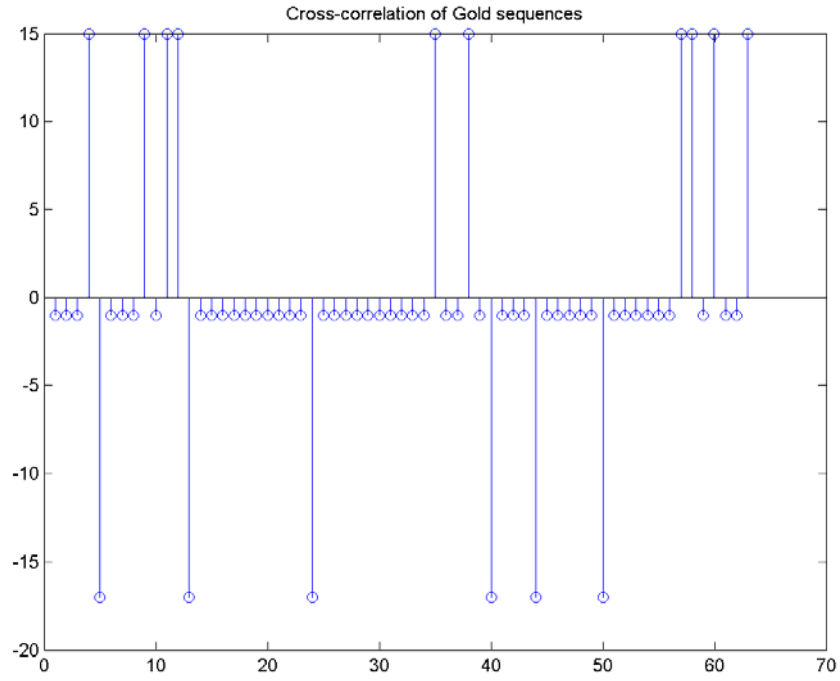

Figure 5-6 Cross correlation of Gold sequence

5.4.3 Kasami sequences

The Kasami sequences are a set of sequences that have good cross correlation properties. There are two classes of Kasami sequences: the small set and the large set. The large set contains all the sequences in the small set.

Kasami sequences have period $N = 2^n - 1$, where *n* is a nonnegative, even integer. Let *u* be a binary sequence of length *N*, and let *w* be the sequence obtained by decimating *u* by $2^{n/2} + 1$. The small set of Kasami sequences is defined by the following formulas, in which *T* denotes the left shift operator, *m* is the shift parameter for *w*, and $\oplus$ denotes addition modulo 2. Note that the small set contains $2^{n/2}$ sequences.

$$K_s(u,n,m) = \begin{cases} u \\ u \oplus T^m w \quad m = 0,\ldots,2^{n/2} - 2 \end{cases}, \text{for } n \text{ even.} \qquad \text{Equation 5-6}$$

For mod (n, 4) = 2, the large set of Kasami sequences is defined as follows. Let *v* be the sequence obtained by decimating the sequence *u* by $2^{n/2+1} + 1$. The large set is defined by the following formulas.

$$K_L = \begin{cases} u & \\ v & \\ u \oplus T^k v & k = 0,\ldots,2^n - 2 \\ u \oplus T^m w & m = 0,\ldots,2^{n/2} - 2 \\ v \oplus T^m w & m = 0,\ldots,2^{n/2} - 2 \\ u \oplus T^k v \oplus T^m w & k = 0,\ldots,2^n - 2; m = 0,\ldots,2^{n/2} - 2 \end{cases} \qquad \text{Equation 5-7}$$

The correlation function for the sequences takes on the following values:
$\{-t(n), -s(n), -1, s(n) - 2, t(n) - 1\}$, where $t(n) = 1 + 2^{(n+2)/2}$, *n* even,
and $s(n) = \frac{1}{2}(t(n) + 1)$.
The following table lists some of the polynomials that can be used to generate the Kasami sequences.

n	N	Polynomial	Set
4	15	[4 1 0]	Small
6	63	[6 1 0]	Large
8	255	[8 4 3 2 0]	Small
10	1023	[10 3 0]	Large
12	4095	[12 6 4 1 0]	Small

Table 5-2

The figures below show the autocorrelation function and cross-correlation function of Kasami sequences of length $N = 63$. Like the Gold sequences, Kasami sequences do not have two-valued autocorrelation function. Yet their autocorrelation function has quite sharp main peak. For $n = 6$, $t(n) = 17, s(n) = 9$. The cross-correlation function takes on 5 values {-17, -9, -1, 7, 15}. The cross-correlation function is low compared to the main autocorrelation peak.

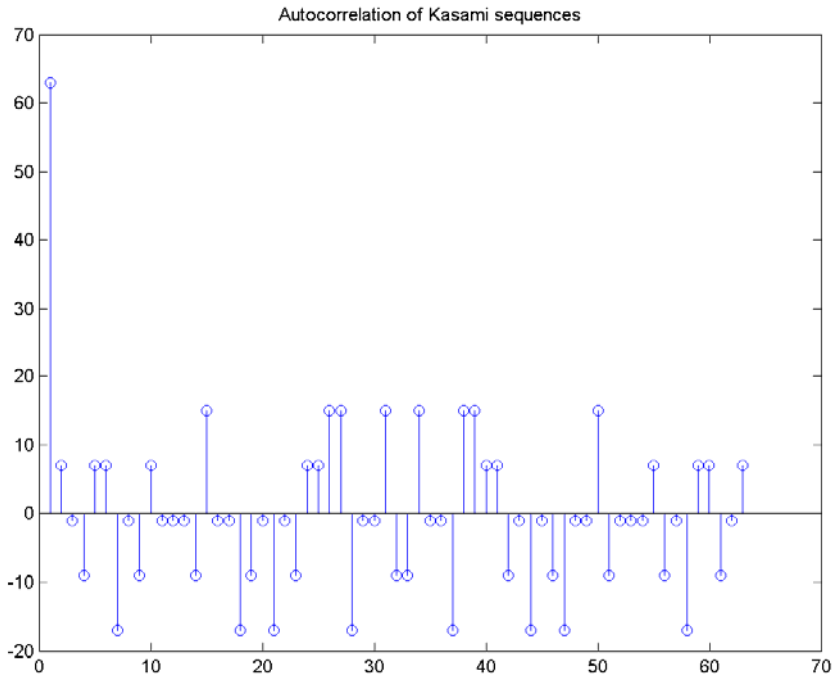

Figure 5-7 Autocorrelation of Kasami sequence

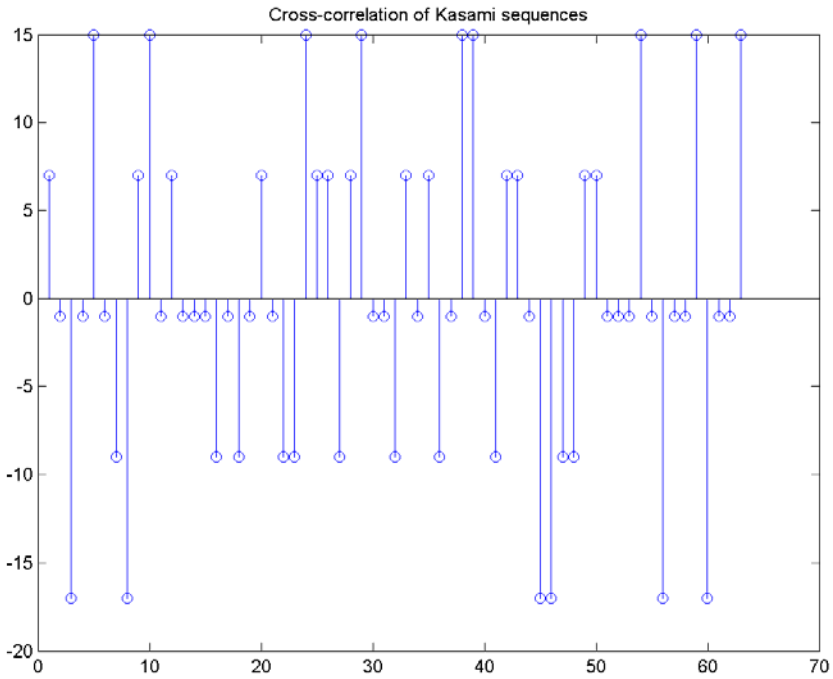

Figure 5-8 Cross correlation of Kasami sequence

5.5 Chaos-based sequence generator

In [GCim 2007], a chaos-based spreading sequence generator is proposed. The sequences are taken from the quantization of the trajectory of a discrete time chaotic dynamical system. According to relevant literatures these sequences have exponential decay in correlation functions.

Simulations are done to examine the correlation properties of this proposed chaos-based sequence and results show that they have correlation properties not so good as the Gold and Kasami PN sequence family do but acceptable. However, not like the Gold and Kasami family, the lengths of sequences are not limited to $N = 2^n, n \geq 5$, n is integer; The sequence length can be arbitrary. In addition, the number of available codes is larger than that the Gold and Kasami families can provide. It is safe to say that for systems with number of channels on level of hundreds, this generator can always provide sufficient sequences for Pulse Sequence Modulation.

We find a method to control the code density of the chaos-based sequence. By adjusting a single parameter of the generator, we can achieve various code densities (the number of one in a binary sequence) from codes of different length. Simulations are done for various lengths and densities. Correlation properties for those less populated sequences are reasonably good.

In conclusion, the chaos-based sequence generator can provides sequences with not so good correlation properties as the Gold and Kasami families do, but with much larger flexibility on code length and code density.

There is one thing needs attention. The Gold and Kasami family sequences are generated with Linear Feedback Shift Register (LFSR) and their correlation properties are studied extensively in literatures and analytical descriptions are given. However, the chaos-based sequences are generated by stochastically dynamic systems, and in my understanding, the inner stochastic characteristics prevent an analytical description of the correlation properties of the sequences. The reported descriptions on correlation of chaos-based sequences are based on statistic analysis. In our discussion, we try to observe the correlation properties through simulation of large number of sequences to represent the statistical feature of the sequences. Given large enough number of tested instance sequences, the observed statistic features should be considered representative.

Review of previous discussion on PN code selection

In our previous discussion, we decided that for our Pulse Sequence Modulation, PN sequences with sharp autocorrelation and orthogonal cross correlation would be the best choice to address the needs of symbol modulation and the multiple-access. The number of orthogonal PN sequences is very limited, and PN sequences with sharp autocorrelation and low cross correlation becomes the suboptimal choice. Different families PN sequences are examined, including Walsh-Hadamard sequence, Barker sequence, m sequence, Gold sequence and Kasami sequence. Gold sequence and Kasami sequence turn out to be the choice since they have sharp autocorrelation and low correlation, and the same time relatively large number of available codes.

One more merit of the Gold and Kasami sequence family is that the autocorrelation side lobe and the cross correlation are predictable. For sequences of length $N = 2^n$, n is a positive integer, the autocorrelation side lobe and the cross correlation take on only several predictable values. For Gold sequence, these values are: $-t(n)$, -1 or $t(n)-2$, where

$$t(n) = \begin{cases} 1 + 2^{(n+1)/2} & n \quad odd \\ 1 + 2^{(n+2)/2} & n \quad even \end{cases}.$$

For Kasami sequence, these values are:
$\{-t(n), -s(n), -1, s(n) - 2, t(n) - 1\}$, where $t(n) = 1 + 2^{(n+2)/2}$, n even,
and $s(n) = \frac{1}{2}(t(n) + 1)$.
When n=6, N=63, $t(n) = 17$, and . The correlation functions take values from {-17, -9, -1, 7, 15}.

These values are computed when antipodal version of the sequences is used. In our PSM demodulation/symbol detection, we aim at detecting the pattern of ones in the sequence and that means, we computed the correlations with a binary version of the sequences. Although no analytical values are given, it is easy to understand that the correlation values are predictable as for the antipodal version. In Figure 4-10 and 4-11 examples of autocorrelation and cross correlation of the binary version of Gold codes. Gold sequences of length 63 are used. Each sequence contains 32 ones. We can see that autocorrelation peak is 32, which is equal to the number of ones in the sequence, and the highest value of autocorrelation side lobe and cross correlation is 20; this is a distinctive difference and this is favorable for demodulation/symbol detection as we explain in Section 4.3.2 Demodulation/symbol detection.

The available number of Gold sequence and Kasami sequence of different length are listed below. According to [GCim 2007], typical spreading sequence lengths for applications of Wireless Sensor Network are less than 256. Here we list code length of up to 1024, but codes with no longer length are investigated.

Gold sequences are available for code order $n \geq 5$, n is integer; Kasami sequences are available for code order $n \geq 4$, n is even integer; large set Kasami sequences are available for mod (n, 4) = 2 only. Detailed information can be found in other section.

Code order n	Code length $N = 2^n$	Code family	Available number
4	15	Kasami (small set)	3
5	31	Gold	33
6	63	Gold	65

6	63	Kasami (large set)	519
7	127	Gold	129
8	255	Gold	257
8	255	Kasami (small set)	15
9	511	Gold	512
10	1023	Gold	1025
10	1023	Kasami (large set)	Very large

Table 5-3

Within available PN codes, the minimal density of '1' for codes with different length is listed below. No lower code density can be achieved in these two code family.

Code length	63	127	512	1023
Minimal density of '1'	38% (24/63)	44% (56/127)	47% (240/512)	47% (480/1027)
Number of Available codes	50	36	136	Can be very large

Table 5-4

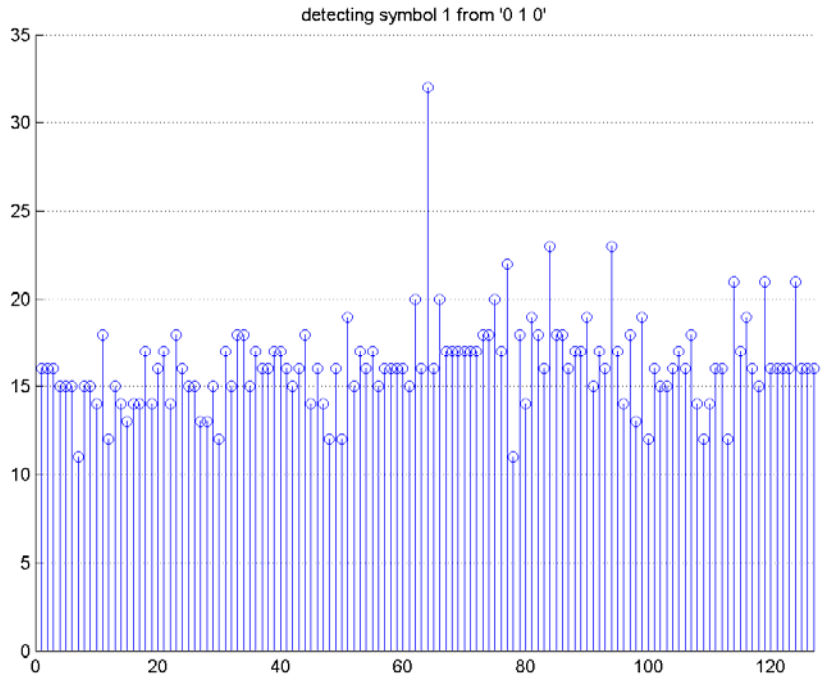

Figure 5-9 Correlation function experienced in the PSM modulated bit sequence

5.5.1 Generation of chaos-based sequence

The technique used to generate the chaos-based sequence is proposed in [GCim 2007], and an analysis on the statistical features of the obtained sequence is provided. A chaos-based spreading sequence generator is proposed. The sequences are taken from the quantization of the trajectory of a discrete time chaotic dynamical system. A chaotic dynamical system is like this: given an initial condition $x_0 \in [0,1]$, and a function M: $[0,1] \mapsto [0,1]$, the state-update equation $x_{k+1} = M(x_k)$ defines a discrete-time dynamical systems whose trajectories are sequences $x_0, x_1, ...x_k, x_{k+1}...$, $x_k \in [0,1]$. The sequences are generated from the trajectories in this way:

- A stretch $x_{k,} x_{k+1}, ..., x_{k+N-1}$ of length N is cut from the virtually infinite trajectory,
- The sequence $y_j = Q(x_j)$ is obtained by quantizing x_j: $Q(x) = +1$ when $x < 1/2$, and $Q(x) = -1$ when $x \geq 1/2$,
- Repeat this antipodal sequence periodically.

The function M is referred as map. Depending on the map M the dynamics of such a system can be very different. For certain maps the system is actually chaotic. In such case the structure of the map M can be linked with the statistical features of the sequence it generates. A family of maps that can be used to generate such chaotic dynamical system is shown below. The statistical features of the sequences depend on the parameter r, $r \in]-1,1[$.

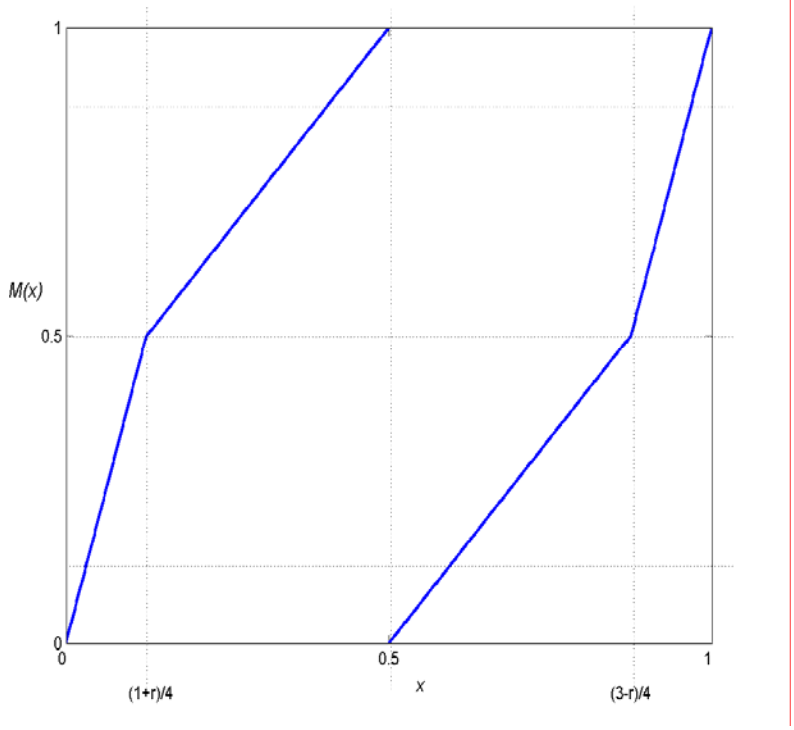

Figure 5-10 The family of maps used for generating the chaos-based sequence, whose statistical features depend on the parameter *r.*

According to [GCim 2007], the quantized sequence can be analyzed by means of well-accepted procedure described in literatures and the following properties of antipodal sequence *y* can be seen for integer $i \le j \le k \le l$:

$$E_y\left[y_i y_j\right] = r^{j-i} \qquad \text{Equation 5-8}$$

$$E_y\left[y_i y_j y_k y_j\right] = r^{j-i+l-k} \qquad \text{Equation 5-9}$$

The $E(\cdot)$ operator gives the mathematic expectation of its argument, with respect to all the possible sequences. These two equations show that the antipodal sequences produced with the map shown in figure 1 have exponentially decaying second- and fourth-order correlations with the rate of decay *r* that may be arbitrarily set to any rational number in $]-1,1[$.

5.5.2 Analysis of sequence correlation properties

Unfortunately, the correlations described in equation 1 and 2 are not the same concept of correlation we use to choosing our PSM sequences. But we can find certain statistical link between them. In the following discussion, without further indicate, we use the term 'correlation' to describe correlation function in the context of PSM sequence properties only.

As described before the chaos-based sequence is generated by quantizing the trajectory of a stochastic process. After quantizing, the obtained sequence can also be seen as a trajectory of an antipodal valued stochastic process. And second order correlation expressed in Equation 1, describes the statistical feature of the relationship between two values of certain distance (j-i) in this stochastic process.

$$E_y\lfloor y_i y_j \rfloor = (+1)*p(y_i y_j = +1) + (-1)*p(y_i y_j = -1)$$
$$\rightarrow \frac{(y_i y_j)_1 + (y_i y_j)_2 + \ldots + (y_i y_j)_M}{M}, M \rightarrow \infty \qquad \text{Equation 5-10}$$

Here $i \le j$, and $p(\cdot)$ is the probability of its argument. It can also be expressed as adding all the possible instance of $(y_i y_j)$ in this stochastic process and dividing the summation by the total number of instances.

Now in our context of PSM sequence, our correlation function is defined like this. For two PSM sequences $y^{(1)}$ and $y^{(2)}$ of length N, the autocorrelation p_{auto} and cross correlation p_{cross} are:

$$p_{auto}^{(1)}(i) = \sum_{j=1}^{N} y_{j+i}^{(1)} y_j^{(1)}, i = 0, \ldots, N-1 \quad \text{Equation 5-11}$$

$$p_{cross}(i) = \sum_{j=1}^{N} y_{j+i}^{(1)} y_j^{(2)}, i = 0, \ldots, N-1$$ Equation 5-12

We can see some similarity between equation3, and equation 4 and 5 since they all contain items of $y_i y_j$. If we used the antipodal chaos-based sequences as PSM sequence, then the statistical relation of item *y* in any of the sequence will be the same, so for the time being, we neglect the upper notation (u) and rewrite the correlation function in such a way

$$\frac{p(i)}{N} = \frac{\sum_{j=1}^{N} y_j y_{j+i}}{N} \qquad \text{Equation 5-13}$$
$$\rightarrow E_y\left[y_j y_{j+i}\right] = r^i, N \rightarrow \infty$$

This means that, for chaos-based sequence of infinite length, the correlation function normalized with the length of the sequence will be decided value r^i.

The chaos-based sequence used in real world will not be of infinite length. The relation described in equation 6 can only give us an impression that, with smaller absolute value of $|r|$, the absolute value of the correlation function $|p(i)|$ will be smaller too. And smaller correlation function means the sequences are less similar to each other. Therefore, generally speaking, smaller $|r|$ tends to lead to less similar or correlated sequences.

The previous analysis is done for antipodal sequences. The sequences used in PSM need to be binary sequences, and they can be easily transformed from the antipodal sequences with a linear transform $y_{\{1,0\}} = (y_{\{+1,-1\}} + 1)/2$. The conclusion of smaller $|r|$ tends to lead to less similar or correlated sequences should hold for binary version of sequences. This conclusion gives us guidance in our simulation.

5.5.3 Method to control the code density of the chaos-based sequences

Code density describes how many '1' are populated in a binary sequence, or code. This measure is interesting in the process of PSM demodulation/symbol detection.

In PSM demodulation we are looking for pattern of '1' that matches with our modulation code in the received bit sequence. In a multiple user scenario, less populated modulation codes lead to lower probability of multiple-access interference. This will be further discussed in system simulation in chapter 8. In this subsection we introduce a method to control the code density of the chaos-based sequence. The code density of a sequence of length N is

$$d_y = \frac{\sum_{j=1}^{N} y_j}{N}, y_j \in \{0,1\} \qquad \text{Equation 5-14}$$

In the chaos-based sequence generator, we can control the code density by adjusting the quantizing constant z.

Recall the generation of the chaos-based sequence: A discrete-time dynamical system is defined with a map shown in figure 1. A trajectory of this system is $x_0, x_1, ...x_k, x_{k+1}..., \ x_k \in [0,1]$. The chaos-based sequences are generated from the trajectory in this way:

- A stretch $x_{k,} x_{k+1},..., x_{k+N-1}$ of length N is cut from the virtually infinite trajectory,
- The sequence $y_j = Q(x_j)$ is obtained by quantizing x_j: $Q(x) = +1$ when $x < 1/2$, and $Q(x) = -1$ when $x \geq 1/2$,
- Repeat this antipodal sequence periodically.

In the quantization step, a constant ½ is set to threshold the real value *x*. We note this constant as z and consider it an adjustable parameter of this generator. With simulation we will see how this constant will affect the behavior of the generator, in respect to code density. Here in the original case, $z = 1/2$. Another adjustment is that we quantize the trajectory to a binary sequence: $Q(x) = 1$ when $x<z$, and $Q(x) = 0$ when $x \geq z$.

By observing the map shown in figure 1 we can see that, in the x-y coordinate, the map is symmetric with the point (0.5, 0.5). If we have a statistic variable *x* of real value with uniform distribution over $[0,1]$, and we map this variable to get $x_{k+1} = M(x_k)$, we will see that the probability of y>0.5 and that of y<0.5 is the same:

$$p(x_{k+1} > 0.5) = p(x_{k+1} < 0.5) = 0.5 \quad \text{Equation 5-15}$$

In turn, if the statistic variable *x* is distributed with equal probability in $[0,1]$ we have

$$p(x_k > 0.5) = p(x_k < 0.5) = 0.5 \qquad \text{Equation 5-16}$$

With a quantizing constant $z = 0.5$, and $y_k = Q(x_k)$, $y_{k+1} = Q(x_{k+1})$ we have:

$$\begin{aligned} &p(y_k = 1) = p(y_k = 0) = 0.5 \Rightarrow \\ &p(y_{k+1} = 1) = p(y_{k+1} = 0) = 0.5 \end{aligned} \quad \text{Equation 5-17}$$

This means, if one bit in the sequence y_k is equally possible to be 1 or 0, then the bit following this bit successively is too equally possible to be 1 or 0. If we set the first value of the trajectory, x_0 to be distributed with equal probability in $[0,1]$, then for its quantized value y_0 we will have $p(y_0 = 1) = p(y_0 = 0) = 0.5$. Combined with Equation 16, we will have $p(y_k = 1) = p(y_k = 0) = 0.5$ for all the bits in the sequence. This leads to a code density of 50%, which is the case for the original generator proposed in [GCim 2007].

If we have all the values with uniform distribution in $[0,1]$, after quantization, we will have a sequence with code density proportional to the quantizing constant z (argument 1, see proof in Appendix). And if the first item in the discrete-time trajectory x_0 has uniform distribution over $[0,1]$, then any item in the trajectory x_k will has uniform distribution over $[0,1]$ (argument 2, see proof in Appendix). Therefore by giving an initial value with uniform distribution over $[0,1]$, we can get sequence with code density proportional to the quantizing constant z. Simulation results shown in Figure 5-11 support our analysis.

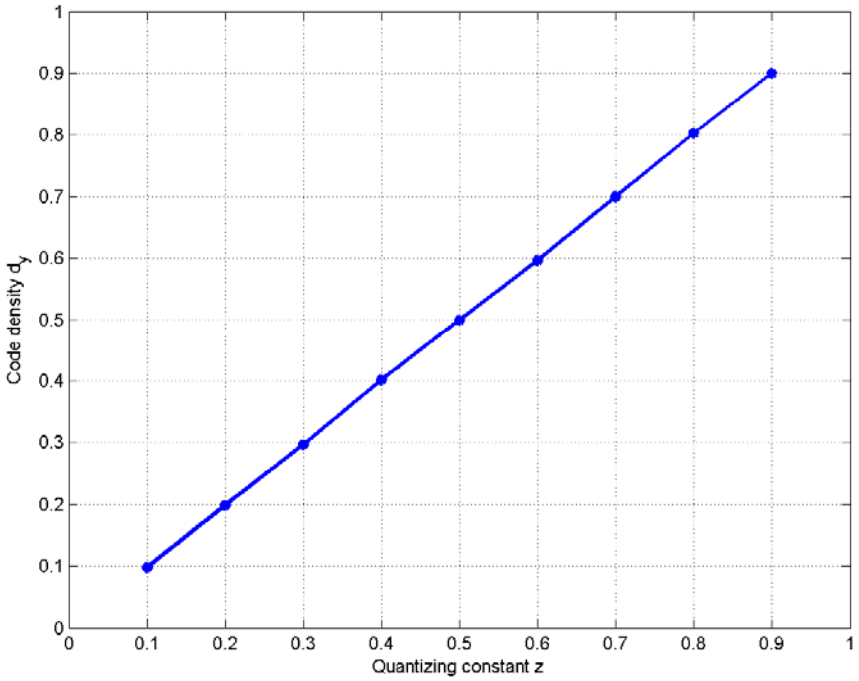

Figure 5-11 code density v.s. quantizing constant z

In this simulation, the initial value of the trajectory has uniform distribution over $[0,1]$. The chaotic dynamic system is defined with the map shown in Figure 5-10. For each quantizing constant z, sequence of length of 100,000 is generated and the code density is computed according to Equation 7. The simulation result is in agreement with our analysis. The conclusion is that we can control the code density by adjusting the quantizing constant z.

It is easy to understand that, this statistical feature can be represented accurately in sequence in large length but may not be represented so clear in a single instance of a sequence with short length, say 127. But still, in large number of instances this feature can be represented clearly. This will be seen in simulations in the following subsection.

5.5.4 Simulation, comparison with Gold codes

Simulations are done to generate chaos-based sequences with different length and with different code density. The correlation properties are also computed.

Figure 5-12 shows the correlations function between 971 chaos-based sequence of length 63 and density 32/63. These sequences are generated from the system introduced previously, and are checked that these 971 sequences are different from each other. The parameter r is set as -0.01, and the quantizing factor is set as 0.5. Compared with Figure 4-10 and Figure 4-11, the autocorrelation and cross correlation of Gold codes, the side lobe of the autocorrelation and the cross correlation of the chaos-based sequence are higher, but still have comparable distinctive difference from the autocorrelation peak. Figure 5-9 shows a more realistic correlation one may experience in the PSM demodulation. Our Figure 5-12 is also comparable to this case.

The reason is that the chaos-based sequence is cut from an infinite long quantized trajectory. For each part of this trajectory, the statistic feature is the same. Therefore, if any two sequences of them are connected together and compute the correlation function with one of these two, just as what is done in Figure 5-9, the statistical feature will be the same as the correlation between these two sequences. This is one difference between the chaos-based sequence and the Gold and Kasami family. In Figure 5-9 highest value excepted for the autocorrelation peak is 23, and in Figure 5-12 is 25. Therefore we say that, for PSM modulation, the correlation properties of the chaos-based sequences are comparably good as that of the Gold and Kasami family. Another example of sequences of length 127 and density 64/127 are shown in Figure 5-13, 688 sequences are generated and are checked to be different from each other. The correlation properties is again comparably good as that shown in Figure 5-14, which is the correlation properties of Gold sequences of length 127, density 64/127.

One thing one can notice here is that, the available numbers of sequences of these two lengths are much larger than that of the Gold and Kasami family. And this is true generally for any other sequence length. What's more, the sequence length of the chaos-based sequence will not be limited to $N = 2^n$. One can generate sequence with arbitrary length and with considerable number of available sequence. This provides us more flexibility in code length.

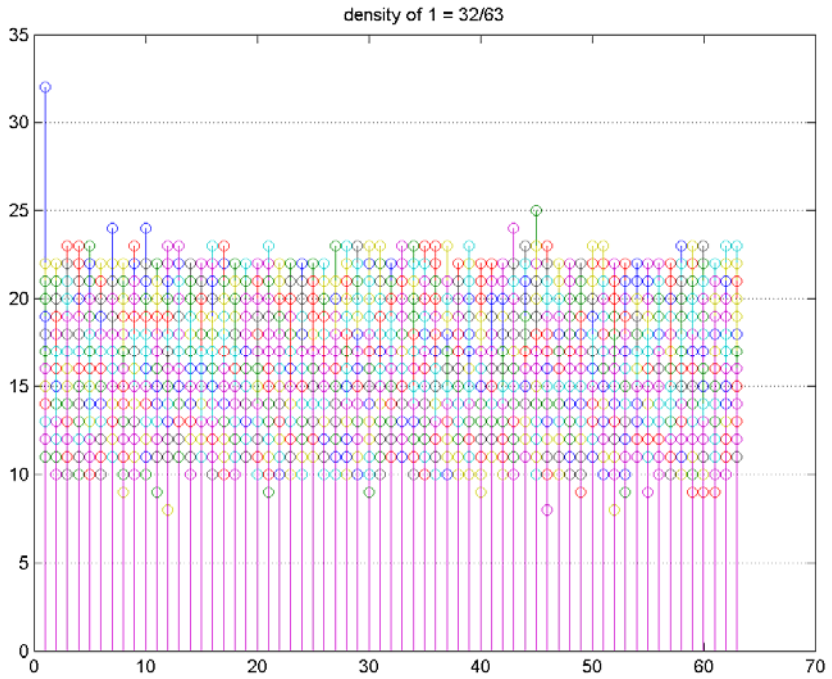

Figure 5-12, correlation function of chaos-based sequences, sequence length 63, density 32/63

Figure 5-13, correlation function of chaos-based sequences, sequence length 127, density 64/127

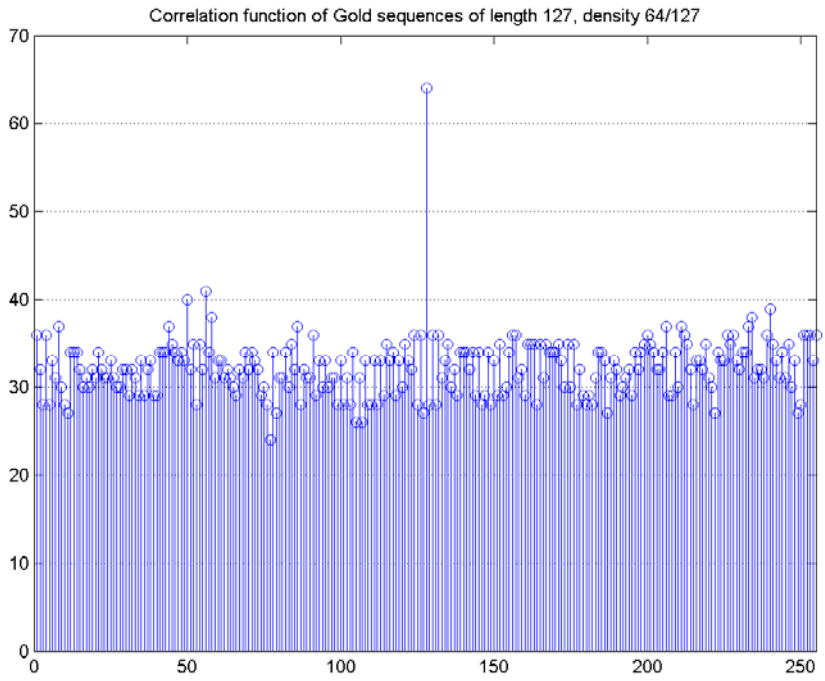

Figure 5-14, correlation property of Gold sequences of length 127, density 64/127

1. Statistical feature of the code density

In this subsection we discuss the statistical feature of the code density given a certain code length and quantizing constant z. It is easy to understand that, for short sequences generated with a certain quantizing constant z, the code density will not be exactly equal to z as the sequence sequences with super long length do. The code density will be distributed over a certain range, with a certain distribution probability profile.

In this simulation a large number of chaos-based sequences of short length are generated. Code length is 100, and for each quantizing constant z, 30,000 code instances are generated. We compute the probability of a certain code density may appear in the 30,000 code instances. The quantizing constant z has value of 0.1, 0.3 and 0.5. From 错误！未找到引用源。 we can see that, the code density is distributed over a range, but with almost highest probability it may consist with the quantizing constant z.

Understanding this, if we want to generate sequences with certain code density, we can just set the quantizing constant z accordingly. We cannot expect all the generated sequences have the exact density as expected, but we have the best chances to get them.

2. Correlation properties of the lower density sequences.

Sequences with lower density are interesting because in our PSM modulation/Multiple Access scheme, lower code density leads to potentially lower multiple access interference (MAI).

The correlation properties we expect from our PSM sequences are high autocorrelation peak and low autocorrelation side lobe and low cross correlation. We now define a measure to quantitatively evaluate how good the expectation is met. We call this peak distinguishablity (PD)

$$PD = \frac{AutocorrelationPeakValue - NonPeakValue}{AutocorrelationPeakValue} * 100\% \qquad \text{Equation 5-18}$$

For orthogonal codes, the non peak value of correlation will be 0, and the PD of orthogonal codes is 100%. The higher the PD is, the sequence is more near to orthogonality. The higher PD a sequence has, the better it meets our expectation. PDs of previously shown examples are listed below. By observing the PD values listed below support the conclusion we state before about these examples.

Figure 5-9	Gold family sequences of length 63 and density 32/63	PD = (32-23)/32=28.1%
Figure 5-12	Chaos-based sequences of length 63 and density 32/63	PD = (32-25)/32=21.9%
Figure 5-14	Gold family sequences of length 127 and density 64/127	PD=(64-41)/64=35.9%
Figure 5-13	Chaos-based sequences of length 127 and density 64/127	PD=(64-45)/64=29.7%

Table 5-5

In Figure 5-16 we show an example of correlation properties of lower density sequences. By setting the quantizing constant z equal to 0.1, we obtained more than 1800 sequence instances with length 200 and code density 10%. All these instances are checked make sure they are different from each other. In all these sequences, we compute the correlation between one sequence and itself, and all

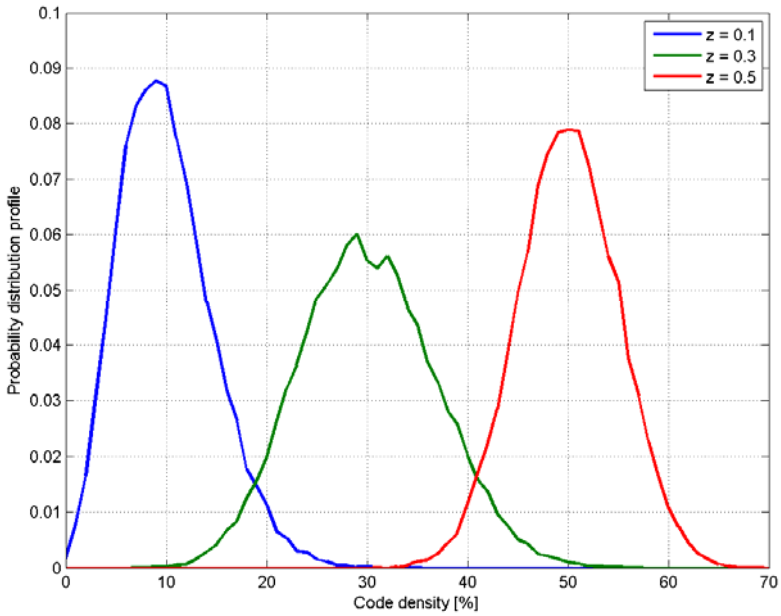

Figure 5-15 Code density distribution profiles, of different quantizing constant z

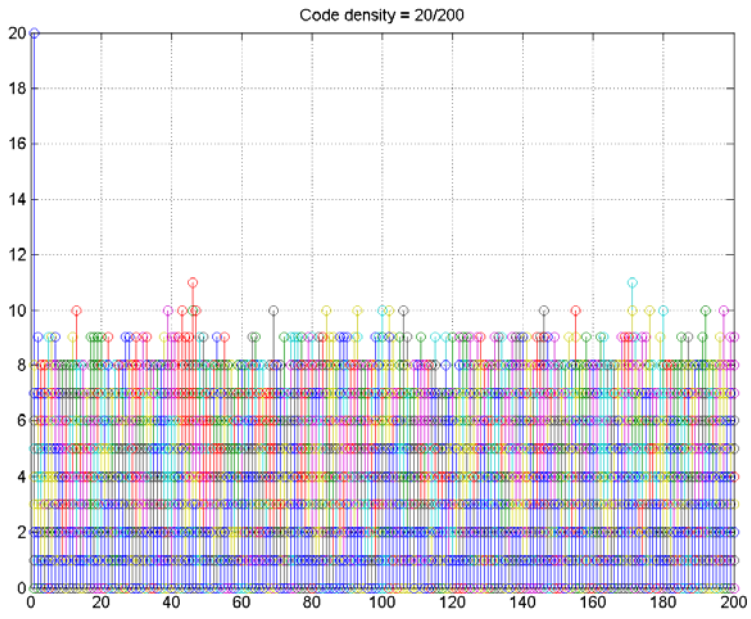

Figure 5-16 Correlation properties of chaos-based sequence of density 20/200

the other sequences and we plot the result together. We found the highest non peak correlation value is 11 and therefore we have our PD = (20-11)/20 = 45%. This result is better than what we get from Gold and Kasami family.
If we do some further analysis to these 1800 sequences, we can see that not all the correlation functions have the same non peak value: most of then are lower than the value seen Figure 5-16, which is the worst case in these 1800 sequences. We list the number of sequences with different correlation non peak values below. We can see that the best PD value we can achieve is 75% and this group has 51 sequences.

Number of highest non peak correlation value	Number of such sequences
5, PD = (20-5)/20 = 75%	51
6, PD = (20-6)/20 = 70%	591
7, PD = (20-7)/20 = 65%	787
8, PD = (20-8)/20 = 60%	302
9, PD = (20-9)/20 = 55%	98
10, PD = (20-10)/20 = 50%	17
11, PD = (20-11)/20 = 45%	2

Table 5-6

The above simulation and analysis let us know that

- With chaos-based generator, we can generate large number of sequences with low density.
- The PD performance of these low density sequences are better than the sequences of the same length but with density of around 50%.
- Some subgroup of sequences has even better PD performance.

5.6 Summary

We compare the candidate codes in their correlation properties, flexibility in code length and code density, number of available codes and implementation of generation hardware. The Gold and Kasami code family provides good correlation properties and very easy implementation of code generator, which is linear feedback shift register. This is good for system that needs to generate codes on each node. However, the flexibility in code length and code density is limited. The chaos-based PN codes provide great flexibility in code length and code density, and have more available codes than the Gold and Kasami family. Its correlation

properties are not as good as the Gold and Kasami but are acceptable. The implementation of the code generator is complicated; it involves an analogue circuit that realizes the chaotic system map function. It may not be suitable to be generated on each node.

Another issue is the complicity of the code management. The Gold and Kasami family are easier to manage for a MAC layer: with a selected polynomial, the generated code is decided. However, the chaos-based PN codes are generated by a chaotic dynamical system and we cannot predict which code will be generated from the generator at a certain moment. This is another reason why the chaos-based PN codes are not suitable to be generated on individual nodes.

6 Simulation and Discussion

In previous chapters we discussed the modulation, transmission, propagation and detection of the UWB signal. The PSM serves both as a modulation method and a multiple access method. The biphasic toggling is a very simple and hardware friendly method which smoothes the spectrum of the PSM signal. The statistic full RAKE receiver takes advantages of the multipath effect of the UWB channel. It collects the multipath components and performs statistic symbol detection.

In this chapter, we discuss some important parameters of the system, and how they will affect the performance of the system. In section 6.1 we discuss a parameter that affects the SER performance of a single channel, the chip duration. The performance of a single channel is limited mainly because of the inter-chip-interference. The inter-chip-interference exists because of the multipath effect of the UWB channel. The Chip duration needs to be long enough to avoid inter-chip-interference.

The multi channel performance of the system is limited because of MAI. Under the PSM modulation and multiple access schemes, MAI exists because of the non-orthognolity of the PSM codes. When the MAI increases to certain extent, the data symbol cannot be detected anymore. From section 6.2 we discuss some parameters in a multi-channel scenario. The aim of the system is to accommodate as many as possible channels and to provide as good as possible SER performance.

Reality of the simulation
In all the simulations in this chapter, the IEEE UWB channel models discussed in chapter 3 are used. I understand that there are more advanced and accurate UWB channel models available now, but the IEEE UWB channel models are what I have when I started this work.

For multi channel simulation, the distance between each transmitter and the receiver is generated randomly, which is more like in a real sensor network. As discussed in section 4.1, the statistic full RAKE receiver is immune to near-far effect. This is confirmed by all the simulation results since in all the simulation, the randomly generated transceiver distance did not affect as it would do to a receiver without immunity to near-far problem. Under the effect of near-far problem the signal from the transmitter which is nearest to the receiver will dominate and will bring severe interference. The existence of one near interfering transmitter is more harmful than the existence of several interfering transmitter at far distance. In our simulation results, no sign of such effect are shown, and this confirms that the near-far problem does not affect the statistic full RAKE receiver.

Another advantage of the statistic full RAKE receiver is that it needs no synchronization with the transmitter. In our simulation, to simulate the non synchronized transmission of the multiple transmitters, a random delay time (which is less than one symbol duration) is added to each transmitter. No degradation is observed in the simulation result after adding this random delay time. This confirms that the statistic full RAKE receiver does not need synchronization with the transmitter.

6.1 Chip duration vs. SER performance

In section 3.3 we discussed a parameter of delay spread of UWB channels. If the chip duration of the system is shorter than the channel delay spread, the multipath replica of the pulse will spread in to the next chip and bring the inter-chip-interference and degrade the system performance of SER.

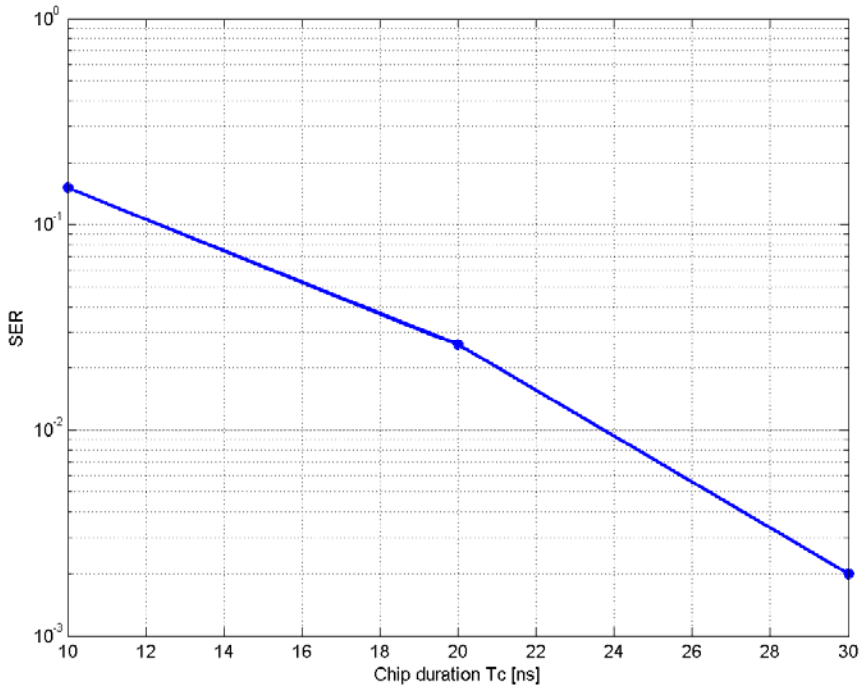

Figure 6-1 SER performance vs. Chip duration

The figure above shows the relation between SER performance and the system chip duration. This simulation is done with CM2 type of channel in the IEEE channel model presented in section 3.3. According to Table 3-1, the RMS delay spread of CM2 channel is 8.03ns and the mean delay spread is 10.36ns. However, we cannot set our chip duration according to these two values because the delay spread of the UWB channel is a statistic parameter, its instance value may exceed its RMS and mean value.

The simulation results show that for CM2 type channel when the chip duration is 10ns, the SER of the system is more than 10%, and this is the result of severe inter-chip-interference. And when the chip duration is set to 30ns, the SER is as low as 0.2% which is quite good. Simulation is done for other type of channel models too. And here we come to a suggestion for the setting of chip duration. For CM1 and CM2 type channels, the chip duration can be set as 30ns and for CM3 and CM4 type channel, the chip duration can be set as 100ns. This setting provides good single channel performance and in the following sections this setting will be used for simulation.

6.2 Code length

The data rate in our system is $R_S = 1/T_S = 1/(N_S * T_C)$, where N_S is code length that represents one data symbol and T_C is the chip duration. The shorter the code length is, the higher data rate the system can provide. However, longer codes tend to give better symbol detection performance in a multiple channel environment.

One way to understand this relation is by comparing the PSM demodulation/symbol detection with a conventional correlation receiver. The PSM demodulation/symbol detection detects the pattern of '1's in the PSM codes. It can be seen as a correlation operation between the received bit sequence and the detection template. In a conventional correlation receiver, the received signal is correlated with the template, and a thresholding operation is performed to detect the correlation peak. In presence of the MAI the detection performance of this receiver is limited by the parameter SINR: signal / interference + noise ratio. The received signal r(t) can be expressed as follow, where s(t) is the expected signal, n(t) is the AWGN noise and i(t) is the interfering signal from other channels.

$$r(t) = s(t) + n(t) + \sum i(t) \quad \text{Equation 6-1}$$

The correlation operation is as follow, where T(t) is the correlation template.

$$\begin{aligned} Z &= \int r(t) * T(t)\, dt \\ &= \int s(t) * T(t)\, dt + \int n(t) * T(t)\, dt + \sum \int i(t) * T(t)\, dt \\ &= S + N + I \end{aligned} \quad \text{Equation 6-2}$$

In Equation 6-2, the first term S is the energy of the expected symbol, or the autocorrelation of the expected symbol, the second term N is the spectrum density of the noise and the third term I is the cross correlation of the target channel and the interfering channels. The parameter SINR is defined as follow:

$$SINR = S / (N + I) \quad \text{Equation 6-3}$$

The higher the energy of the expected symbol is, and the lower the cross correlations between channels are, the higher the SINR is, and the better the receiver will perform.

For the PSM demodulator/symbol detector, the detecting of the code pattern is performed on each RAKE finger. For each RAKE finger, the input signal is a

binary bit sequence. This bit sequence contains the expected code, the interfering code and noise.

$$r(n) = s(n) + n(n) + \sum i(n) \quad \text{Equation 6-4}$$

$$\begin{aligned} Z &= \sum r(n).*T(n) \\ &= \sum s(n).*T(n) + \sum n(n).*T(n) + \sum\left(\sum i(n).*T(n)\right) \\ &= S + N + I \end{aligned} \quad \text{Equation 6-5}$$

In Equation 6-5, the term S is the autocorrelation of the PSM code, the term N is the noise and the term I is the sum of cross correlation of the interfering symbols and the target symbol. The longer the PSM codes are, (with the same code density), the more energy one symbol contains and the higher the term S is. The term N will not grow with the code length since it is the noise spectral density. How the term I will behave as the code length grows depends on the cross correlation property of the PSM codes. In our system we are proposing Gold, Kasami family and chaos-based PN codes. For these two codes, the term I will increase with the code length but not as fast as the term S does. Therefore, increasing the code length will increase the SINR and improve the multi channel performance of the receiver.

Simulation is done to evaluate the multi channel performance of codes of different length and the result is shown in Figure 6-2. Code length of 40, 60 and 80 is used. When 5 channels are transmitting simultaneously, the SER is above 0.1 when code length of 40 is used, it is around 2% when code length of 60 is used and is below 1% when code length of 80 is used. The multi channel performance is improved as the code length grows. The simulation results confirm with our analysis previously in this section. It is easy to understand that this improvement achieved at the cost of data rate of the system.

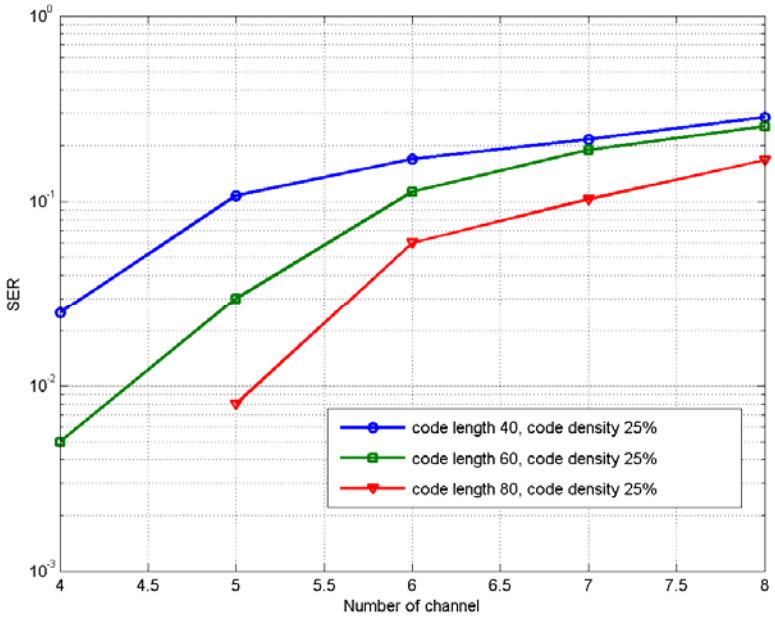

Figure 6-2 code length vs. multi channel performance

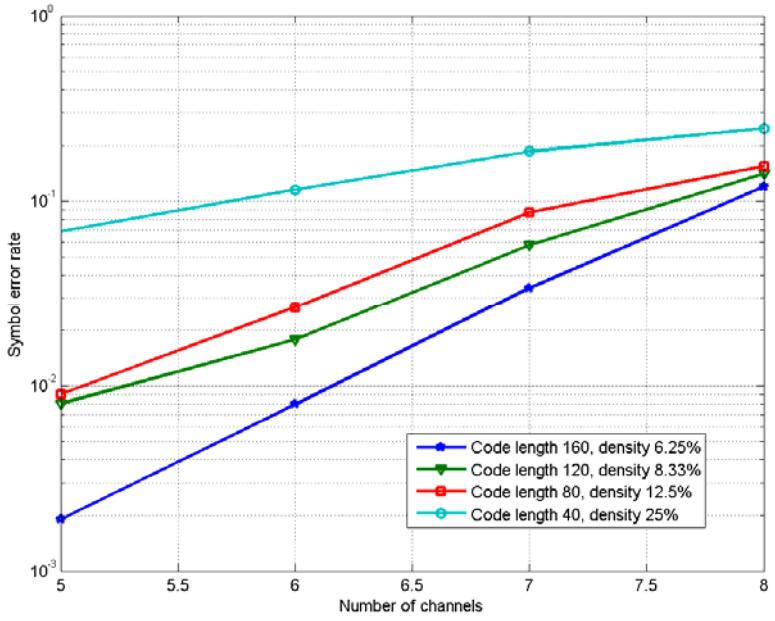

Figure 6-3 Code density vs. multi channel performance

6.3 Code density

The code density is the percentage of '1's in a binary PSM code. We rewrite the definition below, where d_y is the code density and N is the code length

$$d_y = \frac{\sum_{j=1}^{N} y_j}{N}, y_j \in \{0,1\} \qquad \text{Equation 6-6}$$

The code density of PSM codes has impact on MAI. Let us understand this from the point of SIRN. For PSM codes of certain length, the higher density they have, i.e. the more '1's they contains, the higher energy one data symbol contains and therefore the higher the term S will be in the SINR. However, higher density tends to lead to higher cross correlation between codes. To clarify this relation of code density and the interfering term I, we simulate with PSM codes with the same number of '1's. This makes sure that in each simulation the data symbols have the same energy, and the S term is the same in the SINR. We compare the multi channel perform of PSM codes with different density. It is easy to understand that PSM codes with the same number of '1' but different code density have different code length.

$$N = \frac{NumberOfOnes}{d_y} \qquad \text{Equation 6-7}$$

In this simulation, each data symbol contains 10 ones. PSM codes with density 25% has code length of 40, PSM codes with density of 12.5% has code length 0f 80, and so on. From this figure we can see that, the SER becomes lower when the codes have lower density. The multi channel performance is improved as the code density decreases. This confirms with the analysis previously in this section. Again we understand that this improvement is achieved at the cost of data rate of the system.

6.4 Channel activity

A channel is called active when it is transmitting signal. The channel activity is the percentage of time that a channel is active. In the simulations above, the channels are set to be transmitting 100% time; but in a realistic system, the channel activity may be less than 100%. In a wireless sensor network, there is

certain number of nodes and each connection between two nodes forms a channel. A node sends message to other nodes from time to time, and with good probability the activity of the channels are quite low.

In this section we simulate the multi channel performance at different channel activity. The PSM code length of 40 and code density of 25% are used. The results are shown in Figure 6-4. From this figure we can see that, as the channel activity goes down, the SER performance is greatly improved.

This improvement is because, when the channels are transmitting from time to time, and each channel start its data session at a random time, it is less possible that the signals of different channels may overlap and interference each other. Again, transmission at lower channel activity means lower data rate of each channel. But this is more the case in the real world.

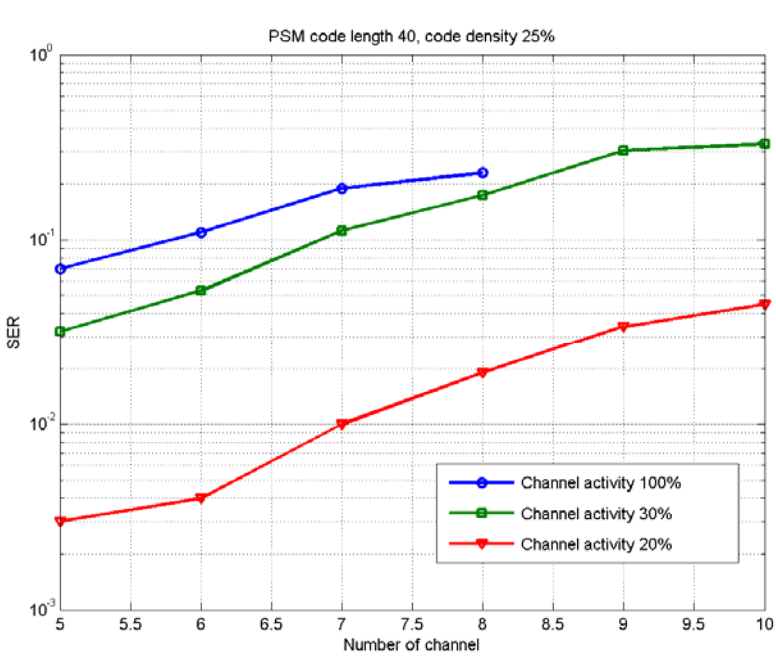

Figure 6-4 Channel activity vs. multi channel performance

6.5 Summary

In this chapter we discuss some important parameters of the system. First of them is the chip duration. The chip duration is important because it needs to be long enough to avoid the inter-chip-interference. The cause of inter-chip-interference is the UWB channel delay spread which is due to multipath effect. So this parameter depends on the condition of transmission environment in which the system is running. In our simulation we are using the IEEE channel model to generate our transmission channels. And the results show that for the CM1 and CM2 types of channel, a chip duration of 30ns can provide good single channel performance, and for CM3 and CM4 types of channel a chip duration of 100ns.

In section 6.2, 6.3 and 6.4 we discuss the multi channel performance of the system, with different PSM code length, code density and system channel activity. The increase of code length, the decrease of code density and a low channel activity all help to improve the multi channel performance of the system. And these improvements are at the cost of system data rate. The symbol rate of the system is

$$R_S = 1/T_S = 1/(N_S * T_C) * ChannelActivity \quad \text{Equation 6-8}$$

For a CM2 type of channel, with chip duration of 30ns, PSM code length of 40 and a channel activity of 20%, the symbol rate of the system is 1.67M symbol/s. With SER less than 5%, we can have 10 channels in this system. If the system needs a symbol rate only on the level of 10K symbol/s, the channel activity can be only 0.2%; surely the system will be able to accommodate much more channels. From these examples we can see the great flexibility on data rate and system capacity (in term of number of channel) of our PHY. With this flexibility this PHY can serve for a very wide range of wireless networks.

7 Conclusion

In this thesis we present a PHY of UWB communication system. At the transmitter part we use the PSM modulation and multiple access method. This method is power efficient than other commonly used modulation and multiple access method, and impose less requirement on DSP and synchronization of the system.

A novel method to smooth the spectrum of the UWB signal, the biphasic toggling method is proposed in this thesis. The purpose of this method is to alleviate the spectrum spikes of the UWB system. Both mathematic analysis and simulation result confirms that the biphasic toggling works well: it brings a 9dB margin in the signal spectrum. In addition, this method is very simple and hardware friendly; it needs only a register and an inverter in the transmitter. No additional hardware is needed at the receiver side to de-toggle the signal.

A lot of discussion has been done on the selection of PSM codes. We compare the candidate codes in their correlation properties, flexibility in code length and code density, number of available codes and implementation of generation hardware, which is linear feedback shift register. The Gold and Kasami code family provides good correlation properties and very easy implementation of code generator. This is good for system that needs to generate codes on each node. However, the flexibility in code length and code density is limited. The chaos-based PN codes provide great flexibility in code length and code density, and have more available codes than the Gold and Kasami family. Its correlation properties are not as good as the Gold and Kasami but are acceptable. The implementation of the code generator is complicated; it involves an analogue circuit that realizes the chaotic system map function. One advantage of the PSM modulation is that, the system sends out pulse only when there is a ‘1’ in the bit sequence; this make the system more power-efficient than other systems. With a code density of 25%, our system will send only 1/4 energy compared to systems with other modulation schemes.

A spatial full RAKE receiver is introduced in chapter 4. This receiver takes advantage of the multipath effect of the UWB channel. Its statistic pulse detection and statistic symbol detection/demodulation are very suitable for the weak signal level of the UWB system. In the statistic pulse detection, a detection threshold that is set according to the noise level. By doing this, the receiver needs no channel estimation as other conventional receivers do. This also makes the receiver immune to near-far problem so that the system needs no power control. By adjusting the thresholding parameters the receiver can work in environment of different noise level.

This system needs no synchronization, and the clock frequency is the chip rate. With chip duration of 30ns, the system needs a clock of 33.3MHz, and the clock drift needs to be less than 11 KHz. The hardware implementation of the transmitter is very simple. The complexity of implementation of the spatial full RAKE receiver depends on, among other factors, the channel condition and the length of the PSM codes. But no synchronization and relatively simple and slow DSP requirement are big favours to the hardware. In conclusion, the PHY we present in this system is suitable for a low data rate, power efficient, simple hardware and low cost UWB system.

Appendix

Proof of argument 1:
The probability distribution function (PDF) of uniform distribution*:

$f(x)=\begin{cases}1/(b-a) & x\in[a,b]\\ 0 & x\notin[a,b]\end{cases}$, where a and b are real number.

If x_k for all k, have PDF of uniform distribution over $[a,b]=[0,1]$:

$$p(x_k\in[0,z])=\int_0^z f(x_k)dx_k=\int_0^z\frac{1}{b-a}dx_k=z$$

$$p(x_k\in[z,1])=\int_z^1 f(x_k)dx_k=\int_z^1\frac{1}{b-a}dx_k=1-z$$

Where z is the quantizing constant and $z\in\,]0,1[$

After quantization, $y_k=Q(x_k)=\begin{cases}1 & x_k\in[0,z]\\ 0 & x\in[z,1]\end{cases}$

$p(y_k=1)=z$ and $p(y_k=0)=1-z$

Code density of the sequence

$$density=\frac{\sum_{k=1}^{M}y_k}{M}\rightarrow p(y_k=1)=z, M\rightarrow\infty$$

Proof of argument 2:
Here we need to proof that in the discrete time dynamic system described by map family shown in Figure 5-10, if the initial value x_0 of a trajectory has uniform distribution over $[0,1]$, then any value in the trajectory x_k will have uniform distribution over $[0,1]$. We prove this by proving the argument that, if x_k has uniform distribution over $[0,1]$, x_{k+1} will have uniform distribution over $[0,1]$.

We prove x_{k+1} has uniform distribution over $[0,1]$, by proving that for any real value $0 \le d_1 \le d_2 \le 1$, $p(x_{k+1} \in [d_1, d_2]) = \frac{d_2 - d_1}{b-a} = d_2 - d_1$.

We define two values c_{11} and c_{12} so that $M(c_{11}) = M(c_{12}) = d_1$, and two values c_{21} and c_{22} so that $M(c_{21}) = M(c_{22}) = d_2$. Consider the nature of the map we assume: $c_{11} \le c_{21} \le c_{12} \le c_{22}$.

We prove this in three cases:

- $0 \le d_1 \le d_2 \le 0.5$

According to the map

$d_1 = \frac{2}{1+r} c_{11}$ and $d_1 = \frac{2}{1-r}(c_{12} - 0.5)$

$d_2 = \frac{2}{1+r} c_{21}$ and $d_2 = \frac{2}{1-r}(c_{22} - 0.5)$

$$
\begin{aligned}
& p(x_{k+1} \in [d_1, d_2]) \\
&= p(M(x_k) \in [d_1, d_2]) \\
&= p(x_k \in [c_{11}, c_{21}]) + p(x_k \in [c_{12}, c_{22}]) \\
&= (c_{21} - c_{11}) + (c_{22} - c_{12}) \\
&= \left(\frac{1+r}{2} d_2 - \frac{1+r}{2} d_1\right) + \left(\frac{1-r}{2} d_2 - \frac{1-r}{2} d_1\right) \\
&= d_2 - d_1
\end{aligned}
$$

- $0.5 \le d_1 \le d_2 \le 1$

Because of the symmetric nature of the map, this case can easily be proved in the same way like above.

- $0 \le d_1 \le 0.5 \le d_2 \le 1$

In this case, having the previous conclusion

$$
\begin{aligned}
& p(x_{k+1} \in [d_1, d_2]) \\
&= p(x_{k+1} \in [d_1, 0.5]) + p(x_{k+1} \in [0.5, d_2]) \\
&= 0.5 - d_1 + d_2 - 0.5 \\
&= d_2 - d_1
\end{aligned}
$$

Proof is done.

*notice that the boundary value will not affect the result of integration, because for any continuous PDF, the probability $p(x = c)$ for what ever real c value, is ultimately small.

Acronyms

ADC	Analogue/Digital Converting
APC	Automatic Power Control
AWGN	Additive White Gaussian Noise
Bps	bit per second
BPSK	Binary Phase Shift Keying
CER	Chip Error Rate
CIR	Channel Impulse Response
DS	Direct Sequence
EGC	Equal Gain Combining
FCC	The Federal Communications Commission
GPS	Global Positioning Systems
DSP	Digital Signal Processing
I.I.D	independent identically distributed (i.i.d)
ISI	Inter-Symbol-Interference
LFSR	Linear Feedback Shift Register
LOS	Line of Sight
MAI	multiple-access-interference
MAC	Media Access Control
MRC	Maximal Ratio Combining
NLOS	non line of sight
OFDM	Orthogonal Frequency Division Multiplexing
OSI	Open Systems Interconnection Basic Reference Model
PAM	Pulse Amplitude Modulation
PD	Peak Distinguishablity
PDF	probability density function
PHY	Physical Layer
PN	Pseudo noise
PPM	Pulse Position Modulation
PSD	Power Spectral Density
PSM	Pulse Sequence Modulation
RMS DS	Root Mean Square delay spread
SINR	Signal Interference/Noise Ratio
SNR	Signal Noise Ratio

SPD	Statistic Pulse Detection
TH	Time Hoping
UWB	Ultra Wideband
WLAN	Wireless Local Area Networks
WPAN	Wireless Personal Area Networks

Bibliography

[FR&O 2002] Federal Communications Commission, *Revision of Part 15 of the Commission's rules Regarding Ultra-Wideband Transmission Systems: First report and order*, Technical Report FCC, adopted February, 2002, released April, 2002.

[Bene 2004] Di Benedetto and Giancola, *Understanding Ultra Wide Band Radio Fundamentals*, Prentice Hall PTR, June 2004.

[Jeff 2005] Jeffrey H. Reed, *An Introduction to Ultra Wideband Communication Systems*, Prentice Hall PTR, second printing, June 2005.

[Mgha 2007] M. Ghavami, L.B. Michael, R. Kohno, *Ultra Wideband signals and systems in communication engineering*, second edition,John Wiley & Sons, Ltd.

[Iano 2004] Ian Oppermann, Matti Hamalainen, and Jari Iinatti, *UWB Theory and Applications*, John Wiley & Sons, Ltd, 2004

[Bsen 2006] Guang-zhong Yang, *Body Sensor Networks*, Springer-Verlag London Limited 2006.

[Wire 2002] Theodore S. Rappaport, *Wireless Communications Principles and Practice*, second edition, Prentice Hall PTR, 2002, 1996.

[IECM 2003] J. R. Foerster, M. Pendergrass and A. F. Molisch, *A Channel Model for Ultrawideband Indoor Communication*, Proc. Of the International Symposium

on Wireless Personal Multimedia communications 2003 (WPMC 2003), October 2003.

[AICT 2006] R. Saadane, D. Aboutajdin and A. M. Hayar, *A Statistical UWB Channel Model Based on Physical Analysis,* Proc. Of AICT/ICIW, 2006 IEEE.

[GCim 2007] G. Cimatti, R. Rovatti, G. Setti, *Chaos-Based Spreading in DS-UWB Sensor networks Increases Available Bit-Rate, IEEE Trams. Circuits Syst I, Reg. papers,* 2007, (accepted for publication).

[Moez 1997] Moe Z. Win, *Power Spectral Density of Binary Digital Pulse Stream in the Presence of Independent Time Jitter,* Military Communication Conference 1997 (MILCOM 97) Proc.

[Srak 2005] Claus Limbodal, Kjetil Meisal, Tor Sverrie Lande, Dag Wisland, *A Spatial RAKE-receiver for real-time UWB-IR applications,* IEEE ICU 2005

[Spar 2005] Claus Limbodal, *A spatial RAKE Receiver for Real-time UWB-IR Applications*, master thesis, University of Oslo.

List of figures